SCIPP 93/49
NSF-ITP-94-30
April 1994

Spin Formalism and Applications to New Physics Searches*

Howard E. Haber

Santa Cruz Institute for Particle Physics
University of California, Santa Cruz, CA 95064†

and

Institute for Theoretical Physics
University of California, Santa Barbara, CA 93106

Abstract

An introduction to spin techniques in particle physics is given. Among the topics covered are: helicity formalism and its applications to the decay and scattering of spin-1/2 and spin-1 particles, techniques for evaluating helicity amplitudes (including projection operator methods and the spinor helicity method), and density matrix techniques. The utility of polarization and spin correlations for untangling new physics beyond the Standard Model at future colliders such as the LHC and a high energy e^+e^- linear collider is then considered. A number of detailed examples are explored including the search for low-energy supersymmetry, a non-minimal Higgs boson sector, and new gauge bosons beyond the $W^\pm$ and Z.

To appear in the Proceedings of the 21st SLAC Summer Institute on
Particle Physics: Spin Structure in High Energy Processes
SLAC, Stanford, CA, 26 July—6 August 1993.

⋆ Work supported in part by the U.S. Department of Energy, grant number DE-FG03-92ER40689 and in part by the National Science Foundation, NSF grant #PHY89-04035.

† Permanent address.

Table of Contents

INTRODUCTION

Every beginning student in particle physics learns how to evaluate Feynman diagrams and compute decay rates and cross sections. In processes involving particles with nonzero spin, one quickly learns the mantra: *average over initial spins and sum over final spins.* Usually, one learns a number of tricks to perform the spin summations so that one never has to worry about the explicit forms for the spin wave functions. However, in the process of summing over spins, one loses a great deal of information. Suppose one is experimentally studying some new physics phenomenon such as a newly discovered particle. In order to maximize the information obtained in the experiment, it is advantageous not to sum over spins. For example, one can study the production of the new particle with polarized beams. One can also study the polarization of the final state by measuring decay angle correlations in the decay chain of the new particle. Clearly, with additional information of this type, one can potentially learn much more about the properties of the new particle and its interactions.

Today, all particle physics phenomena is successfully described by the Standard Model. Precision electroweak measurements at LEP test the Standard Model to better than one part in thousand [1]. So far, no convincing deviation from the Standard Model has been found. Two pieces of the Standard Model remain to be discovered. One is the top quark; evidence for its existence has recently been announced by the CDF collaboration [2]. The other is the Higgs boson. In the Standard Model, electroweak symmetry breaking is triggered by the dynamics of an elementary complex doublet of scalar (Higgs) fields. As a result of these dynamics, the neutral component of the Higgs field acquires a vacuum expectation value. Three of the four Higgs degrees of freedom are absorbed and give mass to the $W^{\pm}$ and Z gauge bosons. A fourth neutral scalar degree of freedom is the Higgs boson. Present limits from LEP imply that the Higgs boson mass must be larger than 60 GeV [3].

However, most theorists believe that the mechanism of electroweak symmetry breaking must be more complex. Theories with elementary scalar fields suffer from the problem of *naturalness* [4]. Simply put, the Standard Model cannot be a complete theory of particle interactions, since it neglects gravity. However, to a very good approximation, it is safe to ignore gravitational interactions at all energy scales below the Planck scale, $M_{\rm PL} \simeq 10^{19}$ GeV. The problem with elementary scalar fields is that the natural value for its mass is given by the largest mass scale at which the scalar field can be viewed as elementary. By natural, I mean that if one attempts to set the scalar mass to be light, radiative corrections drive the mass up to the highest energy scale. Thus, to understand why the Higgs scalar mass (and thus why the scale of electroweak symmetry breaking) is

of order 100 GeV rather than 10^{19} GeV, one must postulate a remarkable fine-tuning of parameters in the fundamental Planck scale theory. Most theorists find this possibility unaesthetic and prefer a less "miraculous" explanation of the large hierarchy between the electroweak scale and the Planck scale. In attempting to devise a theory of electroweak symmetry breaking that avoids this disease, one is led to either assume that the Higgs scalar is not elementary much beyond the scale of 100 GeV, or else a new symmetry exists that can protect scalar fields from acquiring large masses. In all proposed models of these types, there must be new physics associated with the dynamics of electroweak symmetry breaking that exists at or near the scale of electroweak symmetry breaking.

The main goal of the next generation of particle accelerators is to discover the underlying mechanism of electroweak symmetry breaking [5]. That is, one must find the Higgs boson and/or new particles associated with the dynamics of electroweak symmetry breaking that lies at an energy scale of about 1 TeV or below. Assuming that new particles or phenomena are found, it will be crucial to determine the details of the new particle mass spectrum and the nature of their interactions. Spin will play a major role in this enterprise. By employing polarized beams and studying the initial and final state spin correlations, it will be possible to extract detailed information about the new particles and their interactions.

The object of these lectures is to describe some of the basic techniques for making use of spin information to explore new physics beyond the Standard Model. In Lecture 1, I review spin formalism in particle physics and its practical applications to systems of spin-1/2 and spin-1 particles. Most everything in Lecture 1 is well known to practitioners of the field, but is rarely disseminated in elementary graduate courses. I shall highlight the most important results, focusing on the use of helicity states. It is interesting to note that although the material of Lecture 1 is well known, techniques involving the computation of helicity amplitudes are still evolving. New and powerful methods are still being developed today and are permitting the calculation of some multi-particle processes that could not have been envisioned even ten years ago. I will only be able to touch on some of these new methods briefly here. In Lecture 2, I will discuss low-energy supersymmetry as a canonical candidate for physics beyond the Standard Model. I will then show how spin and polarization can be exploited in the detection and elucidation of supersymmetric particles and their interactions. In Lecture 3, I focus on two other examples of the use of spin and polarization for the detection of new phenomena: Higgs bosons at a $\gamma\gamma$ collider, and the detection of new gauge bosons beyond the $W^{\pm}$ and Z at a future hadron collider. I end with a few comments on other areas where spin techniques can play a critical role in the search for new physics.

LECTURE 1:
Spin Formalism and Calculational Techniques

1.1 Helicity states in quantum mechanics

Consider a spinning particle in quantum mechanics with spin vector $\vec{S}$, orbital angular momentum vector $\vec{L}$ and total angular momentum $\vec{J} \equiv \vec{L} + \vec{S}$. In most elementary textbooks of quantum mechanics, it is shown how to construct simultaneous eigenstates of $\vec{J}^2$, J_z, $\vec{L}^2$ and $\vec{S}^2$. Another useful basis is the product basis consisting of simultaneous eigenstates of $\vec{L}^2$, L_z, $\vec{S}^2$ and S_z. Transformations between these two bases involve the Clebsch-Gordon coefficients. However, there is a third basis choice which will prove far more convenient in processes involving relativistic particles. Define the helicity operator Λ as follows

$$\Lambda = \vec{J} \cdot \hat{p} = (\vec{L} + \vec{S}) \cdot \hat{p} = (\vec{r} \times \vec{p} + \vec{S}) \cdot \hat{p} = \vec{S} \cdot \hat{p}, \tag{1.1}$$

which is a scalar operator that commutes with $\vec{J}$ and $\vec{S}^2$. We can now build angular momentum states that are simultaneous eigenstates of $\vec{J}^2$, J_z, $\vec{S}^2$ and Λ. These are the helicity states of a single particle. The helicity states have certain advantages over, say, simultaneous eigenstates of $\vec{J}^2$, J_z, $\vec{L}^2$ and $\vec{S}^2$. In particular, helicity states are (i) invariant under spatial rotations, (ii) invariant under boosts along the particle's momentum (as long as the direction of momentum is not reversed), and (iii) convenient for describing relativistic scattering of both massless and massive particles. Let us explicitly construct the single particle helicity states [6,7]. I shall employ the standard particle physicist's convention of $\hbar = 1$. We shall need to make use of the D and d rotation matrices introduced in most quantum mechanics textbooks. These are defined as follows. The unitary rotation operator acting on the quantum mechanical Hilbert space is [8]

$$U[R(\phi, \theta, \gamma)] \equiv e^{-i\phi J_z} e^{-i\theta J_y} e^{-i\gamma J_z} , \tag{1.2}$$

where the rotation R is specified by three Euler angles. The D and d-matrices are then defined by

$$\begin{aligned} D^{(j)}_{mm'}(R)\, \delta_{jj'} &\equiv \langle jm | U[R(\phi, \theta, \gamma)] | j'm' \rangle \\ &= e^{-i\phi m} e^{-i\gamma m'} d^{j}_{mm'}(\theta)\, \delta_{jj'} . \end{aligned} \tag{1.3}$$

Three important properties that we will need are

$$e^{-i\pi J_y} |jm\rangle = (-1)^{j-m} |j, -m\rangle , \tag{1.4}$$

$$Y_{\ell m}(\theta,\phi) = \sqrt{\frac{2\ell+1}{4\pi}} D^{\ell}_{m0}(\phi,\theta,\gamma)^* \,, \tag{1.5}$$

and the orthogonality relation

$$\int d\Omega\, D^{(j)}_{m\lambda}(R) D^{(j')}_{m'\lambda}(R)^* = \frac{4\pi}{2j+1}\,\delta_{jj'}\delta_{mm'} \,, \tag{1.6}$$

where $d\Omega \equiv d\cos\theta d\phi$ (note that there is no dependence on the angle γ).

Let $\hat{\boldsymbol{p}}$ be a unit vector pointing in a direction specified by a polar angle θ and azimuthal angle ϕ with respect to a fixed z-axis. The three-momentum of a particle will be denoted by $\vec{\boldsymbol{p}} \equiv p\hat{\boldsymbol{p}}$. A plane wave state of helicity λ is constructed by starting with a plane wave eigenstate of S_z (with eigenvalue λ) moving in the z-direction. Applying the rotation operator $U[R(\phi,\theta,-\phi)]$ results in a plane wave moving in the direction of $\vec{\boldsymbol{p}}$. Note that the third argument of R is purely conventional, since for a particle moving in the z-direction, a rotation about $\hat{\boldsymbol{z}}$ has no physical effect. The reason for choosing such a convention is that the rotation $R(\phi,\theta,-\phi)$ is equivalent to a single rotation by an angle θ about an axis $\hat{\boldsymbol{n}}$, where

$$\hat{\boldsymbol{n}} = (-\sin\phi, \cos\phi, 0)\,. \tag{1.7}$$

This result can be proven by verifying that

$$e^{-i\phi J_z} e^{-i\theta J_y} e^{i\phi J_z} = e^{-i\theta(J_y\cos\phi - J_x\sin\phi)} \,, \tag{1.8}$$

which follows from the commutation relations of the angular momentum operators.

The helicity plane-wave state is explicitly given by

$$|\vec{\boldsymbol{p}},\lambda\rangle = U[R(\phi,\theta,-\phi)]\,|p\hat{\boldsymbol{z}},\lambda\rangle \,, \tag{1.9}$$

where

$$J_z\,|p\hat{\boldsymbol{z}},\lambda\rangle = \lambda\,|p\hat{\boldsymbol{z}},\lambda\rangle \,, \tag{1.10}$$

since for $\vec{\boldsymbol{p}} = p\hat{\boldsymbol{z}}$, $J_z = \vec{\boldsymbol{J}}\cdot\hat{\boldsymbol{p}} = \vec{\boldsymbol{S}}\cdot\hat{\boldsymbol{p}} = S_z$. Let us expand in a complete set of eigenstates of $\vec{\boldsymbol{J}}^2$ and J_z,

$$|p\hat{\boldsymbol{z}},\lambda\rangle = \sum_{j=|\lambda|}^{\infty} |p,jm\rangle\,\langle p,jm|p\hat{\boldsymbol{z}},\lambda\rangle \,, \tag{1.11}$$

where the sum is taken over integers (half-integers) for an integer (half-integer) spin particle. Next, apply $U[R]$ to Eq. (1.11) to obtain $|\vec{\boldsymbol{p}},\lambda\rangle$. Inserting a second

complete set of angular momentum states and using Eq. (1.3), one obtains

$$|\vec{\boldsymbol{p}},\lambda\rangle = \sum_{j=|\lambda|}^{\infty} \sum_{m=-j}^{j} |p,jm\rangle\, D^{(j)}_{m\lambda}(R) \langle p,jm|p\hat{\boldsymbol{z}},\lambda\rangle\,. \tag{1.12}$$

This result is the generalization for spinning particles of the well known expansion of plane waves in terms of spherical waves. To see that this is the desired result, multiply Eq. (1.12) by $\langle\vec{\boldsymbol{r}}|$. For spinless particles, $\lambda = 0$, $j = \ell$, and

$$\begin{aligned} &\langle\vec{\boldsymbol{r}}\,|\,\vec{\boldsymbol{p}}\rangle \sim e^{i\vec{\boldsymbol{p}}\,\cdot\,\vec{\boldsymbol{r}}} \\ &\langle\vec{\boldsymbol{r}}\,|\,p,\ell m\rangle \sim i^{\ell} j_{\ell}(pr) Y_{\ell m}(\hat{\boldsymbol{r}}) \\ &\langle p,\ell m\,|\,p\hat{\boldsymbol{z}}\rangle \text{ is a constant independent of } \hat{\boldsymbol{p}},\hat{\boldsymbol{r}}. \end{aligned} \tag{1.13}$$

Eq. (1.12) then reduces to the familiar result

$$e^{i\vec{\boldsymbol{p}}\,\cdot\,\vec{\boldsymbol{r}}} = 4\pi \sum_{\ell m} i^{\ell} j_{\ell}(pr) Y_{\ell m}(\hat{\boldsymbol{r}}) Y^{*}_{\ell m}(\hat{\boldsymbol{p}})\,. \tag{1.14}$$

The overall factor of 4π can be obtained by setting $p = 0$.

Let us return to Eq. (1.12). We can invert this expansion and evaluate the matrix element $\langle p,jm|p\hat{\boldsymbol{z}},\lambda\rangle$ by imposing the orthonormality relation

$$\langle p,jm\lambda|p',j'm'\lambda'\rangle = \frac{1}{p^2}\,\delta(p-p')\delta_{jj'}\delta_{mm'}\delta_{\lambda\lambda'}\,. \tag{1.15}$$

Using Eq. (1.6), one ends up with

$$|p,jm\lambda\rangle = \sqrt{\frac{2j+1}{4\pi}} \int d\Omega\, D^{(j)}_{m\lambda}(R)^{*}\, |\vec{\boldsymbol{p}},\lambda\rangle\ , \tag{1.16}$$

where the rotation R is specified by Euler angles $(\phi,\theta,-\phi)$. Note that I have inserted a helicity label λ on the left-hand side of Eq. (1.16) since $|p,jm\rangle$ is explicitly an eigenstate of Λ. It follows that $|p,jm\lambda\rangle$ are the simultaneous eigenstates of $\vec{\boldsymbol{J}}^2$, J_z, $\vec{\boldsymbol{S}}^2$ and Λ. These are the one-particle helicity states.

In scattering processes, the initial state consists of two particles. It is convenient to work in the center-of-momentum (CM) frame where $\vec{\boldsymbol{p}} \equiv \vec{\boldsymbol{p}}_1 = -\vec{\boldsymbol{p}}_2$. The

total helicity of the two-particle system is defined as

$$\Lambda = \Lambda_1 + \Lambda_2 = \vec{\boldsymbol{J}}_{\mathbf{1}} \cdot \hat{\boldsymbol{p}}_{\mathbf{1}} + \vec{\boldsymbol{J}}_{\mathbf{2}} \cdot \hat{\boldsymbol{p}}_{\mathbf{2}} = (\vec{\boldsymbol{J}}_{\mathbf{1}} - \vec{\boldsymbol{J}}_{\mathbf{2}}) \cdot \hat{\boldsymbol{p}} \,. \tag{1.17}$$

It is also useful to define the relative helicity of the two-particle system as

$$\vec{\boldsymbol{J}} \cdot \hat{\boldsymbol{p}} = (\vec{\boldsymbol{J}}_{\mathbf{1}} + \vec{\boldsymbol{J}}_{\mathbf{2}}) \cdot \hat{\boldsymbol{p}} = \Lambda_1 - \Lambda_2 \,. \tag{1.18}$$

We can construct two-particle helicity states [6] in the same way we obtained the one-particle helicity states above.[⋆] First we define two-particle plane wave states in the CM-frame. However, there is a delicate question of phases that must first be addressed. As in the derivation of the one-particle helicity states, one begins from the state moving along the z-direction and rotates to the desired orientation. But, in the two-particle state in the CM-frame, if $\vec{\boldsymbol{p}}_1 = p\hat{\boldsymbol{z}}$ then $\vec{\boldsymbol{p}}_2 = -p\hat{\boldsymbol{z}}$. Thus, we must define the state $|-p\hat{\boldsymbol{z}}, \lambda\rangle$. This can be done in two different ways: (i) start in the rest frame with a state of helicity λ, boost along the positive z-direction and then rotate to the negative z-axis, or (ii) start in the rest frame with a state of helicity $-\lambda$ and boost along the negative z-axis. These two results yield states that differ by a phase, so a convention is required. I shall choose the Jacob-Wick second particle convention [6] which defines a helicity state of a particle of spin s moving in the negative z-direction to be

$$|-p\hat{\boldsymbol{z}}, \lambda\rangle = (-1)^{s-\lambda} e^{-i\pi J_y} \, |p\hat{\boldsymbol{z}}, \lambda\rangle \ . \tag{1.19}$$

This definition implies that

$$\lim_{p \longrightarrow 0} \langle p\hat{\boldsymbol{z}}, -\lambda| - p\hat{\boldsymbol{z}}, \lambda\rangle = 1 \,, \tag{1.20}$$

where Eq. (1.4) has been used [which explains the origin of the extra phase $(-1)^{s-\lambda}$ in Eq. (1.19)]. The two-particle plane-wave state is then defined by

$$|\vec{\boldsymbol{p}}; \lambda_1 \lambda_2\rangle \equiv U[R(\phi, \theta, -\phi)] \, |p\hat{\boldsymbol{z}}, \lambda_1\rangle \otimes |-p\hat{\boldsymbol{z}}, \lambda_2\rangle \ . \tag{1.21}$$

It follows from Eq. (1.18) that

$$\vec{\boldsymbol{J}} \cdot \hat{\boldsymbol{p}} \, |\vec{\boldsymbol{p}}; \lambda_1 \lambda_2\rangle = \lambda \, |\vec{\boldsymbol{p}}; \lambda_1 \lambda_2\rangle \ , \qquad\qquad \lambda \equiv \lambda_1 - \lambda_2 \,. \tag{1.22}$$

From this point on, the analysis follows the derivation of the one-particle helicity state. The final result for the two-particle helicity state [the analogue of Eq. (1.16),

⋆ Good textbook introductions to helicity formalism in particle physics can be found in Refs. [9] and [10].

with $\lambda \equiv \lambda_1 - \lambda_2$] is

$$|p, jm\,\lambda_1\lambda_2\rangle = \sqrt{\frac{2j+1}{4\pi}} \int d\Omega\, D^{(j)}_{m\lambda}(R)^*\, |\vec{\boldsymbol{p}};\lambda_1,\lambda_2\rangle\ . \tag{1.23}$$

1.2 Helicity amplitudes in decay and scattering processes

From the expression for the two-particle helicity state given in Eq. (1.23), it is straightforward to derive formulae for decay widths and scattering amplitudes in terms of helicity amplitudes [9,10]. Two examples are given below.

First, consider the two-body decay of an unstable particle of spin J. Let us work in the CM-frame. Choose a z-axis and assume that the decaying particle is polarized with J_z quantum number equal to M. The final state particles have spin s_i and helicity λ_i (where $i = 1, 2$). The decay angular distribution for $(J, M) \to (s_1, \lambda_1) + (s_2, \lambda_2)$ is given by

$$\frac{d\Gamma}{d\Omega} = \frac{p_f}{32\pi^2 m^2} \mid \mathcal{M}^{JM}_{\lambda_1\lambda_2}(\theta,\phi) \mid^2 , \tag{1.24}$$

where m is the mass of the decaying particle, p_f is the CM-momentum,[⋆] and

$$\mathcal{M}^{JM}_{\lambda_1\lambda_2}(\theta,\phi) = \sqrt{\frac{2J+1}{4\pi}}\, D^J_{M\lambda}(\phi,\theta,-\phi)^*\, \mathcal{M}^J_{\lambda_1\lambda_2}\,. \tag{1.25}$$

In the above formula, $\lambda \equiv \lambda_1 - \lambda_2$, and $\mathcal{M}^J_{\lambda_1\lambda_2}$ is a reduced decay amplitude which is a function of J, the outgoing helicities, and the particle masses, but is independent of the angles θ and ϕ.

Second, consider the two-body scattering process. Again, it is convenient to work in the CM-frame. Then, the differential cross section for the scattering of particles of definite helicities: $a(\lambda_a) + b(\lambda_b) \longrightarrow c(\lambda_c) + d(\lambda_d)$ is given by

$$\frac{d\sigma}{d\Omega_{\rm CM}} = \frac{1}{64\pi^2 s}\left(\frac{p_f}{p_i}\right) \mid \mathcal{M}_{\lambda_c\lambda_d;\lambda_a\lambda_b}(s,\theta,\phi) \mid^2 , \tag{1.26}$$

where $\sqrt{s}$ is the CM-energy of the process, p_i (p_f) is the initial (final) CM-momentum [explicitly: $p_i = \lambda^{1/2}(s, m_a^2, m_b^2)/2\sqrt{s}$ and for p_f, replace initial state

⋆ Explicitly, $p_f = \lambda^{1/2}(m^2, m_1^2, m_2^2)/2m$, where m_i ($i = 1, 2$) are the masses of the decay products and $\lambda(a,b,c) \equiv (a+b-c)^2 - 4ab$.

masses with final state masses], and the helicity amplitudes for the scattering process are given by

$$\mathcal{M}_{\lambda_c\lambda_d;\lambda_a\lambda_b}(s,\theta,\phi) = \sum_{J=\max\{\lambda_i,\lambda_f\}}^{\infty} (2J+1)\, d^J_{\lambda_i\lambda_f}(\theta) e^{i(\lambda_i-\lambda_f)\phi} \mathcal{M}^J_{\lambda_c\lambda_d;\lambda_a\lambda_b}(s)\,, \quad (1.27)$$

summed over integers (half-integers) for integer (half-integer) λ_i and λ_f, where

$$\lambda_i \equiv \lambda_a - \lambda_b\,, \qquad \lambda_f \equiv \lambda_c - \lambda_d\,. \quad (1.28)$$

In the above formula, $\mathcal{M}^J_{\lambda_c\lambda_d;\lambda_a\lambda_b}(s)$ is a reduced matrix element which is independent of scattering angle. Note that if all particles are spinless (take $\lambda_i = \lambda_f = 0$ and $J = \ell$, where ℓ is the orbital angular momentum), then Eq. (1.27) reduces to the usual partial wave expansion of nonrelativistic quantum mechanics. [In verifying this result, use the fact that $d^\ell_{00}(\theta) = P_\ell(\cos\theta)$, which follows from Eq. (1.5).]

If the decay and scattering processes are mediated by parity (P) and/or time-reversal (T) invariant interactions, then there are nontrivial constraints on the reduced matrix elements. Additional restrictions are obtained if the initial and/or final state particles are identical. These constraints are summarized below [6,9].

(a) Parity

$$\begin{aligned} \mathcal{M}^J_{\lambda_1\lambda_2} &= \eta\eta_1\eta_2(-1)^{s_1+s_2-J}\mathcal{M}^J_{-\lambda_1,-\lambda_2}\,, \\ \mathcal{M}^J_{\lambda_c\lambda_d;\lambda_a\lambda_b}(s) &= (\eta_c\eta_d/\eta_a\eta_b)(-1)^{s_c+s_d-s_a-s_b}\mathcal{M}^J_{-\lambda_c-\lambda_d;-\lambda_a-\lambda_b}(s)\,, \end{aligned} \quad (1.29)$$

where η_i is the intrinsic parity of particle i. Note that in the first formula above, η is the intrinsic parity of the decaying spin-J particle.

(b) Time-reversal

$$\mathcal{M}^J_{\lambda_c\lambda_d;\lambda_a\lambda_b}(s) = \mathcal{M}^J_{\lambda_a\lambda_b;\lambda_c\lambda_d}(s)\,. \quad (1.30)$$

(c) Identical particles

$$\begin{aligned} \mathcal{M}^J_{\lambda_1\lambda_2} &= (-1)^J\mathcal{M}^J_{\lambda_2\lambda_1}\,, \\ \mathcal{M}^J_{\lambda_c\lambda_d;\lambda_a\lambda_b}(s) &= \begin{cases} (-1)^J\mathcal{M}^J_{\lambda_c\lambda_d;\lambda_b\lambda_a}(s), & a,\, b \text{ identical}, \\ (-1)^J\mathcal{M}^J_{\lambda_d\lambda_c;\lambda_a\lambda_b}(s), & c,\, d \text{ identical}. \end{cases} \end{aligned} \quad (1.31)$$

Note that in the case of identical particles, J must be an integer.

In actual computations of decay and scattering processes from Feynman diagrams, one can compute the helicity amplitudes by employing explicit representations for the spin wave functions. Then, the reduced amplitudes can be identified from Eqs. (1.25) or (1.27).

1.3 Explicit spin-$\frac{1}{2}$ and spin-1 wave functions

In this section we summarize the explicit forms for the spin wave functions for spin-1/2 and spin-1 particles (see *e.g.*, Ref. [11]). There are some delicate phase choices to be made in writing down these explicit forms. Sometimes, these choices actually matter, so I have been careful to be consistent in my presentation of the formulae below.

(1) Spin-$\frac{1}{2}$ helicity states

The explicit form of the Dirac spinors depends on the choice of representation for the γ-matrices. Consider first the standard or "low energy" representation (using the metric and γ-matrix conventions of Bjorken and Drell [12]):

$$\gamma^0 = \begin{pmatrix} 1 & 0 \\ 0 & -1 \end{pmatrix}, \qquad \gamma^i = \begin{pmatrix} 0 & \sigma^i \\ -\sigma^i & 0 \end{pmatrix}, \qquad \gamma_5 = i\gamma^0\gamma^1\gamma^2\gamma^3 = \begin{pmatrix} 0 & 1 \\ 1 & 0 \end{pmatrix}, \tag{1.32}$$

where the σ^i are the usual Pauli matrices. The charge-conjugation matrix is defined by[⋆]

$$C = i\gamma^0\gamma^2 = \begin{pmatrix} 0 & i\sigma^2 \\ i\sigma^2 & 0 \end{pmatrix}. \tag{1.33}$$

The free-particle solutions to the Dirac equation are four-component spinors

$$u(p) = \sqrt{2m} \begin{pmatrix} \cosh\frac{\zeta}{2}\,\chi \\ \sinh\frac{\zeta}{2}\,\vec{\boldsymbol{\sigma}}\cdot\hat{\boldsymbol{p}}\,\chi \end{pmatrix}, \tag{1.34}$$

where χ is a two-component spinor, $p = (E\,;\vec{\boldsymbol{p}})$ and

$$\begin{aligned} \cosh\frac{\zeta}{2} &= \left(\frac{E+m}{2m}\right)^{1/2}, \\ \sinh\frac{\zeta}{2} &= \left(\frac{E-m}{2m}\right)^{1/2}. \end{aligned} \tag{1.35}$$

Note that the rapidity ζ is simply related to the energy and three-momentum by $E = m\cosh\zeta$ and $p = m\sinh\zeta$. The overall normalization factor in Eq. (1.34) has been chosen so that $\bar{u}u = 2m$. This ensures a smooth $m \to 0$ limit; that is, for

⋆ The reader should be cautioned that this definition of C differs from that of Ref. [12] (and other standard texts) by a minus sign. The choice of sign is conventional.

a massless spinor, take $\sqrt{2m}\cosh\zeta/2 = \sqrt{2m}\sinh\zeta/2 = \sqrt{E}$ in Eq. (1.34). The four-component antiparticle spinor is defined as

$$v(p) = C\bar{u}^T(p)\,, \tag{1.36}$$

where C is the charge conjugation matrix [Eq. (1.33)] and $\bar{u} \equiv u^\dagger\gamma^0$.

In order to construct the spin-1/2 helicity states, one chooses the two-component spinors χ in Eq. (1.34) to be eigenstates of $\frac{1}{2}\vec{\boldsymbol{\sigma}}\cdot\hat{\boldsymbol{p}}$, *i.e.*,

$$\tfrac{1}{2}\vec{\boldsymbol{\sigma}}\cdot\hat{\boldsymbol{p}}\,\chi_\lambda = \lambda\chi_\lambda, \qquad \lambda = \pm\tfrac{1}{2}\,. \tag{1.37}$$

If $\hat{\boldsymbol{p}}$ is a unit vector with polar angle θ and azimuthal angle ϕ with respect to a fixed z-axis, then the two-component spinors are

$$\chi_{1/2}(\hat{\boldsymbol{p}}) = \begin{pmatrix} \cos\frac{\theta}{2} \\ e^{i\phi}\sin\frac{\theta}{2} \end{pmatrix}, \qquad \chi_{-1/2}(\hat{\boldsymbol{p}}) = \begin{pmatrix} -e^{-i\phi}\sin\frac{\theta}{2} \\ \cos\frac{\theta}{2} \end{pmatrix}. \tag{1.38}$$

One can also construct $\chi_\lambda(\hat{\boldsymbol{p}})$ from $\chi_\lambda(\hat{\boldsymbol{z}})$ by employing the spin-1/2 rotation operator

$$\chi_\lambda(\hat{\boldsymbol{p}}) = e^{-i\theta\hat{\boldsymbol{n}}\cdot\vec{\boldsymbol{\sigma}}/2}\,\chi_\lambda(\hat{\boldsymbol{z}})\,, \tag{1.39}$$

where $\hat{\boldsymbol{n}}$ is defined in Eq. (1.7). Note that the two-component helicity spinors satisfy

$$\chi_{-\lambda}(\hat{\boldsymbol{p}}) = -2\lambda i\sigma^2\chi^*_\lambda(\hat{\boldsymbol{p}})\,. \tag{1.40}$$

The explicit forms for the four-component helicity spinors are

$$\begin{aligned} u(p,\lambda) &= \sqrt{2m}\begin{pmatrix} \cosh\frac{\zeta}{2}\,\chi_\lambda(\hat{\boldsymbol{p}}) \\ 2\lambda\sinh\frac{\zeta}{2}\,\chi_\lambda(\hat{\boldsymbol{p}}) \end{pmatrix}, \\ v(p,\lambda) &= \sqrt{2m}\begin{pmatrix} \sinh\frac{\zeta}{2}\,\chi_{-\lambda}(\hat{\boldsymbol{p}}) \\ -2\lambda\cosh\frac{\zeta}{2}\,\chi_{-\lambda}(\hat{\boldsymbol{p}}) \end{pmatrix}. \end{aligned} \tag{1.41}$$

In the case of a two-particle helicity state, one must choose an appropriate definition for $\chi_\lambda(-\hat{\boldsymbol{p}})$ in the second particle spinor in order to be consistent with the Jacob-Wick second particle convention. First, note that if $\hat{\boldsymbol{p}}$ is pointing in the direction specified by polar and azimuthal angles (θ,ϕ), then $-\hat{\boldsymbol{p}}$ points in the direction

specified by $(\pi - \theta, \phi \pm \pi)$ [the choice of sign is made so that $0 \leq \phi \leq 2\pi$]. It follows from Eq. (1.38) that[†]

$$\chi_{-\lambda}(-\hat{\boldsymbol{p}}) = \xi_\lambda \, \chi_\lambda(\hat{\boldsymbol{p}}) \,, \tag{1.42}$$

where the phase $\xi_\lambda \equiv (-1)^{s-\lambda} \, e^{-2i\lambda\phi}$ for a particle of spin s. For $s = 1/2$, it is convenient to write $\xi_\lambda = 2\lambda e^{-2i\lambda\phi}$. For second particle spinors in the Jacob-Wick convention, the overall phase of $\chi_\lambda(-\hat{\boldsymbol{p}})$ is modified by choosing $\xi_\lambda \equiv 1$.

With the explicit forms for the helicity spinors, one can derive a number of useful relations. We list three such relations below, which we will make use of later in this lecture:

$$v(p,\lambda) = -2\lambda \, \gamma_5 \, u(p,-\lambda) \,, \tag{1.43}$$

and

$$\begin{aligned} u(-p,-\lambda) &= \xi_\lambda \, \gamma^0 u(p,\lambda) \,, \\ v(-p,-\lambda) &= \xi_{-\lambda} \, \gamma^0 v(p,\lambda) \,, \end{aligned} \tag{1.44}$$

where $-p \equiv (E\,; -\vec{\boldsymbol{p}})$ and ξ_λ is defined below Eq. (1.42).

In high energy processes, the chiral or "high energy" representation of the Dirac matrices and spinors is more useful if an explicit representation is needed. For the record, I note that

$$\begin{aligned} \gamma_c^\mu &= S \gamma_s^\mu \, S^\dagger \,, \\ \psi_c &= S \psi_s \,, \end{aligned} \tag{1.45}$$

where the subscripts s and c refer to the standard and chiral representations respectively, ψ is either a u or v-spinor and

$$S = \frac{1}{\sqrt{2}} \begin{pmatrix} 1 & -1 \\ 1 & 1 \end{pmatrix} . \tag{1.46}$$

For example,

$$u(p) = \frac{1}{\sqrt{2(E+m)}} \begin{pmatrix} (m + E - \vec{\boldsymbol{p}} \cdot \vec{\boldsymbol{\sigma}})\chi \\ (m + E + \vec{\boldsymbol{p}} \cdot \vec{\boldsymbol{\sigma}})\chi \end{pmatrix} = \begin{pmatrix} \sqrt{p \cdot \sigma}\chi \\ \sqrt{p \cdot \overline{\sigma}}\chi \end{pmatrix} , \tag{1.47}$$

where $\sigma^\mu = (1; \vec{\boldsymbol{\sigma}})$ and $\overline{\sigma}^\mu = (1; -\vec{\boldsymbol{\sigma}})$. See *e.g.*, Refs. [10] and [13] for further details on this representation.

---

† An equivalent result for $\chi_\lambda(-\hat{\boldsymbol{p}})$, which can be obtained from Eq. (1.39), is

$$\chi_\lambda(-\hat{\boldsymbol{p}}) = -2\lambda e^{-2i\lambda\phi} \, i \, \hat{\boldsymbol{n}} \cdot \vec{\boldsymbol{\sigma}} \, \xi_{-\lambda} \chi_\lambda(\hat{\boldsymbol{p}}) \,,$$

where the phase ξ_λ is defined below Eq. (1.42).

Although the explicit forms for spinors are occasionally useful in practical computations, it is often more useful to employ the helicity projection operators which are independent of the specific Dirac matrix representation. For a massive spin-1/2 particle with four-momentum $p^\mu = (E\,;\,\vec{\boldsymbol{p}})$, the spin four-vector is defined as

$$s^\mu = (2\lambda)\frac{1}{m}\,(|\vec{\boldsymbol{p}}|\,;\,E\hat{\boldsymbol{p}})\ , \tag{1.48}$$

where $2\lambda = \pm 1$ is twice the spin-1/2 particle helicity. The spin four-vector satisfies

$$\begin{aligned} s\cdot p &= 0\,,\\ s\cdot s &= -1\,. \end{aligned} \tag{1.49}$$

Note that in the rest frame, $s = 2\lambda\,(0\,;\,\hat{\boldsymbol{p}})$, while in the high energy limit (where $E \gg m$), $s = 2\lambda p/m$.

The helicity spinors satisfy the Dirac equation and are eigenstates of $\gamma_5 \not{s}$ with unit eigenvalue. Explicitly, we have

$$\begin{aligned} \not{p}u(p,\lambda) &= mu(p,\lambda)\,, & \gamma_5\not{s}\,u(p,\lambda) &= u(p,\lambda)\,,\\ \not{p}v(p,\lambda) &= -mv(p,\lambda)\,, & \gamma_5\not{s}\,v(p,\lambda) &= v(p,\lambda)\,. \end{aligned} \tag{1.50}$$

From these results, one can derive the helicity projection operators for a massive spin-1/2 particle:

$$\begin{aligned} u(p,\lambda)\bar{u}(p,\lambda) &= \tfrac{1}{2}(1+\gamma_5\not{s})\,(\not{p}+m)\,,\\ v(p,\lambda)\bar{v}(p,\lambda) &= \tfrac{1}{2}(1+\gamma_5\not{s})\,(\not{p}-m)\,. \end{aligned} \tag{1.51}$$

To apply the above formulae to the massless case, recall that in the $m \to 0$ limit, $s = 2\lambda p/m + \mathcal{O}(m/E)$. Inserting this result in Eq. (1.50), it follows that the massless helicity spinors are eigenstates of γ_5

$$\begin{aligned} \gamma_5 u(p,\lambda) &= 2\lambda u(p,\lambda)\,,\\ \gamma_5 v(p,\lambda) &= -2\lambda v(p,\lambda)\,. \end{aligned} \tag{1.52}$$

Applying the same limiting procedure to Eq. (1.51) and using the mass-shell condition ($\not{p}\not{p} = p^2 = m^2$), one obtains the helicity projection operators for a massless spin-1/2 particle

$$\begin{aligned} u(p,\lambda)\bar{u}(p,\lambda) &= \tfrac{1}{2}(1+2\lambda\gamma_5)\,\not{p}\,,\\ v(p,\lambda)\bar{v}(p,\lambda) &= \tfrac{1}{2}(1-2\lambda\gamma_5)\,\not{p}\,. \end{aligned} \tag{1.53}$$

(2) Spin-1 helicity states

Let $k^\mu = (k^0\,;\,\vec{\boldsymbol{k}}\,)$ be the four-momentum of a spin-1 particle moving in the direction $\hat{\boldsymbol{k}}$ which points in a direction specified by polar and azimuthal angles θ and ϕ. The spin-1 wave function (or polarization four-vector) for the helicity $\lambda = \pm 1$ states is given by

$$\epsilon^\mu(k,\pm 1) = \sqrt{\tfrac{1}{2}}e^{\pm i\phi}(0\,;\,\mp\cos\theta\cos\phi + i\sin\phi\,,\,-i\cos\phi \mp \cos\theta\sin\phi\,,\,\pm\sin\theta)\,. \tag{1.54}$$

Note that the above result holds both for massless and massive spin-1 particles. If the mass $m \neq 0$, one must also list the polarization four-vector of the longitudinal ($\lambda = 0$) state

$$\epsilon^\mu(k,0) = \left(\frac{|\vec{\boldsymbol{k}}|}{m};\ \frac{k^0}{m}\,\hat{\boldsymbol{k}}\right)\,. \tag{1.55}$$

The spin-1 polarization vectors satisfy

$$\begin{aligned} &k\cdot\epsilon(k,\lambda) = 0\,,\\ &\epsilon(k,\lambda)\cdot\epsilon(k,\lambda')^* = -\delta_{\lambda\lambda'}\,. \end{aligned} \tag{1.56}$$

In addition, the overall phase of ϵ has been chosen such that

$$\epsilon(k,-\lambda) = (-1)^\lambda\,\epsilon(k,\lambda)^*\,. \tag{1.57}$$

For spin-1 particles moving in the $-\hat{\boldsymbol{k}}$ direction, one can check that

$$\epsilon^\mu(-k,-\lambda) = -\xi_\lambda\,g_{\mu\mu}\,\epsilon^\mu(k,\lambda)\,, \tag{1.58}$$

where $-k \equiv (k^0;\,-\vec{\boldsymbol{k}})$ and $g_{\mu\nu} = \mathrm{diag}\,(1,-1,-1,-1)$ [but there is *no* implied sum over μ]. The definition of ξ_λ is the one appropriate for $s = 1$ [see below Eq. (1.42)]; *i.e.*, $\xi_\lambda = (-1)^{1-\lambda}\,e^{-2i\lambda\phi}$. As before, for a second particle in the Jacob-Wick convention, the overall phase of $\epsilon^\mu(-k,\lambda)$ is modified by choosing $\xi_\lambda = 1$.

1.4 Spin projection operator methods

All particle physics students learn how to use projection operators to compute spin-summed and averaged cross-sections in quantum field theory. These methods also apply when the incoming and/or outgoing particles are in definite spin states.

Many examples of such computations can be found in Ref. [14]. Here, I shall illustrate the method in the computation of the squared matrix element for

$$e^+(p_2,\lambda_2) + e^-(p_1,\lambda_1) \to \mu^+(p_4,\lambda_4) + \mu^-(p_3,\lambda_3)\,, \tag{1.59}$$

where each lepton is in a definite helicity state as specified by the corresponding λ (and the p_i are the corresponding four-momenta). There is one tree-level Feynman diagram shown below.

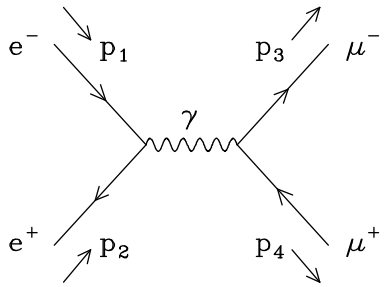

Applying QED Feynman rules, the helicity amplitudes are

$$\mathcal{M}_{\lambda_3\lambda_4;\lambda_1\lambda_2} = \frac{e^2}{s}\bar{u}(p_3,\lambda_3)\gamma^\mu v(p_4,\lambda_4)\bar{v}(p_2,\lambda_2)\gamma_\mu u(p_1,\lambda_1)\,, \tag{1.60}$$

where $s = (p_1+p_2)^2$ is the CM-energy squared. Squaring the amplitude, and making use of the helicity projection operators [Eq. (1.51)], one obtains

$$\begin{aligned}|\mathcal{M}_{\lambda_3\lambda_4;\lambda_1\lambda_2}|^2 = \frac{e^4}{16s^2}\,&\mathrm{Tr}\;\gamma^\mu(1+\gamma_5\not{s}_4)(\not{p}_4-m_\mu)\gamma^\nu(1+\gamma_5\not{s}_3)(\not{p}_3+m_\mu)\\ &\times\mathrm{Tr}\;\gamma_\mu(1+\gamma_5\not{s}_1)(\not{p}_1+m_e)\gamma_\nu(1+\gamma_5\not{s}_2)(\not{p}_2-m_e)\,.\end{aligned} \tag{1.61}$$

Although this expression is complicated, it can be worked out by hand. However, it is instructive to simplify the computation by evaluating the squared amplitude in the high energy limit. In this case, I can neglect all masses and replace $\not{s}_i$ with $\pm 2\lambda$ [where the plus (minus) sign is chosen for (anti-)particles]. Eq. (1.61) then reduces to

$$\begin{aligned}|\mathcal{M}_{\lambda_3\lambda_4;\lambda_1\lambda_2}|^2 &= \frac{e^4}{16s^2}\,\mathrm{Tr}\;\gamma^\mu(1-2\lambda_4\gamma_5)\not{p}_4\gamma^\nu(1+2\lambda_3\gamma_5)\not{p}_3\\ &\qquad\times\mathrm{Tr}\;\gamma_\mu(1+2\lambda_1\gamma_5)\not{p}_1\gamma_\nu(1-2\lambda_2\gamma_5)\not{p}_2\\ &= \tfrac{1}{4}e^4\left[(1+\cos^2\theta)(1-4\lambda_1\lambda_2)(1-4\lambda_3\lambda_4)\right.\\ &\qquad\left.+2\cos\theta(2\lambda_1-2\lambda_2)(2\lambda_3-2\lambda_4)\right]\,.\end{aligned} \tag{1.62}$$

Keep in mind that the λ_i can take on the values $\pm\frac{1}{2}$.

Eq. (1.62) is easy to understand. First, note that if $\lambda_1 = \lambda_2$ and/or if $\lambda_3 = \lambda_4$, then $\mathcal{M}_{\lambda_3\lambda_4;\lambda_1\lambda_2} = 0$. This is a consequence of angular momentum conservation, which is illustrated in the diagram below.

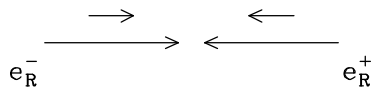

The long arrows indicate the direction of three-momentum (in the CM-frame), while the short arrows indicate the direction of helicity (which is either parallel or antiparallel to the momentum depending on whether λ is positive or negative, respectively). For example, in the above configuration, if we choose the positive z-axis to lie along the electron direction, then the total $J_z = 0$, which is in conflict with $J_z = \pm 1$, which is required since helicity is conserved in QED when fermion masses can be neglected. By the same reasoning, the allowed configurations would include the possibilities shown below.

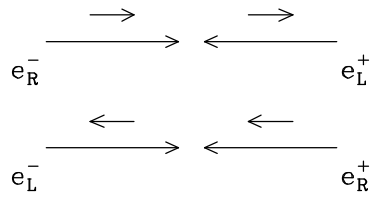

For these configurations, the squared amplitude takes the following form

$$|\mathcal{M}_{\lambda_3-\lambda_3;\lambda_1,-\lambda_1}|^2 = e^4\,[1 + (2\lambda_1)(2\lambda_3)\cos\theta]^2 \ . \tag{1.63}$$

This amplitude vanishes at $\cos\theta = -1$ [$\cos\theta = 1$] if $\lambda_1 = \lambda_3$ [$\lambda_1 = -\lambda_3$]. This result can also be seen to be a consequence of angular momentum conservation; that is, the amplitude vanishes when $J_z = \pm 1$ in the initial state but $J_z = \mp 1$ in the final state.

1.5 The spinor helicity method

For scattering processes with more than two particles in the final state, the spin projection operator methods quickly become unwieldy. In this section, I shall give a brief introduction to the spinor helicity method [15-19] which is a powerful technique for computing helicity amplitudes for multiparticle processes involving massless spin-1/2 and spin-1 particles. Although generally applied to tree-level processes, more general techniques have been developed recently which are applicable to one-loop (and multiloop) diagrams [20]. The spinor helicity techniques are ideal for QCD where light quark masses can almost always be neglected. Generalizations of these methods that incorporate massive spin-1/2 and spin-1 particles exist,

although the complications that are introduced are substantial. The reader can study the papers of Ref. [16] to learn about these techniques for massive particles; in this section, I shall restrict my discussion to the massless case.

We begin by recalling that massless helicity spinors are eigenstates of γ_5 [see Eq. (1.52)]. Combining this result with Eq. (1.43) yields

$$v(p,\lambda) = -2\lambda\gamma_5 u(p,-\lambda) = u(p,-\lambda)\,, \tag{1.64}$$

and we see that particle and antiparticle massless spinors of opposite helicity are the same.* With this observation, it is clear that the algebra of massless spinors should simplify significantly. Here, I shall describe the spinor-helicity technique of Xu, Zhang and Chang [17] (denoted henceforth by XZC), which is a modification of techniques developed by the CALKUL collaboration [18]. Following XZC, I shall introduce a very useful notation for massless spinors

$$\begin{aligned} |p\pm\rangle &\equiv u(p,\pm\tfrac{1}{2}) = v(p,\mp\tfrac{1}{2})\,, \\ \langle p\pm| &\equiv \bar{u}(p,\pm\tfrac{1}{2}) = \bar{v}(p,\mp\tfrac{1}{2})\,. \end{aligned} \tag{1.65}$$

These massless spinors have the following properties

1. Massless Dirac equation

$$\not{p}\,|p\pm\rangle = \langle p\pm|\,\not{p} = 0\,. \tag{1.66}$$

2. Chirality conditions

$$\begin{aligned} (1\pm\gamma_5)\,|p\mp\rangle &= 0\,, \\ \langle p\pm|\,(1\pm\gamma_5) &= 0\,. \end{aligned} \tag{1.67}$$

3. Other massless spinor properties

$$\langle p\pm|\,\gamma^\mu\,|p\pm\rangle = 2p^\mu\,, \tag{1.68}$$

$$|p\pm\rangle\,\langle p\pm| = \tfrac{1}{2}(1\pm\gamma_5)\not{p}\,, \tag{1.69}$$

from which the following "completeness"-type relation follows

$$|p+\rangle\,\langle p+| + |p-\rangle\,\langle p-| = \not{p}\,. \tag{1.70}$$

$\star$ Eq. (1.64) motivates the choice of overall sign in the definition of the charge conjugation matrix C [Eq. (1.33)].

4. Vanishing spinor-products

$$\begin{aligned} \langle p+|q+\rangle = \langle p-|q-\rangle = 0 \qquad & \text{for any } p, q\,, \\ \langle p+|p-\rangle = 0\,. & \end{aligned} \tag{1.71}$$

Eq. (1.71) shows that only a few of the possible spinor-products are non-zero. It is therefore convenient to introduce the following notation for spinor-products:

$$\begin{aligned} \langle pq\rangle \equiv \langle p-|q+\rangle = -\langle qp\rangle\,, \\ [\,pq\,] \equiv \langle p+|q-\rangle = -[\,qp\,]\,. \end{aligned} \tag{1.72}$$

These two quantities are related by

$$\langle pq\rangle^* = -[\,pq\,]\,, \tag{1.73}$$

where all spinors are assumed to have positive energy.† It follows that

$$|\langle pq\rangle|^2 = |[\,pq\,]|^2 = 2p\cdot q\,, \tag{1.74}$$

which indicates that the spinor-products are roughly the square roots of dot products. Other useful relations can be found in Appendix A of Ref. [19].

Next, XZC introduced a convenient expression for the massless spin-1 polarization vector. Let k be the four-momentum of the massless spin-1 particle. Let p be a "reference" four-vector (usually taken to be another four-momentum vector in the scattering process of interest). The XZC spin-1 polarization vectors are given by

$$\epsilon^\mu(k,\pm 1) = \pm\frac{1}{\sqrt{2}}\,\frac{\langle p\mp|\,\gamma^\mu\,|k\mp\rangle}{\langle p\mp|k\pm\rangle}\,. \tag{1.75}$$

The only restriction on p is that it not be parallel to k. One can immediately check that $\epsilon^\mu(k,\lambda)$ [where $\lambda = \pm 1$] so defined satisfies Eq. (1.56), which means that it is a valid polarization four-vector. Note that

$$\epsilon^*(k,\lambda) = \epsilon(k,-\lambda)\,, \tag{1.76}$$

which implies that the choice of phase in the above definition of $\epsilon(k,\pm 1)$ differs from that of Eq. (1.54).

† In Ref. [19], calculations are performed assuming that all particle momenta are outgoing. As a result, energy-momentum conservation implies that some spinors have negative energy, in which case Eq. (1.73) is replaced by $\langle pq\rangle^* = -\mathrm{sign}(p\cdot q)[\,pq\,]$.

To appreciate the significance of the reference four-vector p, one can check that if p is changed then ϵ^μ is shifted by a factor proportional to k^μ. This does not affect Eq. (1.56) since $k^2 = 0$ for massless spin-1 particles. Moreover, this shift does not affect the final result for any observable (in particular the sum of amplitudes of any gauge invariant set of Feynman diagrams remains unchanged). Thus, the presence of the arbitrary four-vector p just reflects the gauge invariance of the theory of massless spin-1 particles.

The following additional properties of $\epsilon^\mu(k,\lambda)$ defined in Eq. (1.75) are noteworthy:

$$p \cdot \epsilon(k,\lambda) = 0\,, \tag{1.77}$$

$$\sum_\lambda \epsilon_\mu(k,\lambda)\epsilon^*_\nu(k,\lambda) = -g_{\mu\nu} + \frac{p_\mu k_\nu + p_\nu k_\mu}{p\cdot k}\,, \tag{1.78}$$

$$\not\epsilon(k) = \frac{\pm\sqrt{2}}{\langle p \mp | k \pm\rangle}\left(|k\mp\rangle\langle p\mp| + |p\pm\rangle\langle k\pm|\right)\,. \tag{1.79}$$

We are now ready to apply the XZC technology to a real calculation. Consider the process:

$$\gamma(k_1,\lambda_1) + \gamma(k_2,\lambda_2) \to q(p_1,\lambda_3) + \overline{q}(p_2,\lambda_4)\,, \tag{1.80}$$

which is relevant as a background to Higgs production in $\gamma\gamma$ collisions (to be discussed in Lecture 3). In the following computation, I shall neglect the quark masses. Two tree-level diagrams contribute to this process

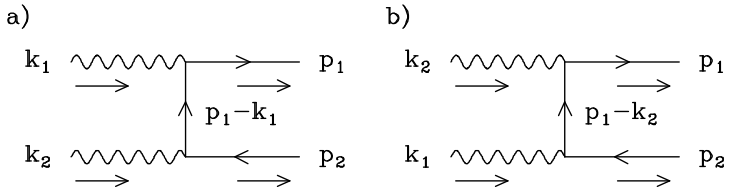

where the separated arrows above indicate the flow of four-momenta. The corresponding amplitudes are

$$\begin{aligned}
\mathcal{M}_a &= -e^2 e_q^2 \bar{u}(p_1)\not\epsilon_1 \frac{\not p_1 - \not k_1}{(p_1-k_1)^2}\not\epsilon_2 v(p_2)\,,\\
\mathcal{M}_b &= -e^2 e_q^2 \bar{u}(p_1)\not\epsilon_2 \frac{\not p_1 - \not k_2}{(p_1-k_2)^2}\not\epsilon_1 v(p_2)\,,
\end{aligned} \tag{1.81}$$

where e_q is the quark charge in units of e. It is easy to check that the helicity amplitudes with $\lambda_1 = \lambda_2$ and/or with $\lambda_3 = \lambda_4$ are zero. This leaves four non-zero

helicity amplitudes corresponding to

$$(\lambda_3,\lambda_4;\lambda_1,\lambda_2) = (\pm\tfrac{1}{2},\mp\tfrac{1}{2};+1,-1),\ (\pm\tfrac{1}{2},\mp\tfrac{1}{2};-1,+1)\,. \tag{1.82}$$

Consider first $\mathcal{M}(+\frac{1}{2},-\frac{1}{2};-1,+1)$. I shall use the following notation for the photon polarization four-vectors

$$\begin{aligned} \not\epsilon_1 &\equiv \not\epsilon(k_1,+1) = \not\epsilon(k_1,p_2,+1)\,,\\ \not\epsilon_2 &\equiv \not\epsilon(k_2,-1) = \not\epsilon(k_2,p_1,-1)\,, \end{aligned} \tag{1.83}$$

where the reference momentum chosen in each case is indicated. Note that one can choose different reference momentum for different photons. The decision on which reference momenta to choose is somewhat of an art; experience will teach you which choices lead to the most simplification in a given computation. Writing the amplitudes given in Eq. (1.81) using the XZC bracket notation, and using the fact that all external particles are massless,

$$\begin{aligned} \mathcal{M}_a(+\tfrac{1}{2},-\tfrac{1}{2};-1,+1) &= \frac{e^2e_q^2}{2p_1\cdot k_1}\langle p_1+|\not\epsilon_1(\not p_1-\not k_1)\not\epsilon_2|p_2+\rangle\,,\\ \mathcal{M}_b(+\tfrac{1}{2},-\tfrac{1}{2};-1,+1) &= \frac{e^2e_q^2}{2p_1\cdot k_2}\langle p_1+|\not\epsilon_2(\not p_1-\not k_2)\not\epsilon_1|p_2+\rangle\,. \end{aligned} \tag{1.84}$$

Next, we employ Eq. (1.79) to write

$$\begin{aligned} \not\epsilon_1 &= \frac{\sqrt{2}}{\langle p_2-|k_1+\rangle}\left(|k_1-\rangle\langle p_2-| + |p_2+\rangle\langle k_1+|\right)\,,\\ \not\epsilon_2 &= \frac{-\sqrt{2}}{\langle p_1+|k_2-\rangle}\left(|k_2+\rangle\langle p_1+| + |p_1-\rangle\langle k_2-|\right)\,. \end{aligned} \tag{1.85}$$

Using Eq. (1.71), it follows that $\mathcal{M}_b = 0$ since $\langle p_1+|k_2+\rangle = \langle p_1+|p_1-\rangle = 0$. Thus,

$$\begin{aligned} \mathcal{M}(+\tfrac{1}{2},-\tfrac{1}{2};-1,+1) &= \frac{-e^2e_q^2\langle p_1+|k_1-\rangle\langle p_2-|\not p_1-\not k_1|p_1-\rangle\langle k_2-|p_2+\rangle}{p_1\cdot k_1\langle p_2-|k_1+\rangle\langle p_1+|k_2-\rangle}\\ &= \frac{e^2e_q^2\langle p_1+|k_1-\rangle\langle p_2-|k_1+\rangle\langle k_1+|p_1-\rangle\langle k_2-|p_2+\rangle}{p_1\cdot k_1\langle p_2-|k_1+\rangle\langle p_1+|k_2-\rangle}\,, \end{aligned} \tag{1.86}$$

where we have used $\not p_1\,|p_1-\rangle = 0$ [Eq. (1.66)] and $\not k = |k_1+\rangle\langle k_1+| + |k_1-\rangle\langle k_1-|$

[Eq. (1.70)]. Finally, we convert to the spinor-product notation [Eq. (1.72)]. Writing $2p_1 \cdot k_1 = |[\, p_1 k_1 \,]|^2$, it follows that

$$\begin{aligned} \mathcal{M}\left(+\tfrac{1}{2},-\tfrac{1}{2};-1,+1\right) &= -2e^2e_q^2\,\frac{[\, k_1p_1\,]\langle k_2p_2\rangle}{[\, k_1p_1\,]^*[\, p_1k_2\,]}\,, \\ &= -2e^2e_q^2\,e^{i\alpha}\,\frac{\langle k_2p_2\rangle}{[\, p_1k_2\,]}\,, \end{aligned} \tag{1.87}$$

where I have noted that $e^{i\alpha} \equiv [\, k_1p_1\,]/[\, k_1p_1\,]^*$ is a pure phase. Thus, we arrive at the final and very simple result

$$|\mathcal{M}\left(+\tfrac{1}{2},-\tfrac{1}{2};-1,+1\right)|^2 = 4e^4e_q^4\,\frac{k_2\cdot p_2}{k_2\cdot p_1}\,. \tag{1.88}$$

By parity and identical particles [Eqs. (1.29) and (1.31)], the remaining non-zero helicity amplitudes immediately follow. We collect the complete set of non-zero helicity amplitudes below

$$\begin{aligned} |\mathcal{M}\left(+\tfrac{1}{2},-\tfrac{1}{2};-1,+1\right)|^2 &= |\mathcal{M}\left(-\tfrac{1}{2},+\tfrac{1}{2};+1,-1\right)|^2 = 4e^4e_q^4\,\frac{k_2\cdot p_2}{k_2\cdot p_1}\,, \\ |\mathcal{M}\left(+\tfrac{1}{2},-\tfrac{1}{2};+1,-1\right)|^2 &= |\mathcal{M}\left(-\tfrac{1}{2},+\tfrac{1}{2};-1,+1\right)|^2 = 4e^4e_q^4\,\frac{k_1\cdot p_2}{k_1\cdot p_1}\,. \end{aligned} \tag{1.89}$$

Finally, it is conventional to introduce the kinematic invariants

$$\begin{aligned} t &= -2p_1\cdot k_1 = -2p_2\cdot k_2\,, \\ u &= -2p_1\cdot k_2 = -2p_2\cdot k_1\,. \end{aligned} \tag{1.90}$$

From Eq. (1.89), we immediately obtain the squared amplitude for $\gamma\gamma \to q\overline{q}$ averaged over initial spins and summed over final spins and colors ($N_c = 3$)

$$|\mathcal{M}|^2_{ave} = 2N_ce^4e_q^4\left(\frac{t}{u}+\frac{u}{t}\right)\,. \tag{1.91}$$

1.6 The Bouchiat-Michel formulae

Instead of trying to generalize the methods of the previous section to the case of massive fermions, I shall introduce yet another method for evaluating helicity amplitudes. This method is well suited for scattering processes in which the initial state consists of two equal mass fermions. First, one introduces three four-vectors

s^a_μ, $a = 1,2,3$ such that the s^a and p/m form an orthonormal set of four-vectors. That is,

$$\begin{aligned} p \cdot s^a &= 0\,, \\ s^a \cdot s^b &= -\delta^{ab}\,, \\ s^a_\mu\, s^a_\nu &= -g_{\mu\nu} + \frac{p_\mu p_\nu}{m^2}\,, \end{aligned} \tag{1.92}$$

where repeated indices (such as the index a above) are implicitly summed over unless otherwise stated. A convenient choice for the s^a is

$$\begin{aligned} s^{1\mu} &= (0\,;\, \cos\theta\cos\phi,\, \cos\theta\sin\phi,\, -\sin\theta)\,, \\ s^{2\mu} &= (0\,;\, -\sin\phi,\, \cos\phi,\, 0)\,, \end{aligned} \tag{1.93}$$

and

$$s^{3\mu} = \left(\frac{|\vec{\boldsymbol{p}}\,|}{m}\,;\, \frac{E}{m}\,\hat{\boldsymbol{p}}\right)\,, \tag{1.94}$$

in a coordinate system where $\hat{\boldsymbol{p}} = (\sin\theta\cos\phi,\, \sin\theta\sin\phi,\, \cos\theta)$. Note that s^3 is identical to the positive helicity spin vector; that is, $2\lambda s^3 = s$ [see Eq. (1.48)]. From these explicit forms, it is easy to derive a number of useful properties[⋆]

$$\begin{aligned} &\epsilon^{\mu\nu\lambda\sigma} p_\mu s^1_\nu s^2_\lambda s^3_\sigma = m\,, \\ &s^a_\mu s^b_\nu - s^a_\nu s^b_\mu = \frac{\epsilon^{abc}\epsilon_{\mu\nu\lambda\sigma} p^\lambda s^{c\sigma}}{m}\,, \\ &\not{s}^a \not{s}^b = -\delta^{ab} + \frac{i\epsilon^{abc}\gamma_5 \not{p}\, \not{s}^c}{m}\,, \end{aligned} \tag{1.95}$$

where $\epsilon_{0123} = -\epsilon^{0123} \equiv 1$. One can check that the helicity spinors satisfy [21]

$$\begin{aligned} \gamma_5 \not{s}^a u(p,\lambda') &= \tau^a_{\lambda\lambda'}\, u(p,\lambda)\,, \\ \gamma_5 \not{s}^a v(p,\lambda') &= \tau^a_{\lambda'\lambda}\, v(p,\lambda)\,, \end{aligned} \tag{1.96}$$

where the τ^a are the Pauli matrices,[†] and there is an implicit sum over the repeated label $\lambda = \pm\frac{1}{2}$. In Eq. (1.96), the second formula may be obtained from the first one by using Eq. (1.43) and noting that $4\lambda\lambda'\tau^a_{-\lambda,-\lambda'} = -\tau^a_{\lambda'\lambda}$. Consequently, the

⋆ I do not distinguish between upper and lower Latin indices. Thus, ϵ^{abc} is the usual Levi-Cevita tensor in three space dimensions with $\epsilon^{123} = 1$.

† The first (second) row and column of the τ-matrices correspond to $\lambda = 1/2$ $(-1/2)$. Thus, for example, $\tau^3_{\lambda\lambda'} = 2\lambda\delta_{\lambda\lambda'}$ (no sum over λ).

helicities λ and λ' that label τ^a appear in the second formula of Eq. (1.96) in reversed order. Finally, note that for $a = 3$, Eq. (1.96) reduces to a result previously obtained [see Eq. (1.50)].

Using Eq. (1.96), one can derive the following formulae first introduced by Bouchiat and Michel [22] for spin-1/2 particles of mass m

$$\begin{aligned} u(p,\lambda')\bar{u}(p,\lambda) &= \tfrac{1}{2}\left[\delta_{\lambda\lambda'} + \gamma_5 \not{s}^a \tau^a_{\lambda\lambda'}\right](\not{p} + m)\,, \\ v(p,\lambda')\bar{v}(p,\lambda) &= \tfrac{1}{2}\left[\delta_{\lambda'\lambda} + \gamma_5 \not{s}^a \tau^a_{\lambda'\lambda}\right](\not{p} - m)\,. \end{aligned} \tag{1.97}$$

Note that the Bouchiat-Michel formulae are generalizations of the helicity projection operators. The former [Eq. (1.97)] reduces to the latter [Eq. (1.51)] when $\lambda = \lambda'$ after using $2\lambda s^3 = s$. Although the above results apply to the $m \neq 0$ case, the $m = 0$ limit of the Bouchiat-Michel formulae can be easily obtained. Noting that $s^3 = p/m + \mathcal{O}(m/E)$ in the high energy limit, and using the mass-shell condition ($p^2 = m^2$), it follows that the $m \to 0$ limit is smooth. The end result is

$$\begin{aligned} u(p,\lambda')\bar{u}(p,\lambda) &= \tfrac{1}{2}(1 + 2\lambda\gamma_5)\not{p}\,\delta_{\lambda\lambda'} + \tfrac{1}{2}\gamma_5[\not{s}^1\tau^1_{\lambda\lambda'} + \not{s}^2\tau^2_{\lambda\lambda'}]\not{p}\,, \\ v(p,\lambda')\bar{v}(p,\lambda) &= \tfrac{1}{2}(1 - 2\lambda\gamma_5)\not{p}\,\delta_{\lambda'\lambda} + \tfrac{1}{2}\gamma_5[\not{s}^1\tau^1_{\lambda'\lambda} + \not{s}^2\tau^2_{\lambda'\lambda}]\not{p}\,. \end{aligned} \tag{1.98}$$

As expected, when $\lambda = \lambda'$, we recover the helicity projection operators for massless spin-1/2 particles [Eq. (1.53)].

I shall now illustrate how one can use the Bouchiat-Michel formulae to evaluate helicity amplitudes involving two equal-mass spin-1/2 particles. A typical amplitude involving a fermion-antifermion pair takes the form

$$\mathcal{M}_{\lambda_1\lambda_2} = \bar{u}(p_1,\lambda_1)\,\Gamma\, v(p_2,\lambda_2)\,, \tag{1.99}$$

where Γ can contain Dirac matrices, spin-1 polarization vectors, *etc.* In the CM-frame, $\vec{\boldsymbol{p}}_{\mathbf{1}} = -\vec{\boldsymbol{p}}_{\mathbf{2}} = \vec{\boldsymbol{p}}$. Using the notation $-p \equiv (E\,;\,-\vec{\boldsymbol{p}})$,

$$\begin{aligned} \mathcal{M}_{\lambda_1\lambda_2} &= \bar{u}(p,\lambda_1)\,\Gamma\, v(-p,\lambda_2) \\ &= -2\lambda_2\,\bar{u}(p,\lambda_1)\,\Gamma\,\gamma_5\, u(-p,-\lambda_2) \\ &= -2\lambda_2\,\bar{u}(p,\lambda_1)\,\Gamma\,\gamma_5\gamma^0 u(p,\lambda_2) \\ &= -\lambda_2\,\mathrm{Tr}\left\{\Gamma\,\gamma_5\gamma^0[\delta_{\lambda_1\lambda_2} + \gamma_5\tau^a_{\lambda_1\lambda_2}\not{s}^a](\not{p} + m)\right\}\,, \end{aligned} \tag{1.100}$$

where Eqs. (1.43) and (1.44) have been used (with the Jacob-Wick second particle convention, *i.e.*, $\xi_\lambda = 1$) to manipulate the amplitude into a form where the

Bouchiat-Michel formulae [Eq. (1.97)] can be applied. By performing the trace, one completes the direct evaluation of the helicity amplitude. As a trivial example, set $\Gamma = 1$ in Eq. (1.100). The result is

$$\begin{aligned}\bar{u}(p,\lambda_1)v(-p,\lambda_2) &= \lambda_2 m\tau^a_{\lambda_1\lambda_2}\,\mathrm{Tr}\,(\gamma^0 \not{\hat{p}}\,\gamma^a) \\ &= 4\lambda_2\,|\vec{\boldsymbol{p}}\,|\tau^3_{\lambda_1\lambda_2} \\ &= 2|\vec{\boldsymbol{p}}\,|\delta_{\lambda_1\lambda_2}\,.\end{aligned} \tag{1.101}$$

Alternative and related methods for directly evaluating expressions such as Eq. (1.99) can be found in Ref. [23].

1.7 Density matrix techniques in unstable particle production and decay

A typical process in high energy physics starts with a two-body collision of particles of definite spin. If the beams are polarized, then the initial particles are in definite helicity states. If the beams are unpolarized, then one must average over initial spins. Particles that are produced in the collision are often unstable. A complete quantum mechanical description of the scattering process including the decay of all unstable intermediate states must account for possible interference effects between the production and decay processes. In this section, I shall always work in the narrow width approximation; *i.e.*, the width of the unstable particle is small compared to its mass. This approximation is very good in many cases of interest. In practical terms, it implies that the Breit-Wigner resonance shape can be approximated by a δ-function in cross-section calculations. Explicitly,

$$\frac{1}{(s-m^2)^2+m^2\Gamma^2} \approx \frac{\pi}{m\Gamma}\delta(s-m^2)\,. \tag{1.102}$$

For the scattering process, $A+B\to C_1+C_2+\ldots$, if C_1 is spinless and decays via $C_1\to D_1+D_2+\ldots$, then in the narrow width approximation, the total cross section is [10]

$$\sigma_{\mathrm{T}} \approx \sigma(A+B\to C_1+C_2+\ldots)\,\mathrm{BR}(C_1\to D_1+D_2+\ldots)\,, \tag{1.103}$$

where the branching ratio is defined by

$$\mathrm{BR}(C_1\to D_1+D_2+\ldots) = \frac{\Gamma(C_1\to D_1+D_2+\ldots)}{\Gamma}\,, \tag{1.104}$$

and Γ is the total width of particle C_1. Thus, in the narrow width approximation, there is no correlation between the production and decay of a spinless particle. On

the other hand, if the unstable particle has non-zero spin, a proper computation should take into account spin correlations between the production and decay. This is most easily done by introducing the concept of density matrices. Good textbook introductions to density matrices in particle physics can be found in Refs. [9] and [10]. In addition, see Ref. [24] for a comprehensive treatment of polarization phenomena using helicity amplitude techniques. In this section, I shall illustrate the use of density matrices in two simple examples. Further details on the material in this section can be found in Refs. [25–29].

As a first example, consider the process

$$\begin{aligned} A + B \to C_1 + C_2 + \ldots \\ \qquad\quad \lfloor\!\!\rightarrow D_1 + D_2 + \ldots \end{aligned} \tag{1.105}$$

where C_1 is a spin-1/2 fermion. Let $\mathcal{M}_\lambda$ [$\mathcal{N}_\lambda$] be the matrix element for production [decay] of C_1 with helicity λ. We then define the production and decay density matrix elements, respectively, as follows

$$\begin{aligned} \rho^P_{\lambda\lambda'} &= \sum \mathcal{M}_\lambda \mathcal{M}^*_{\lambda'} \,, \\ \rho^D_{\lambda\lambda'} &= \sum \mathcal{N}_\lambda \mathcal{N}^*_{\lambda'} \,, \end{aligned} \tag{1.106}$$

where the summation sign indicates that one should average over initial spins and sum over the final spins of all particles excluding C_1. (More complicated density matrices can be defined if other initial or final state particles are also prepared or observed in definite helicity states.) These matrices are sometimes referred to as helicity density matrices to emphasize the fact that they are defined with respect to states of definite helicity (other choices are possible). Note that the diagonal elements $\rho_{\lambda\lambda}$ correspond to the usual squared matrix element for the production or decay of the particle of helicity λ. The total squared matrix element for the process $A + B \to (D_1 + D_2 + \ldots) + C_2 + \ldots$ is then given by

$$\sum |\mathcal{M}_{\rm total}|^2 = {\rm Tr}(\rho^P \rho^D) \equiv \rho^P_{\lambda\lambda'} \rho^D_{\lambda'\lambda} \,. \tag{1.107}$$

The meaning of the summation sign here is similar to its use above. The nontrivial spin correlations between production and decay are evident in the above formulae, since the total squared matrix element contains terms involving products of the off-diagonal density matrix elements.

Since C_1 is assumed to be a spin-1/2 particle, the most general forms for ρ^P and ρ^D can be deduced from the Bouchiat-Michel formulae. In particular, Eq. (1.97)

implies that the spin-1/2 density matrices must be linear in $\delta_{\lambda\lambda'}$ and in $\tau^a_{\lambda\lambda'}s^a_\mu$. Thus, we may write*

$$\begin{aligned}\rho^P_{\lambda\lambda'} &= A\delta_{\lambda\lambda'} + \tau^a_{\lambda\lambda'}s^a_\mu B^\mu\,,\\ \rho^D_{\lambda\lambda'} &= C\delta_{\lambda\lambda'} + \tau^b_{\lambda\lambda'}s^b_\nu D^\nu\,,\end{aligned} \tag{1.108}$$

where A, B, C, and D are functions of the kinematic invariants of the problem. These results should be compared with the more traditional expression

$$\rho^D = C(I + \vec{\boldsymbol{P}}\cdot\vec{\boldsymbol{\tau}})\,, \tag{1.109}$$

where I is the 2×2 identity matrix and $\vec{\boldsymbol{P}}$ is the polarization vector of the decaying spin-1/2 particle. Comparing the two equations above yields $P^b = s^b_\nu D^\nu/C$, which can be inverted [using the second equation of Eq. (1.92)] to give: $D^\nu = -CP^a s^a_\nu$.

In a parity-conserving process, there are restrictions of the form of the density matrices. These can be derived from the parity constraints on helicity amplitudes [see Eq. (1.29)]. The end result is that the density matrix elements must satisfy [10]

$$\rho_{-\lambda,-\lambda'} = (-1)^{\lambda-\lambda'}\rho_{\lambda\lambda'}\,. \tag{1.110}$$

For the 2×2 spin-1/2 density matrix, this constraint implies that the two off-diagonal elements are opposite in sign. Using Eq. (1.109), it follows that for parity conserving interactions $P_x = P_z = 0$ while P_y may be non-zero (*i.e.*, the polarization vector is normal to the production plane), which is a well known result. Equivalently, in the notation of Eq. (1.108), B_μ and D_μ must be proportional to s^2_μ.

Using the general forms for the density matrix elements shown in Eq. (1.108), it is easy to compute the total amplitude squared [Eq. (1.107)] for the process shown in Eq. (1.105). Using $\mathrm{Tr}\,\tau^a = 0$ and $\mathrm{Tr}\,\tau^a\tau^b = 2\delta^{ab}$, we obtain [using Eq. (1.92)]

$$\mathrm{Tr}\,(\rho^P\rho^D) = 2\left[AC + B^\mu\left(-g_{\mu\nu} + \frac{p_\mu p_\nu}{m^2}\right)D^\nu\right]\,. \tag{1.111}$$

The term in Eq. (1.111) involving B and D describes quantum mechanical correlations between the production and decay processes.

⋆ Note that in the definitions presented above, Tr ρ is equal to the helicity-averaged squared amplitude. In the literature, one often finds that density matrices are normalized such that Tr $\rho = 1$, although I will not follow this convention here.

As a second example, consider the process

$$\begin{array}{l} A + B \to C_1 + C_2 \\ \qquad\quad \big\lfloor \quad \big\lfloor \to F_1 + F_2 + \ldots \\ \qquad\quad \big\lfloor \to D_1 + D_2 + \ldots \end{array} \tag{1.112}$$

where C_1 and C_2 are both spin-1/2 particles. Let $\mathcal{M}_{\lambda\mu}$ be the matrix element for the production of C_1 and C_2 with helicities λ and μ, respectively. Let $\mathcal{N}^{(1)}_\lambda$ $[\mathcal{N}^{(2)}_\lambda]$ be the matrix element for the decay of C_1 $[C_2]$ with helicity λ $[\mu]$. We then define the production and decay density matrix elements, respectively, as follows:

$$\begin{aligned} \rho^P_{\lambda\lambda';\mu\mu'} &= \sum \mathcal{M}_{\lambda\mu}\mathcal{M}^*_{\lambda'\mu'} \,, \\ \rho^{D_1}_{\lambda\lambda'} &= \sum \mathcal{N}^{(1)}_\lambda \mathcal{N}^{(1)*}_{\lambda'} \,, \\ \rho^{D_2}_{\mu\mu'} &= \sum \mathcal{N}^{(2)}_\mu \mathcal{N}^{(2)*}_{\mu'} \,, \end{aligned} \tag{1.113}$$

where the summation sign indicates that one should average over initial spins and sum over final spins of all particles excluding C_1 and C_2. Then, the total squared matrix element for the process $A + B \to (D_1 + D_2 + \ldots) + (F_1 + F_2 + \ldots)$ is given by

$$\sum |\mathcal{M}_{\text{total}}|^2 = \rho^P_{\lambda\lambda';\mu\mu'}\rho^{D_1}_{\lambda'\lambda}\rho^{D_2}_{\mu'\mu} \,. \tag{1.114}$$

Following the same steps as above, we use the Bouchiat-Michel formulae to write down the general forms for the density matrix elements:

$$\begin{aligned} \rho^P_{\lambda\lambda';\mu\mu'} =& A\delta_{\lambda\lambda'}\delta_{\mu\mu'} + \delta_{\mu\mu'}\tau^a_{\lambda\lambda'}s^a_{1\alpha}B^\alpha + \delta_{\lambda\lambda'}\tau^b_{\mu\mu'}s^b_{2\beta}C^\beta + \tau^a_{\lambda\lambda'}\tau^b_{\mu\mu'}s^a_{1\alpha}s^b_{2\beta}D^{\alpha\beta} \,, \\ \rho^{D_1}_{\lambda\lambda'} =& E\delta_{\lambda\lambda'} + \tau^c_{\lambda\lambda'}s^c_{1\rho}F^\rho \,, \\ \rho^{D_2}_{\mu\mu'} =& G\delta_{\mu\mu'} + \tau^d_{\mu\mu'}s^d_{2\sigma}H^\sigma \,. \end{aligned} \tag{1.115}$$

Restrictions in the case of parity conservation can be obtained as before. If parity is conserved in the production process, then B and C are both proportional to s^2 (note that there is no restriction on D). If parity is conserved in the decay process, then F and H are each proportional to s^2.

The total squared amplitude for the process shown in Eq. (1.112) is

$$\rho^P_{\lambda\lambda';\mu\mu'}\rho^{D_1}_{\lambda'\lambda}\rho^{D_2}_{\mu'\mu} = 4\left[AEG + B^\alpha\left(-g_{\alpha\rho} + \frac{p_{1\alpha}p_{1\rho}}{m_1^2}\right)F^\rho G\right.$$
$$\left. + C^\beta\left(-g_{\beta\sigma} + \frac{p_{2\beta}p_{2\sigma}}{m_2^2}\right)H^\sigma E + F^\rho\left(-g_{\rho\alpha} + \frac{p_{1\rho}p_{1\alpha}}{m_1^2}\right)D^{\alpha\beta}\left(-g_{\beta\sigma} + \frac{p_{2\beta}p_{2\sigma}}{m_2^2}\right)H^\sigma\right]. \tag{1.116}$$

Note that all terms in Eq. (1.116) apart from the first term proportional to AEG reflect the non-trivial correlations between the production of C_1 and C_2 and their subsequent decays.

To gain a better understanding of these results, I shall give another derivation of Eq. (1.116) which is more physically motivated, following the analysis of Ref. [27]. For simplicity, I shall consider the case of $B = C = 0$. Let $\vec{\boldsymbol{w}}_1$ and $\vec{\boldsymbol{w}}_2$ be the polarizations of C_1 and C_2 in their rest frames. For example, if we define an orthonormal set of axes $\hat{\boldsymbol{e}}_i$ in three-space, then the components of $\vec{\boldsymbol{w}}_1$ are given by

$$w_{1i} = \frac{(\text{number of } C_1 \text{ with spin along } + \hat{\boldsymbol{e}}_i) - (\text{number of } C_1 \text{ with spin along } - \hat{\boldsymbol{e}}_i)}{(\text{number of } C_1 \text{ with spin along } + \hat{\boldsymbol{e}}_i) + (\text{number of } C_1 \text{ with spin along } - \hat{\boldsymbol{e}}_i)} \tag{1.117}$$

and so on. Now, compute the production cross-section for $A+B \to C_1(\vec{\boldsymbol{s}}_1)+C_2(\vec{\boldsymbol{s}}_2)$, *i.e.*, the probability distribution for producing C_1 with its spin in the direction of $\vec{\boldsymbol{s}}_1$ in its rest frame, and C_2 with its spin in the direction of $\vec{\boldsymbol{s}}_2$ in its rest frame. We take $\vec{\boldsymbol{s}}_1$ and $\vec{\boldsymbol{s}}_2$ to be unit vectors. Symbolically, we write

$$d\sigma(A + B \to C_1 + C_2) = C + D_{ij}s_{1i}s_{2j}\,, \tag{1.118}$$

where there is an implicit sum over $i, j = 1, 2, 3$.

Next, consider the problem of computing the decay distribution of C_1 (or C_2) of arbitrary polarization $\vec{\boldsymbol{w}}$. We allow for the possibility of a mixed state so that the norm of $\vec{\boldsymbol{w}}$ need not be unity. (In general, $|\vec{\boldsymbol{w}}| \leq 1$.) For example, the decay of an unpolarized state would correspond to $\vec{\boldsymbol{w}} = 0$. Now, the decay distributions for C_1 and C_2 (in their respective rest frames) are schematically given by

$$\begin{aligned} d\Gamma(C_1 \to D_1 + D_2 + \ldots) &= A_1 + B_1\,\vec{\boldsymbol{q}}_1 \cdot \vec{\boldsymbol{w}}_1\,, \\ d\Gamma(C_2 \to F_1 + F_2 + \ldots) &= A_2 + B_2\,\vec{\boldsymbol{q}}_2 \cdot \vec{\boldsymbol{w}}_2\,, \end{aligned} \tag{1.119}$$

where $\vec{\boldsymbol{q}}_1$ and $\vec{\boldsymbol{q}}_2$ are final state momenta of one of the decay products of C_1 and C_2 respectively. Using Eq. (1.118), The number of C_1 having spin along the direction $\hat{\boldsymbol{e}}_i$ with the polarization of C_2 in a certain direction $\vec{\boldsymbol{s}}_2$ is proportional to $C + D_{ij}s_{2j}$;

whereas the corresponding number of C_1 having spin along the direction $-\hat{\boldsymbol{e}}_{\boldsymbol{i}}$ is $C - D_{ij}s_{2j}$. Hence, using Eq. (1.117), one finds

$$w_{1i} = \frac{(C + D_{ij}s_{2j}) - (C - D_{ij}s_{2j})}{(C + D_{ij}s_{2j}) + (C - D_{ij}s_{2j})} = \frac{D_{ij}s_{2j}}{C} \,. \tag{1.120}$$

Inserting this result into the formula for $d\Gamma(C_1 \to D_1 + D_2 + \ldots)$ [see Eq. (1.119)], we symbolically have:

$$d\sigma \otimes d\Gamma(C_1 \to D_1 + D_2 + \ldots) \propto CA_1 + B_1(q_1)_i D_{ij} s_{2j} \,. \tag{1.121}$$

Similarly, we may compute w_{2j} (holding fixed the angular distribution of C_1). The result is:

$$w_{2j} = \frac{CA_1 + B_1(q_1)_i D_{ij} - [CA_1 - B_1(q_1)_i D_{ij}]}{CA_1 + B_1(q_1)_i D_{ij} + [CA_1 - B_1(q_1)_i D_{ij}]} = \frac{B_1(q_1)_i D_{ij}}{CA_1} \,. \tag{1.122}$$

Substituting this into the formula for $d\Gamma(C_2 \to F_1 + F_2 + \ldots)$ [see Eq. (1.119)], one ends up with the combined angular distribution of the decay products of C_1 and C_2 at fixed production angle

$$d\sigma \otimes d\Gamma(C_1 \to D_1 + D_2 + \ldots) \otimes d\Gamma(C_2 \to F_1 + F_2 + \ldots) \propto CA_1A_2 + B_1B_2(q_1)_i(q_2)_j D_{ij} \,. \tag{1.123}$$

In Eqs. (1.121) and (1.123), I have omitted the overall normalization. But, this factor is easily obtained by considering the case of $B_1 = B_2 = 0$. Then, the joint probability distribution is [normalized to our previous calculation; see Eq. (1.116)] equal to $4A_1A_2C$.

Finally, we need to convert the results of Eq. (1.123) into a covariant form. Recall that $\vec{\boldsymbol{q}}_{\mathbf{1}}$ is the momentum in the C_1 rest frame and $\vec{\boldsymbol{q}}_{\mathbf{2}}$ is the momentum in the C_2 rest frame. If one defines $(\vec{\boldsymbol{d}}_{\boldsymbol{j}})_i \equiv D_{ij}$, then it is easy to check that the covariant expression which reduces to $\vec{\boldsymbol{q}}_{\mathbf{1}} \cdot \vec{\boldsymbol{d}}_{\boldsymbol{j}}$ in the frame where $\vec{\boldsymbol{p}}_{\mathbf{1}} = 0$ is

$$-q_1 \cdot d_j + \frac{q_1 \cdot p_1 d_j \cdot p_1}{m_1^2} = q_1^\mu d_j^\nu \left(-g_{\mu\nu} + \frac{p_{1\mu}p_{1\nu}}{m_1^2} \right) \,, \tag{1.124}$$

since if $p_1 = (m_1\,;0)$, then $-q_1 \cdot d_j + (q_1)_0(p_1)_0 \equiv \vec{\boldsymbol{q}}_{\mathbf{1}} \cdot \vec{\boldsymbol{d}}_{\boldsymbol{j}}$ as desired. Thus, Eq. (1.123) becomes

$$d\sigma \otimes d\Gamma_1 \otimes d\Gamma_2 \propto CA_1A_2 + B_1B_2 q_1^\mu \left(-g_{\mu\nu} + \frac{p_{1\mu}p_{1nu}}{m_1^2} \right) D^{\nu\rho} \left(-g_{\rho\sigma} + \frac{p_{2\rho}p_{2\sigma}}{m_2^2} \right) q_2^\sigma \,, \tag{1.125}$$

which is precisely the expression obtained in Eq. (1.116) in the case of $B = C = 0$, with appropriate identification of the corresponding variables.

LECTURE 2:
Applications to Low-Energy Supersymmetry

2.1 Raison-d'être for new physics beyond the Standard Model

The search for the origin of electroweak symmetry breaking and new physics beyond the Standard Model provides the central focus for particle physics experiments envisioned at the next generation of colliders. With the recent demise of the SSC, the only hadron supercollider now on the drawing boards is the LHC which will be constructed at CERN. LHC is a proton-proton supercollider operating at a CM-energy of $\sqrt{s} \simeq 14$ TeV, with an instantaneous luminosity of 10^{33} cm^{-2} sec^{-1}, and an eventual capability to reach luminosities above 10^{34} cm^{-2} sec^{-1} [30]. Meanwhile, the e^+e^- physics community is vigorously engaged in the development of an e^+e^- linear collider with CM-energy of $\sqrt{s} = 500$ GeV and luminosity in excess of 10^{33} cm^{-2} sec^{-1}, with eventual upgrades to CM energies of 1 TeV (and perhaps beyond) and luminosities above 10^{34} cm^{-2} sec^{-1} [31]. There is an active international collaboration involved in the design of this collider, which has been recently dubbed the International Linear Collider (ILC). Its proponents envision a formal proposal for constructing the ILC to be ready later in this decade, with completion of construction sometime in the following decade.

There are three fundamental goals of the LHC and ILC. The first goal is to discover the Higgs boson [32] (assuming that it has not already been discovered at LEP-II). If the Standard Model Higgs boson (or the Higgs bosons of an extended elementary Higgs sector) is not realized in nature, then one expects to ascertain the dynamics responsible for electroweak symmetry breaking. If elementary Higgs scalars exist, then they are probably light (less than 200 GeV in mass) and weakly-coupled. An alternative picture is one in which the dynamics responsible for electroweak symmetry breaking involves strong forces. In such an approach, any Higgs-like scalar is almost certainly composite, heavy (with mass on the order of 1 TeV) and strongly coupled. Technicolor is the standard paradigm for such approaches [33].

The second goal of the future supercolliders is to elucidate the structure of the effective low-energy gauge group and associated matter multiplets. If the Standard Model is the correct description of physics at the electroweak scale, then the correct low-energy gauge group is SU(3)×SU(2)×U(1), associated with three generations of quarks, charged leptons and massless neutrinos. However, one cannot be certain at present that this is the whole story. It is still possible that physics at the 1 TeV scale contains:

1. New gauge bosons beyond the $W^\pm$ and Z (which would indicate that the Standard Model gauge group must be enlarged).

2. Massive neutrinos (very small masses for left-handed neutrinos and large masses of order 1 TeV for right-handed neutrinos).

3. New quark and lepton generations with the same quantum numbers as the known generations.[⋆]

4. Mirror fermions, whose left and right handed couplings are opposite relative to those of the Standard Model fermions [34].

5. Fermions with exotic quantum numbers (*e.g.*, new vector-like D-quark and E-lepton which could arise in an E_6 model of grand unification) [35].

The discovery of any one of these particles would dramatically alter theoretical attempts to extend our understanding of physics beyond the 1 TeV scale.

The third goal of the future supercolliders is to search for new physics beyond the Standard Model associated with the dynamics of electroweak symmetry breaking. Despite the great success of the Standard Model of particle physics, most theorists strongly believe that the successes of the Standard Model will not persist to higher energy scales. This belief arises from attempts to embed the Standard Model in a more fundamental theory. We know that the Standard Model cannot be the ultimate theory, valid to arbitrarily high energy scales. Even in the absence of grand unification of strong and electroweak forces at a very high energy scale [36], it is clear that the Standard Model must be modified to incorporate the effects of gravity at the Planck scale [$M_{\rm PL} = (c\hbar/G_N)^{1/2} \simeq 10^{19}$ GeV].[†] In this context, it is a mystery why the ratio $m_W/M_{\rm PL} \simeq 10^{-17}$ is so small. This is called the hierarchy problem [37,38]. Moreover, in the Standard Model, the scale of the electroweak interactions derives from an elementary scalar field which acquires a

---

⋆ Precision electroweak measurements at LEP do place some constraints. Since the Z width implies the existence of exactly three light neutrinos, any fourth generation neutrino must have mass greater than $m_Z/2$. Second, precision measurement of the ρ-parameter (where $\rho = m_W^2/m_Z^2 \cos^2\theta_W = 1$ to better than 1%) places strong constraints on the splittings between masses of any new fourth generation weak doublet states.

† The Planck scale arises as follows. The gravitational potential energy of a particle of mass M, $G_N M^2/r$ (where G_N is Newton's gravitational constant), evaluated at a Compton wavelength, $r = \hbar/Mc$, is of order the rest mass, Mc^2, when

$$G_N M^2 \left(\frac{Mc}{\hbar}\right) \sim Mc^2 \,,$$

which implies that $M^2 \sim c\hbar/G_N$. When this happens, the gravitational energy is large enough to induce pair production, which means that quantum gravitational effects can no longer be neglected. Thus, the Planck scale, $M_{\rm PL} = (c\hbar/G_N)^{1/2}$, represents the energy scale at which gravity and all other forces of elementary particles must be incorporated into the same theory.

vacuum expectation value of $v = 2m_W/g = 246$ GeV. However, if one couples a theory of scalar particles to new physics at some arbitrarily high scale Λ, radiative corrections to the scalar squared-mass are of $\mathcal{O}(\Lambda^2)$, due to the quadratic divergence in the scalar self-energy (which indicates quadratic sensitivity to the largest energy scale in the theory). Thus, the "natural" mass for any scalar particle is Λ (which is presumably equal to $M_{\rm PL}$). Of course, in order to have a successful electroweak theory, the Higgs mass must be of order the electroweak scale. The fact that the Higgs mass cannot be equal to its natural value of $M_{\rm PL}$ is called the "naturalness" problem [4].

Theorists have been hard at work for more than a decade in an attempt to circumvent the problems raised above. The proposed solutions involve removing the quadratic divergences from the theory that are the root cause of the naturalness problem. Two classes of solutions have been proposed. In one class, the elementary scalars are removed altogether. One then must add new fundamental fermions and new fundamental forces. For example, in technicolor models, new fermions F are introduced such that $\langle F\overline{F}\rangle \neq 0$ due to technicolor forces, which results in the breaking of the electroweak interactions [33]. Other models of this class are composite models, where some (or all) of the particles that we presently regard as fundamental are bound states of more fundamental fermions [39]. In this class of models, the physics that is responsible for electroweak symmetry breaking is strong and its implementation requires non-perturbative techniques. I believe that it is fair to say that no compelling realistic model of this type exists at present. I will say no more about this approach. The second class of models are those in which new particles are introduced to the Standard Model in such a way that all quadratic divergences exactly cancel. Since one retains the Higgs scalars as elementary, the cancellation of quadratic divergences can only be the result of a new symmetry [40]. This symmetry is called supersymmetry which relates fermions to bosons. Because fermion self-energies have no quadratic divergences, it is possible in a theory with a symmetry that relates fermions to bosons to guarantee that no quadratic divergences arise in scalar self-energies.

In this lecture I will focus on low-energy supersymmetry as a compelling model for physics beyond the Standard Model [41]. Low-energy supersymmetric models contain a rich phenomenology of new particles and interactions. Moreover, polarization and spin correlations provide essential tools for disentangling the supersymmetric spectrum and checking that the underlying interactions have a supersymmetric origin. I will first review the ingredients of low-energy supersymmetry and define the minimal supersymmetric extension of the Standard Model. Then, I will discuss some theoretical biases on the parameters of this model, which are based on additional assumptions about physics at a very high energy scale (near

the Planck scale). Finally, I will survey how to exploit polarization and utilize spin information to study supersymmetric phenomenology at future supercolliders.

2.2 Introduction to low-energy supersymmetry

Supersymmetry is an attractive theoretical framework that may permit the consistent unification of particle physics and gravity, which takes place at an energy of order the Planck scale [42-44]. However, supersymmetry is clearly not an exact symmetry of nature, and therefore must be broken. In theories of "low-energy" supersymmetry, the effective scale of supersymmetry breaking is tied to the electroweak scale [45,38]. In this way, it is hoped that supersymmetry will ultimately explain the origin of the large hierarchy between the W and Z masses and the Planck scale.

The minimal supersymmetric extension of the Standard Model (MSSM) consists of taking the Standard Model and adding the corresponding supersymmetric partners [46]. In addition, the MSSM contains two $Y = \pm 1$ Higgs doublets, which is the minimal structure for the Higgs sector of an anomaly-free supersymmetric extension of the Standard Model that generates mass for both "up"-type and "down"-type quarks (and charged leptons) [47,48]. Supersymmetric interactions consistent with (global) B–L conservation (where B is baryon number and L is lepton number) are included. Finally, the most general soft-supersymmetry-breaking terms are added [49]. If supersymmetry is relevant for explaining the scale of electroweak interactions, then the mass parameters that occur in the soft-supersymmetry-breaking terms must be of order 1 TeV or below [50]. Some bounds on these parameters exist due to the absence of supersymmetry particle production at current accelerators, as well as the absence of any evidence for virtual supersymmetric particle exchange in a variety of Standard Model processes [51].

As a consequence of B–L invariance, the MSSM possesses a discrete R-parity invariance, where $R = (-1)^{3\,(B-L)+2S}$ for a particle of spin S [52]. Note that this formula implies that all the ordinary Standard Model particles have even R-parity, whereas the corresponding supersymmetric partners have odd R-parity. The conservation of R-parity in scattering and decay processes has a crucial impact on supersymmetric phenomenology. For example, starting from an initial state involving ordinary (R-even) particles, it follows that supersymmetric particles must be produced in pairs. In general, these particles are highly unstable and decay quickly into lighter states. However, R-parity invariance also implies that the lightest supersymmetric particle (LSP) is absolutely stable, and must eventually be produced at the end of a decay chain of a heavy unstable supersymmetric particle. In order to be consistent with cosmological constraints, the LSP is almost

certainly electrically and color neutral [53]. Consequently, the LSP is weakly-interacting in ordinary matter, *i.e.*, it behaves like a neutrino and will escape detectors without being directly observed. Thus, the canonical signature for (R-parity conserving) supersymmetric theories is missing (transverse) energy, due to the escape of the LSP. Some model builders attempt to relax the assumption of R-parity conservation [54]. Models of this type must break B–L and are therefore strongly constrained, although such models cannot be completely ruled out at present. In R-parity violating models, the LSP would be unstable, and this fact (among others) leads to a phenomenology of broken-R-parity models that is very different from that of the MSSM.

In the MSSM, supersymmetry breaking is induced by the soft-supersymmetry breaking terms mentioned above. These terms parametrize our ignorance of the fundamental mechanism of supersymmetry breaking. The parameters of the MSSM are conveniently described by considering separately the supersymmetry-conserving sector and the supersymmetry-breaking sector. A careful discussion of the conventions used in defining the MSSM parameters can be found in Ref. [55]. Among the parameters of the supersymmetry conserving sector are: (i) gauge couplings: g_s, g, and g', corresponding to the Standard Model gauge group SU(3)×SU(2)×U(1), respectively; (ii) Higgs Yukawa couplings: λ_e, λ_u, and λ_d (which are 3×3 matrices in flavor space); and (iii) a supersymmetry-conserving Higgs mass parameter μ. The supersymmetry-breaking sector contains the following set of parameters: (i) gaugino Majorana masses M_3, M_2 and M_1 associated with the SU(3), SU(2), and U(1) subgroups of the Standard Model; (ii) scalar mass matrices for the squarks and sleptons; (iii) Higgs-squark-squark trilinear interaction terms (the so-called "A-parameters") and corresponding terms involving the sleptons; and (iv) three scalar Higgs mass parameters—two diagonal and one off-diagonal mass terms for the two Higgs doublets. Explicitly, the tree-level Higgs potential in the MSSM reads

$$\begin{aligned} V_{\rm Higgs} = {} & m_{1H}^2|H_1|^2 + m_{2H}^2|H_2|^2 - m_{12}^2(H_1^0 H_2^0 - H_1^- H_2^+ + \text{h.c.}) \\ & + \tfrac{1}{8}(g^2+g'^2)\left(|H_1|^2 - |H_2|^2\right)^2 + \tfrac{1}{2}g^2|H_1^* H_2|^2\,, \end{aligned} \tag{2.1}$$

where H_1 and H_2 are weak SU(2) scalar doublets with hypercharges $Y=-1$ and $+1$, respectively.* These mass parameters m_{iH}^2 $(i=1,2)$ and m_{12}^2 can be re-expressed in terms of the two Higgs vacuum expectation values, $v_i \equiv \langle H_i^0\rangle$, $(i=1,2)$, and one physical Higgs mass. Here, v_1 (v_2) is the vacuum expectation

$\star$ The diagonal Higgs squared mass parameters actually receive a contribution from the supersymmetry conserving parameter μ as well. That is, $m_{iH}^2 \equiv |\mu|^2 + m_i^2$ $(i=1,2)$, where m_i^2 $(i=1,2)$ and m_{12}^2 are parameters of the supersymmetry breaking sector. Conventionally, one writes $m_{12}^2 \equiv B\mu$, which defines the parameter B.

value of the Higgs field that couples exclusively to down-type (up-type) quarks and leptons. Note that $v_1^2 + v_2^2 = (246\ \text{GeV})^2$ is fixed by the W mass, while the ratio

$$\tan\beta = \frac{v_2}{v_1} \tag{2.2}$$

is a free parameter of the model.†

The MSSM contains a number of possible new sources of CP violation. For example, gaugino mass parameters, the A-parameters, and μ may be complex. Some combination of these complex phases must be less than of order 10^{-2}–10^{-3} (for a supersymmetry-breaking scale of 100 GeV) to avoid generating electric dipole moments for the neutron, electron, and atoms in conflict with observed data [56]. However, these complex phases have little impact on the direct searches for supersymmetric particles. Nevertheless, if supersymmetric particles are discovered, it will be challenging to attempt to measure the CP-violating phases by precision measurements of supersymmetric couplings.

Before describing the supersymmetric particle sector, let us consider the Higgs sector of the MSSM [32]. There are five physical Higgs particles in this model: a charged Higgs pair ($H^\pm$), two CP-even neutral Higgs bosons (denoted by h^0 and H^0 where $m_{h^0} \leq m_{H^0}$) and one CP-odd neutral Higgs boson (A^0). The properties of the Higgs sector are determined by the Higgs potential. The strengths of the Higgs self-interaction terms are directly related to the gauge couplings by supersymmetry (and are not affected at tree-level by supersymmetry-breaking). As a result, $\tan\beta$ [defined in Eq. (2.2)] and one Higgs mass determine: the Higgs spectrum, an angle α [which indicates the amount of mixing of the original $Y = \pm 1$ Higgs doublet states in the physical CP-even scalars], and the Higgs boson couplings. When one-loop radiative corrections are incorporated, additional parameters of the supersymmetric model enter via virtual loops. The impact of these corrections can be significant [57,58]. For example, at tree-level, the MSSM predicts $m_{h^0} \leq m_Z$ [47,48]. If true, this would imply that experiments to be performed at LEP-II operating at its maximum energy and luminosity would rule out the MSSM if h^0 were not found. However, this Higgs mass bound need not be respected when radiative corrections are incorporated. For example, in Ref. [57], the following

† In the MSSM, it is conventional to choose the phases of the Higgs fields such that v_1 and v_2 are real and positive. Moreover, one can check that the Higgs sector is automatically CP-conserving (at tree-level). Thus, the physical neutral Higgs states are CP-eigenstates. The parameter m_{12}^2 in Eq. (2.1) is directly related to the mass of the CP-odd neutral state, A^0, via $m_{A^0}^2 = m_{12}^2/\sin\beta\cos\beta$. Thus, m_{12}^2 is real and positive in the standard convention where $\tan\beta$ is positive.

upper bound was obtained for m_{h^0} (assuming $m_{A^0} > m_Z$) in the limit of $m_Z \ll m_t \ll M_{\widetilde{t}}$ [where top-squark ($\widetilde{t}_L$–$\widetilde{t}_R$) mixing is neglected]

$$m_{h^0}^2 \lesssim m_Z^2 + \frac{3g^2 m_Z^4}{16\pi^2 m_W^2}\left\{\ln\left(\frac{M_{\widetilde{t}}^2}{m_t^2}\right)\left[\frac{2m_t^4 - m_t^2 m_Z^2}{m_Z^4}\right] + \frac{m_t^2}{3m_Z^2}\right\}. \tag{2.3}$$

For a top-squark mass of $M_{\widetilde{t}} = 1$ TeV, Eq. (2.3) yields a positive mass shift for m_{h^0} of about 20 GeV for $m_t = 150$ GeV, and 40 GeV for $m_t = 180$ GeV. Even if $\tan\beta = 1$ (so that $m_{h^0} = 0$ at tree-level), there is a large positive shift in $m_{h^0}^2$ due to radiative corrections of similar size.

Consider next the supersymmetric particle sector of the MSSM. The supersymmetric partners of the gauge and Higgs bosons are fermions, whose names are obtained by appending "ino" at the end of the corresponding Standard Model particle name. The *gluino* is the color octet Majorana fermion partner of the gluon with mass $M_{\widetilde{g}} = |M_3|$. The supersymmetric partners of the electroweak gauge and Higgs bosons (the *gauginos* and *Higgsinos*) can mix. As a result, the physical mass eigenstates are model-dependent linear combinations of these states, called *charginos* and *neutralinos*, which are obtained by diagonalizing the corresponding mass matrices.

The chargino mass matrix depends on M_2, μ, $\tan\beta$ and m_W. In the $\widetilde{W}^+$–$\widetilde{H}^+$ basis, the chargino mass matrix is [59]

$$X = \begin{pmatrix} M_2 & \sqrt{2}m_W \sin\beta \\ \sqrt{2}m_W\cos\beta & \mu \end{pmatrix}. \tag{2.4}$$

In general, two unitary 2×2 matrices U and V are required to diagonalize the chargino mass-squared matrix

$$\mathcal{M}^2_{\widetilde{\chi}^+} = VX^\dagger XV^{-1} = U^* XX^\dagger (U^*)^{-1}. \tag{2.5}$$

The two mass eigenstates are denoted by $\widetilde{\chi}_1^+$ and $\widetilde{\chi}_2^+$ with corresponding squared masses

$$\begin{aligned} M^2_{\widetilde{\chi}_1^+,\widetilde{\chi}_2^+} =& \tfrac{1}{2}\left[|\mu|^2 + |M_2|^2 + 2m_W^2\right] \mp \Big\{\left(|\mu|^2 + |M_2|^2 + 2m_W^2\right)^2 \\ & - 4|\mu|^2|M_2|^2 - 4m_W^4\sin^2 2\beta + 8m_W^2 \sin 2\beta\,\mathrm{Re}(\mu M_2)\Big\}^{1/2}, \end{aligned} \tag{2.6}$$

where the states are ordered such that $M_{\widetilde{\chi}_1^+} \leq M_{\widetilde{\chi}_2^+}$. If CP-violating effects are ignored (in which case, M_2 and μ are real parameters), then one can choose a

convention where $\tan\beta$ and M_2 are positive. (Note that the relative sign of M_2 and μ is meaningful. The sign of μ is convention-dependent; the reader is warned that both sign conventions appear in the literature.) The sign convention for μ fixed by Eq. (2.4) is used by the LEP collaborations [60] in their plots of exclusion contours in the M_2 *vs.* μ plane derived from the non-observation of $Z \to \widetilde{\chi}_1^+\widetilde{\chi}_1^-$. The mixing matrix elements U_{ij} and V_{ij} [see Eq. (2.5)] will appear in the chargino Feynman rules. If CP is conserved, the U and V can be chosen to be orthogonal matrices.

The neutralino mass matrix depends on M_1, M_2, μ, $\tan\beta$, m_Z, and the weak mixing angle θ_W. In the $\widetilde{B}$–$\widetilde{W}$–$\widetilde{H}_1^0$–$\widetilde{H}_2^0$ basis,* the neutralino Majorana mass matrix is [59]

$$Y = \begin{pmatrix} M_1 & 0 & -m_Z c_\beta s_W & m_Z s_\beta s_W \\ 0 & M_2 & m_Z c_\beta c_W & -m_Z s_\beta c_W \\ -m_Z c_\beta s_W & m_Z c_\beta c_W & 0 & -\mu \\ m_Z s_\beta s_W & -m_Z s_\beta c_W & -\mu & 0 \end{pmatrix}, \tag{2.7}$$

where $s_\beta = \sin\beta$, $c_\beta = \cos\beta$, *etc.* The 4×4 unitary matrix Z diagonalizes the neutralino mass matrix

$$\mathcal{M}_{\widetilde{\chi}^0} = Z^* Y Z^{-1}\,, \tag{2.8}$$

where the diagonal elements of $\mathcal{M}_{\widetilde{\chi}^0}$ can be either positive or negative. The four mass eigenstates are denoted by $\widetilde{\chi}_i^0$ $(i = 1, 2, 3, 4)$, with corresponding mass eigenvalues $\eta_i M_{\widetilde{\chi}_i^0}$. The physical neutralino masses are defined to be positive, with $M_{\widetilde{\chi}_1^0} \leq M_{\widetilde{\chi}_2^0} \leq M_{\widetilde{\chi}_3^0} \leq M_{\widetilde{\chi}_4^0}$. The sign of the mass eigenvalue ($\eta_i = \pm 1$) is physically relevant and corresponds to the CP quantum number of the Majorana neutralino state. The mixing matrix elements Z_{ij} will appear in the neutralino Feynman rules. If CP is conserved, then Z can be chosen to be an orthogonal matrix.

It is common practice in the literature to reduce the supersymmetric parameter freedom by requiring that all three gaugino mass parameters are equal at some grand unification scale. Then, at the electroweak scale, the gaugino mass parameters can be expressed in terms of one of them (say, M_2). The other two gaugino mass parameters are given by

$$M_3 = (g_s^2/g^2)M_2 \qquad M_1 = (5g'^2/3g^2)M_2\,. \tag{2.9}$$

Having made this assumption, the chargino and neutralino masses and mixing angles depend only on three unknown parameters: the gluino mass, μ, and $\tan\beta$.

$\star$ $\widetilde{B}$ and $\widetilde{W}^3$ are superpartners of the U(1)-hypercharge and SU(2)-weak neutral gauge bosons.

The supersymmetric partners of the quarks and leptons are spin-zero bosons: the *squarks*, charged *sleptons*, and *sneutrinos*. For a given fermion f, there are two supersymmetric partners $\widetilde{f}_L$ and $\widetilde{f}_R$ which are scalar partners of the corresponding left and right-handed fermion. (There is no $\widetilde{\nu}_R$.) However, in general, $\widetilde{f}_L$ and $\widetilde{f}_R$ are not mass-eigenstates since there is $\widetilde{f}_L$-$\widetilde{f}_R$ mixing which is proportional in strength to the corresponding element of the scalar mass-squared-matrix [61]

$$M^2_{LR} = \begin{cases} m_d(A_d - \mu \tan\beta), & \text{for "down"-type } f, \\ m_u(A_u - \mu \cot\beta), & \text{for "up"-type } f, \end{cases} \tag{2.10}$$

where m_d (m_u) is the mass of the appropriate "down" ("up") type quark or lepton. Here, A_d and A_u are (unknown) soft-supersymmetry-breaking A–parameters and μ and $\tan\beta$ have been defined earlier. The signs of the A parameters are also convention dependent; see Ref. [55]. Due to the appearance of the *fermion* mass in Eq. (2.10), one expects M_{LR} to be small compared to the diagonal squark and slepton masses, with the possible exception of the top-squark, since m_t is large, and the bottom squark if $\tan\beta \gg 1$. The (diagonal) L and R-type squark and slepton masses are given by [43].

$$\begin{aligned}
M^2_{\widetilde{u}_L} &= M^2_{\widetilde{Q}} + m_u^2 + m_Z^2 \cos 2\beta (\tfrac{1}{2} - \tfrac{2}{3}\sin^2\theta_W)\,, \\
M^2_{\widetilde{u}_R} &= M^2_{\widetilde{U}} + m_u^2 + \tfrac{2}{3} m_Z^2 \cos 2\beta \sin^2\theta_W\,, \\
M^2_{\widetilde{d}_L} &= M^2_{\widetilde{Q}} + m_d^2 - m_Z^2 \cos 2\beta (\tfrac{1}{2} - \tfrac{1}{3}\sin^2\theta_W)\,, \\
M^2_{\widetilde{d}_R} &= M^2_{\widetilde{D}} + m_d^2 - \tfrac{1}{3} m_Z^2 \cos 2\beta \sin^2\theta_W\,, \\
M^2_{\widetilde{\nu}} &= M^2_{\widetilde{L}} + \tfrac{1}{2} m_Z^2 \cos 2\beta\,, \\
M^2_{\widetilde{e}_L} &= M^2_{\widetilde{L}} + m_e^2 - m_Z^2 \cos 2\beta (\tfrac{1}{2} - \sin^2\theta_W)\,, \\
M^2_{\widetilde{e}_R} &= M^2_{\widetilde{E}} + m_e^2 - m_Z^2 \cos 2\beta \sin^2\theta_W\,.
\end{aligned} \tag{2.11}$$

The soft-supersymmetry-breaking parameters: $M_{\widetilde{Q}}$, $M_{\widetilde{U}}$, $M_{\widetilde{D}}$, $M_{\widetilde{L}}$, and $M_{\widetilde{E}}$ are unknown parameters. In the equations above, the notation of first generation fermions has been used and generational indices have been suppressed. Further complications such as intergenerational mixing are possible, although there are some constraints from the nonobservation of flavor-changing neutral currents (FCNC) [62].

One way to guarantee the absence of significant FCNC's mediated by virtual supersymmetric particle exchange is to posit that the diagonal soft-supersymmetry-breaking scalar mass matrices are proportional to the unit matrix (in flavor space) at some energy scale (normally taken to be the Planck scale) [63]. Renormalization group evolution is used to determine the low-energy values for the scalar mass

parameters listed above. This assumption substantially reduces the MSSM parameter freedom. For example, supersymmetric grand unified models with universal scalar masses at the Planck scale typically give [64] $M_{\widetilde{L}} \approx M_{\widetilde{E}} < M_{\widetilde{Q}} \approx M_{\widetilde{U}} \approx M_{\widetilde{D}}$ with the squark masses somewhere between a factor of 1–3 larger than the slepton masses (neglecting generational distinctions). More specifically, the first two generations are thought to be nearly degenerate in mass, while $M_{\widetilde{Q}_3}$ and $M_{\widetilde{U}_3}$ are typically reduced by a factor of 1–3 from the other soft-supersymmetry-breaking scalar masses because of renormalization effects due to the heavy top quark mass. As a result, four flavors of squarks (with two squark eigenstates per flavor) and $\widetilde{b}_R$ will be nearly mass-degenerate and somewhat heavier than six flavors of approximately mass-degenerate sleptons (with two per flavor for the charged sleptons and one per flavor for the sneutrinos). On the other hand, the $\widetilde{b}_L$ mass and the diagonal $\widetilde{t}_L$ and $\widetilde{t}_R$ masses are reduced compared to the common squark mass of the first two generations. In addition, third generation squark masses are sensitive to the strength of the respective $\widetilde{q}_L$–$\widetilde{q}_R$ mixing as discussed below Eq. (2.10).

Two additional theoretical frameworks are often introduced to further reduce the MSSM parameter freedom [42,43,65]. The first is that of grand unified theories (GUTs) and the desert hypothesis (*i.e.*, no new physics between the TeV-scale and the GUT-scale). In the absence of low-energy supersymmetry, the simplest models of this type fail because the three SU(3)×SU(2)×U(1) gauge couplings fail to unify at a common scale [66,67]. Remarkably, in the case of the MSSM (with a supersymmetry-breaking scale of order 1 TeV or below), the three gauge couplings do unify at a common energy scale of order 10^{16} GeV (with only very mild assumptions about the GUT-scale theory) [66,68]. Unification constraints on the Higgs-fermion Yukawa couplings may also exist but are more GUT-model dependent [69]. The second theoretical framework is that of minimal supergravity theory, which can impose nontrivial constraints on the soft-supersymmetry breaking parameters. Referring to the parameter list given above Eq. (2.1), the Planck-scale values of the soft-supersymmetry-breaking parameters in the simplest supergravity models take the following form: (i) a universal gaugino mass $m_{1/2}$ [assuming grand unification; Eq. (2.9) is a consequence of this assumption]; (ii) a universal diagonal scalar mass parameter m_0 [whose consequences were described in the preceding paragraph]; (iii) a universal A-parameter, A_0; and (iv) three scalar Higgs mass parameters [*cf.* Eq. (2.1)]—two common diagonal squared-masses given by $|\mu_0|^2 + m_0^2$ and an off-diagonal squared-mass given by $B_0\mu_0$ (which defines the Planck-scale supersymmetry-breaking parameter B_0), where μ_0 is the Planck-scale value of the μ-parameter. As before, renormalization group evolution is used to compute the low-energy values of the supersymmetry-breaking parameters, and determines the supersymmetric particle spectrum. Moreover, in this approach, electroweak symmetry breaking is induced radiatively if one of the Higgs diagonal squared-masses

is forced negative by the evolution. This occurs in models with a large Higgs-top quark Yukawa coupling (*i.e.*, large m_t). As a result, the two Higgs vacuum expectation values (or equivalently, m_Z and $\tan\beta$) can be expressed as a function of the Planck-scale supergravity parameters. The simplest procedure [64] is to remove μ_0 and B_0 in favor of m_Z and $\tan\beta$ (the sign of μ_0 is not fixed in this process). In this case, the MSSM spectrum and its interactions are determined by m_0, A_0, $m_{1/2}$, $\tan\beta$, and the sign of μ_0 (in addition to the parameters of the Standard Model). Combining both grand unification and the minimal supergravity approach yield the most constrained version of the MSSM.

2.3 Polarization and spin analysis as tools for supersymmetry searches

First, let us briefly consider supersymmetry searches at hadron colliders. The supersymmetric particles with the largest production cross sections are the squarks and gluinos [70]. These particles have non-trivial color quantum numbers and are produced in gluon-gluon and quark-antiquark collisions. (Gluinos and squarks can also be produced in association via gluon-quark and gluon-antiquark collisions.) Since gluinos are color octets, their production cross-section is larger than that of the color-triplet squarks. However, because there are twelve squark types (six flavors, with two mass eigenstates per flavor), with at least eight types rather close in mass (as discussed in the previous section), the total cross section for the production of squarks of all types is competitive with the gluino cross sections.

One can also directly produce sleptons, neutralinos and charginos at hadron colliders via the Drell-Yan mechanism (virtual s-channel gauge boson exchange in $q\bar{q}$ annihilation). However, these processes are mediated by the electroweak interactions, so their cross sections are substantially smaller than those of squarks and gluinos. On the plus side, the sleptons, neutralinos and charginos states are expected to be lighter than the squarks and gluinos. Nevertheless, gluinos and squarks remain the most likely supersymmetric candidates for discovery at the LHC.

The phenomenology of squarks and gluinos at hadron colliders is well known [71]. Can one exploit polarization and spin analysis to untangle such signals if they are discovered? For a review of spin effects at supercollider energies, see Refs. [72] and [73]. Here I will quote one attempt to answer this question if polarized beams were available at a future hadron collider. Suppose the initial proton beams have helicity λ and λ', respectively. Consider the process $p(\lambda) + p(\lambda') \to \text{ jet} + X$, and denote some differential cross section for this process by $d\sigma_{\lambda\lambda'}$. Then, one can define the double helicity asymmetry

$$A_{LL} = \frac{d\sigma_{++} - d\sigma_{+-}}{d\sigma_{++} + d\sigma_{+-}}\,. \tag{2.12}$$

In the parton model, this asymmetry is obtained from

$$A_{LL}d\sigma = \sum_{ij} \frac{1}{1+\delta_{ij}} \int dx_a dx_b \left[\Delta f_i(x_a)\Delta f_j(x_b) + (i \leftrightarrow j)\right] \hat{a}_{LL}^{ij} d\hat{\sigma}_{ij} \,, \qquad (2.13)$$

where $\Delta f \equiv f_+ - f_-$, and $f_{2\lambda}$ is the parton distribution in a polarized proton of helicity λ. The sum over i and j in Eq. (2.13) is taken over all possible elementary scattering processes $i + j \to k + \ell$, in which the observed jet originates from one of the final state partons.

Note that A_{LL} is generally nonzero, even in parity conserving interactions. (In contrast, single helicity asymmetries are nonzero only in parity non-conserving processes.) One can work out expressions for the elementary partonic cross sections ($d\hat{\sigma}_{ij}$) and the partonic double helicity asymmetries ($\hat{a}_{LL}^{ij}$), and derive predictions for A_{LL} based on the partonic subprocesses of QCD in the Standard Model. Predictions for A_{LL} (at zero rapidity) as a function of transverse momentum tend to be small and positive, of order a few percent [74]. Consider now the contributions to A_{LL} from supersymmetric particle production. Due to helicity conservation, in the limit of zero mass squarks and gluinos, the production of $\widetilde{q}$ and $\widetilde{g}$ has the property that $\hat{a}_{LL} = -1$. This result is diluted somewhat when the squark and gluino masses are taken into account. Nevertheless, it continues to be true that jet events of a supersymmetric origin would have $A_{LL} < 0$. Whether this is an observable effect under realistic experimental conditions remains to be proven.

For the rest of this lecture, I will consider the search for supersymmetry at e^+e^- colliders. In particular, I will exhibit some of the power of the ILC for disentangling the supersymmetric particle interactions and testing model assumptions in the MSSM. The advantages of an e^+e^- collider for a detailed study of the supersymmetric spectrum (over the corresponding search for supersymmetry at a hadron supercollider) are:

1. In an e^+e^- collider, Standard Model backgrounds to new physics signals tend to be of the same order of magnitude in cross section as the signals themselves. This is true because all tree-level cross sections of processes produced at e^+e^- colliders are electroweak in strength, so all two-body tree-level cross sections are roughly a unit of R (where one unit of R is equal to the cross section for $e^+e^- \to \gamma^* \to \mu^+\mu^-$).
2. The beam energy constraint can be used (assuming that beamstrahlung effects are negligible). That is, the CM-energy of the final state is known to be equal to the CM-energy of the e^+e^- collider. In contrast, at hadron colliders, the CM-energy of the final state partons is generally not known unless it can be directly measured.

3. $W^{\pm}$ and Z bosons can be detected in their two-jet decay modes. This is very difficult in hadron colliders, where QCD backgrounds are severe.

4. Polarized beams can provide a powerful tool for studying new physics and rejecting Standard Model background. The SLC has demonstrated the feasibility of polarized beams at a linear e^+e^- collider. Although it is possible in principle to polarize the beams at a hadron collider, the interest in doing so has been limited. (Perhaps these lectures will encourage more study of the feasibility of polarized beams at future hadron supercolliders and their potential in detecting and elucidating new physics.)

5. Complex final states are more easily managed at e^+e^- colliders due to the relative cleanliness of the environment (*e.g.*, smaller multiplicities, less gluon radiation, *etc.*).

6. The production rates for uncolored and colored particles with electroweak quantum numbers are similar (of order one unit of R).

The main disadvantages of e^+e^- linear colliders as compared to hadron supercolliders are:

1. The CM-energy of future hadron supercolliders are significantly larger than any e^+e^- linear collider that will exist during the same era. Of course, at a hadron collider, the new physics reach is determined by the CM-energy of the relevant parton-parton interaction, which is of order 10% of the pp CM-energy. Even so, the physics reach of the LHC is substantially larger than that of a 500 GeV ILC. Since the goal of the next generation of colliders is to uncover the mechanism of electroweak symmetry breaking, the LHC is therefore essential for maximizing the probability for the discovery of new physics at the TeV energy scale.

2. It is very difficult to directly produce colored particles that are singlets under the electroweak gauge group (such as the gluino) at an e^+e^- collider.* In contrast, such particles are produced with significant cross sections at hadron colliders (via gluon-gluon scattering), and under most circumstances are easily observed.

In summary, hadron colliders and e^+e^- colliders are complementary. The LHC is likely to be the discovery machine for new physics beyond the Standard Model. Sorting out the nature of the new physics will primarily be the job of the ILC.

$\star$ Gluinos can be more easily studied at e^+e^- colliders if they are lighter than squarks, assuming that the production of squark pairs is kinematically allowed. In this case, the dominant squark decay, $\widetilde{q} \to q\widetilde{g}$, provides the gluino source.

Polarized beams at the ILC provide an effective tool in studies of supersymmetric particle production. A comprehensive analysis by Tsukamoto *et al.* [75] demonstrates that one can make precision measurements of the MSSM parameters and test various theories for these parameters at the ILC. I will briefly describe some of their work here; for a more detailed description of their methods and strategies, see Ref. [75].

First, based on the theoretical remarks at the end of section 2.2, one expects that the lightest states of the MSSM are the sleptons, charginos and neutralinos. The lightest supersymmetric particle is assumed to be $\widetilde{\chi}_1^0$. However, since $\widetilde{\chi}_1^0$ behaves like a neutrino in particle detectors, one cannot detect $e^+e^- \to \widetilde{\chi}_1^0\widetilde{\chi}_1^0$. Consider next $e^+e^- \to \widetilde{\chi}_1^0\widetilde{\chi}_2^0$, where $\widetilde{\chi}_2^0 \to \widetilde{\chi}_1^0 + f\bar{f}$ (and f can be either a quark or lepton). Note that the $\widetilde{\chi}_1^0\widetilde{\chi}_2^0$ final state is produced via t-channel selectron-exchange or via s-channel Z-exchange. There is no s-channel virtual photon exchange; as a result, the cross section for this process tends to be less than that for charged supersymmetric particle production. Thus, one should first focus on charged slepton production $e^+e^- \to \widetilde{\ell}_{L,R}^+\widetilde{\ell}_{L,R}^-$ ($\ell = e, \mu, \tau$), which is mediated at tree-level by

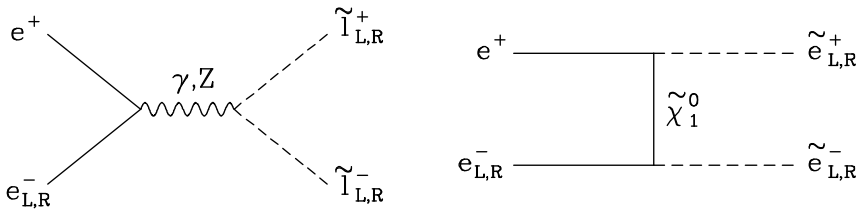

and on pair-production of the lightest charginos $e^+e^- \to \widetilde{\chi}_1^+\widetilde{\chi}_1^-$ which is mediated at tree-level by the following graphs.

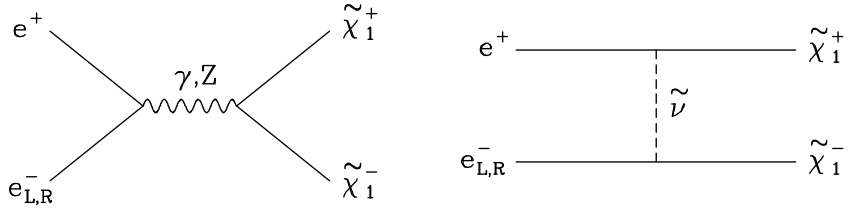

I assume that the initial electron beam is polarized. There are two main advantages of employing a polarized electron beam. First, it provides another handle for determining the supersymmetric parameters. For example, by controlling the electron polarization, one can affect the relative strengths of the competing Feynman diagrams depicted above. That permits the isolation of neutralino couplings in slepton production and sneutrino couplings in chargino production. In particular, note that $\tilde{e}_L^+\tilde{e}_R^-$ (or $\tilde{e}_L^-\tilde{e}_R^+$) production occurs only via $\widetilde{\chi}_i^0$-exchange, since the γ and Z couplings to slepton pairs is diagonal at tree-level. Furthermore, only

the $\widetilde{B}$ component of the $\widetilde{\chi}_1^0$ contributes to $\widetilde{e}_R^{\pm}$ production; clearly this requires an incoming e_R^- beam. In $\widetilde{\chi}_1^+\widetilde{\chi}_1^-$ production, $\widetilde{\nu}$ exchange is absent in the case of an incoming e_R^- beam, since the $\widetilde{\nu}$ is the superpartner of the neutrino which possesses only left-handed couplings. Moreover, the e_R^- beam enhances the higgsino components of the produced $\widetilde{\chi}_1^{\pm}$. Second, controlling the polarization enhances the ability to separate Standard Model backgrounds from the above signals. For example, one of the main Standard Model backgrounds to the processes considered above is $e^+e^- \to W^+W^-$. This background can be significantly reduced by employing an e_R^- beam, because (i) W^+W^- production via s-channel exchange is suppressed and (ii) the t-channel neutrino exchange contribution to W^+W^- production (which is particularly large in the forward direction due to the exchange of a massless particle) is completely absent.

Tsukamoto *et al.* [75] describe the following strategy for the supersymmetric particle search at the ILC using a polarized electron beam. Suppose that the supersymmetric particle spectrum satisfies $M_{\widetilde{\chi}_1^0} < M_{\widetilde{\ell}_R^{\pm}} < M_{\widetilde{\chi}_2^0}, M_{\widetilde{\chi}_1^+} < M_{\widetilde{\ell}_L^{\pm}}, M_{\widetilde{\nu}}$. For example, the cross sections for slepton pair production for a representative set of parameters for three choices of electron beam polarization is shown in Fig. 1. Then, in the first stage of the supersymmetric particle search, $\tilde{e}_R^{\pm}$ and $\tilde{\mu}_R^{\pm}$ will be discovered.* A detailed experimental analysis will then produce measurements of $M_{\tilde{e}_R^{\pm}}$, $M_{\tilde{\mu}_R^{\pm}}$, $M_{\widetilde{\chi}_1^0}$, $\sigma_L(\widetilde{e}_R)$, $\sigma_R(\widetilde{e}_R)$, $\sigma_L(\widetilde{\mu}_R)$, $\sigma_R(\widetilde{\mu}_R)$, and the slepton angular distributions. The notation here should be obvious; for example, $\sigma_L(\widetilde{e}_R) = \sigma(e^+e_L^- \to \tilde{e}_R^+\tilde{e}_R^-)$, *etc.* The $\widetilde{\chi}_1^0$ will also be discovered by virtue of the decay $\widetilde{\ell}_R \to \ell\widetilde{\chi}_1^0$ ($\ell = e, \mu$). The ability to separate the supersymmetric signal from Standard Model background can be enhanced with polarization. For example, one potentially important background to slepton pair production is $e^+e^- \to W^+W^- \to \ell^+\ell^-$ + missing energy, which yields the same type of final state as the signal events. However, this background can be suppressed by employing a right-handed electron beam, since W-bosons couple only to e_L^-. The power of polarization in the background suppression is illustrated in Fig. 2. When the full analysis is performed, it is found that the supersymmetric particle masses can be measured rather accurately, typically to within a few GeV. With the information of the masses and cross sections, one can already deduce important information about the supersymmetric spectrum. Assuming the relation of gaugino mass parameters given in Eq. (2.9), a measurement of $M_{\widetilde{\chi}_1^0}$ is sufficient to provide an upper bound on the mass of the lightest chargino. One finds that for $M_{\widetilde{\chi}_1^{\pm}} \geq m_W$, the light chargino mass is bounded by $M_{\widetilde{\chi}_1^{\pm}} \leq (M_2/M_1)M_{\widetilde{\chi}_1^0} \simeq 2M_{\widetilde{\chi}_1^0}$, where Eq. (2.9) was applied in the last step. One also tests the universality of scalar

$\star$ Discovery of the $\widetilde{\tau}_R^{\pm}$ is somewhat more involved and will be neglected in the following discussion.

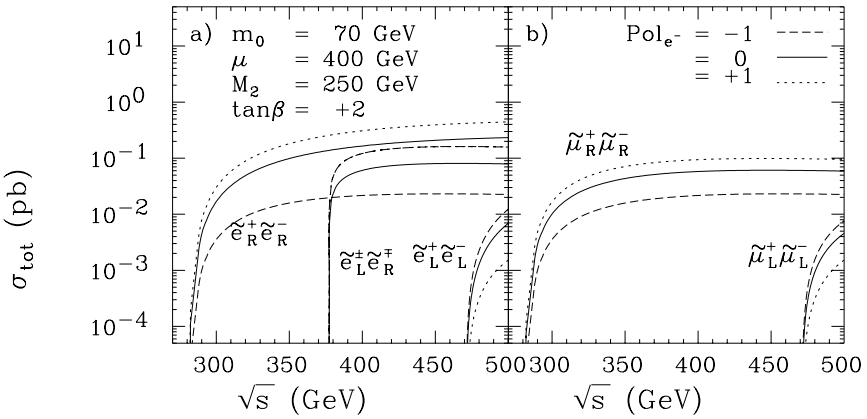

Fig. 1. Total cross sections for slepton production: (a) $e^+e^- \to \tilde{e}^+_R\tilde{e}^-_R$, $e^+e^- \to \tilde{e}^\pm_L\tilde{e}^\mp_R$, and $e^+e^- \to \tilde{e}^+_L\tilde{e}^-_L$, (b) $e^+e^- \to \tilde{\mu}^+_R\tilde{\mu}^-_R$ and $e^+e^- \to \tilde{\mu}^+_L\tilde{\mu}^-_L$, where dashed, solid, and dotted lines correspond to electron beam polarizations of -1, 0, and $+1$, respectively. The cross sections were evaluated at the lowest order, without including initial state radiation nor beam effects. Taken from Ref. [75].

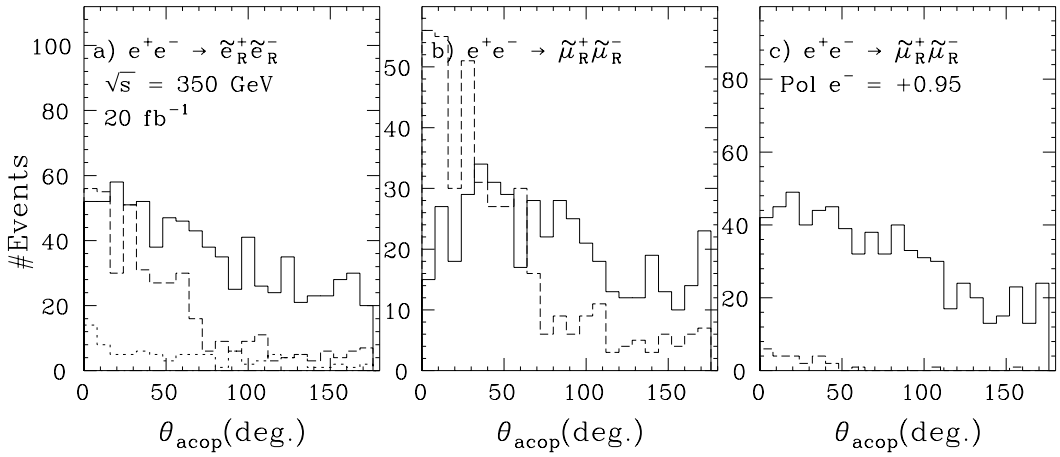

Fig. 2. Acoplanarity angle distributions for final-state leptons from right-handed slepton-pair productions (solid) at $\sqrt{s} = 350$ GeV with an integrated luminosity of 20 fb^{-1} after including the initial state radiation and the beamstrahlung effects: (a) $e^+e^- \to \tilde{e}^+_R\tilde{e}^-_R$ with $P = 0$, (b) $e^+e^- \to \tilde{\mu}^+_R\tilde{\mu}^-_R$ with $P = 0$, and (c) $\bar{\mu}^+_R\bar{\mu}^-_R$ with $P = +0.95$. The dashed lines indicate the W^+W^- background, while the dotted line represents that from the $e^{\pm}\overset{(-)}{\nu}_e W^\mp$ process. Taken from Ref. [75].

masses by comparing the values of $M_{\tilde{e}_R^\pm}$ and $M_{\tilde{\mu}_R^\pm}$. Finally, adding in the cross section measurements and angular distributions allows one to check the assignment of slepton quantum numbers and provides some constraints on the parameters of the neutralino mass matrix.

Proceeding in the scenario under consideration, in the second stage of the supersymmetric particle search the next particle to be discovered is $\widetilde{\chi}_1^\pm$. Experimental observables include: $M_{\widetilde{\chi}_1^\pm}$, $\sigma_L(\widetilde{\chi}_1^\pm)$, $\sigma_R(\widetilde{\chi}_1^\pm)$, and the chargino angular distribution. The chargino mass search is very similar to the search for a new heavy charged lepton. Assuming that squarks and the charged Higgs boson are much heavier than m_W, the dominant decay of the chargino is $\widetilde{\chi}_1^\pm \to \widetilde{\chi}_1^0 W^\pm$, where the final state W is either real or virtual. According to the analysis of Ref. [75], the chargino and neutralino masses can be measured to an accuracy of about 5%. Moreover, by comparing the relative chargino production rates using left-handed and right-handed electron beams, one can distinguish between the higgsino and gaugino components of $\widetilde{\chi}_1^\pm$, and separate out the sneutrino-exchange contribution. For example, gauginos and the sneutrino couple only to left-handed electrons, while higgsinos couple to both e_L^- and e_R^-. Thus, one can perform a global fit using the measured masses of $\widetilde{\chi}_1^\pm$ and $\widetilde{\chi}_1^0$, $\sigma_R(\widetilde{e}_R)$ [from stage 1 of the search], and the chargino pair cross sections $\sigma_L(\widetilde{\chi}_1^\pm)$ and $\sigma_R(\widetilde{\chi}_1^\pm)$ to reconstruct the sneutrino mass and the four unknown parameters, M_1, M_2, μ and $\tan\beta$ of the neutralino mass matrix. One can now begin to test models of the supersymmetry breaking parameters. For example, having deduced M_1 and M_2, one can directly test the unification of gaugino mass parameters [Eq. (2.9)].

Finally, in the third stage of the supersymmetric particle search, $\tilde{e}_L^\pm$ is discovered in associated production of $\tilde{e}_L^\mp \tilde{e}_R^{\pm\star}$. Note that for the associated production, there is no s-channel gauge boson exchange contribution, since the γ and Z couple diagonally to slepton pairs at tree-level. Thus, only the t-channel neutralino exchange contributes in this case. If the electron beam is polarized, then there are four possible cross sections to consider:

$$\begin{aligned}
\sigma_L(\tilde{e}_L^- \tilde{e}_R^+) &\equiv \sigma(e^+ e_L^- \to \tilde{e}_L^- \tilde{e}_R^+)\,, \\
\sigma_R(\tilde{e}_R^- \tilde{e}_L^+) &\equiv \sigma(e^+ e_R^- \to \tilde{e}_R^- \tilde{e}_L^+)\,, \\
\sigma_L(\tilde{e}_R^- \tilde{e}_L^+) &\equiv \sigma(e^+ e_L^- \to \tilde{e}_R^- \tilde{e}_L^+)\,, \\
\sigma_R(\tilde{e}_L^- \tilde{e}_R^+) &\equiv \sigma(e^+ e_R^- \to \tilde{e}_L^- \tilde{e}_R^+)\,.
\end{aligned} \tag{2.14}$$

In fact, $\sigma_L(\tilde{e}_R^- \tilde{e}_L^+) = \sigma_R(\tilde{e}_L^- \tilde{e}_R^+) = 0$, since chirality is conserved at the $\ell\widetilde{\ell}\widetilde{\chi}^0$ vertex. That is, in the $e\widetilde{e}\widetilde{\chi}^0$ interaction, e_L^- [e_R^-] couples exclusively to $\tilde{e}_L^-$ [$\tilde{e}_R^-$]. The fact that

$\star$ One may also be able to discover the sneutrino in $e^+e^- \to \tilde{\nu}\overline{\tilde{\nu}}$, which is mediated by s-channel Z-decay and t-channel chargino exchange. See *e.g.*, Ref. [76].

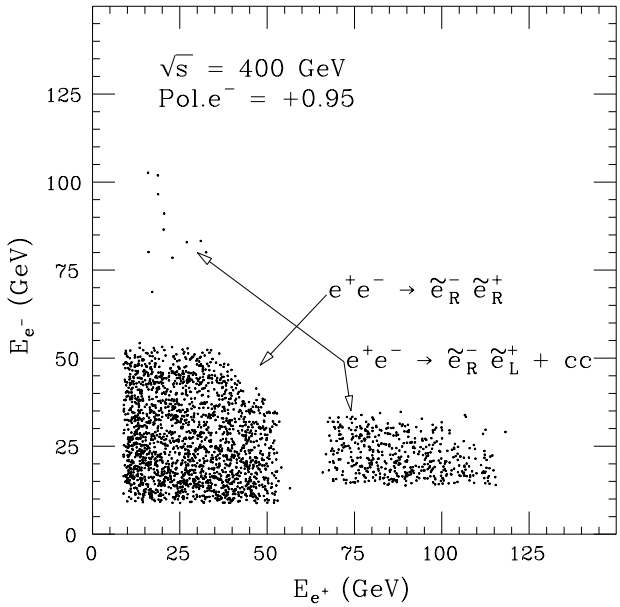

Fig. 3. The scatter plot of e^+ energies at $\sqrt{s} = 400$ GeV with an integrated luminosity of 20 fb^{-1} and an electron beam polarization of $P = +0.95$ for $e^+e^- \to \tilde{e}_L^{\pm}\tilde{e}_R^{\mp}$ and $e^+e^- \to \tilde{e}_R^+\tilde{e}_R^-$, including the initial state radiation and the beamstrahlung effects. Taken from Ref. [75].

one can speak of a chirality for the scalar sleptons is a deep consequence of supersymmetry which associates scalar particles with each left and right-handed fermion component. As a result, the experimental observables in the stage 3 analysis are: $M_{\tilde{e}_L^{\pm}}$, $\sigma_L(\tilde{e}_L^-\tilde{e}_R^+)$, $\sigma_R(\tilde{e}_R^-\tilde{e}_L^+)$ and the angular distribution of the final state sleptons. However, one can test experimentally the absence of $\sigma_L(\tilde{e}_R^-\tilde{e}_L^+)$ and $\sigma_R(\tilde{e}_L^-\tilde{e}_R^+)$ directly with polarized beams. In Fig. 3, the results of a Monte Carlo simulation of Ref. [75] are displayed. This figure illustrates a case in which the initial electron beam is almost purely right-handed electron beam. The final state sleptons are assumed to decay via $\widetilde{\ell} \to \ell\widetilde{\chi}_1^0$, so the experimentally observed process is $e^+e_R^- \to e^-e^+ +$ missing energy. Since $M_{\tilde{e}_L^{\pm}} > M_{\tilde{e}_R^{\pm}}$, one expects that in the associated slepton production, the final state positron energy should be larger than the corresponding electron energy.† This is indeed the case, as shown in Fig. 3. The few events seen with $E_{e^-} > E_{e^+}$ correspond to $\sigma_L(\tilde{e}_L^-\tilde{e}_R^+)$ since the plot assumes that the initial electron beam is not 100% polarized. Such a plot if observed in a real experiment would constitute strong evidence for the absence of $\sigma_R(\tilde{e}_L^-\tilde{e}_R^+)$ and support the notion of the association of chirality for sleptons. With the measurement

† In addition, one also expects events arising from $e^+e^- \to \tilde{e}_R^-\tilde{e}_R^+$ which should be symmetric about $E_{e^-} = E_{e^+}$.

of $M_{\tilde{e}_L^\pm}$ and the associated slepton pair cross sections, one can make additional checks of parameters already obtained in stages 1 and 2 above and test additional model predictions. For example, in models based on minimal supergravity, one obtains relations among slepton masses of the same generation. These relations can be checked and provide additional probes of the structure of the theory at the grand unification scale.

If the energy of the ILC is sufficiently high, one may be able to reach the squark threshold. The phenomenology of squark pair production at a future e^+e^- linear collider has been recently treated in detail in Ref. [77]. As in the case of $\widetilde{\mu}^+\widetilde{\mu}^-$ production, only s-channel γ and Z-exchange diagrams contribute. Again, polarizing the electron beam can play a critical role in separating out the $\widetilde{q}_L\overline{\widetilde{q}}_L$ and $\widetilde{q}_R\overline{\widetilde{q}}_R$ final states. The cross sections are very sensitive to the electron helicity, as shown in Fig. 4. In particular, there is a strong tendency for left [right] handed electrons to produce $\widetilde{q}_L\overline{\widetilde{q}}_L$ [$\widetilde{q}_R\overline{\widetilde{q}}_R$] final states. Thus, by controlling the polarization of the electron beam, one can separately determine the masses of $\widetilde{q}_L$ and $\widetilde{q}_R$. A Monte-Carlo simulation of Ref. [77], shown in Fig. 5, suggests that a mass difference of 10 GeV between $\widetilde{q}_L$ and $\widetilde{q}_R$ could be detected.

Clearly, polarization is a valuable tool for dissecting the properties of supersymmetric particles. One still must check that the observed sleptons and squarks have spin-zero, while the charginos and neutralinos have spin-1/2. Threshold behavior of cross sections provides some indication, although this requires that one study the production rates as a function of the CM-energy of the collider. The spin of the final state particles can also be determined by careful measurement of the distribution of final state decay products. These methods are well-known and have been used often in the past to determine the quantum numbers of hadronic resonances. To describe these methods in detail would take us beyond the scope of these lectures. Instead, I will refer you to some of the old textbooks of the field (see *e.g.*, Refs. [9,10]), which perhaps should be better known to the current young generation of particle physicists!

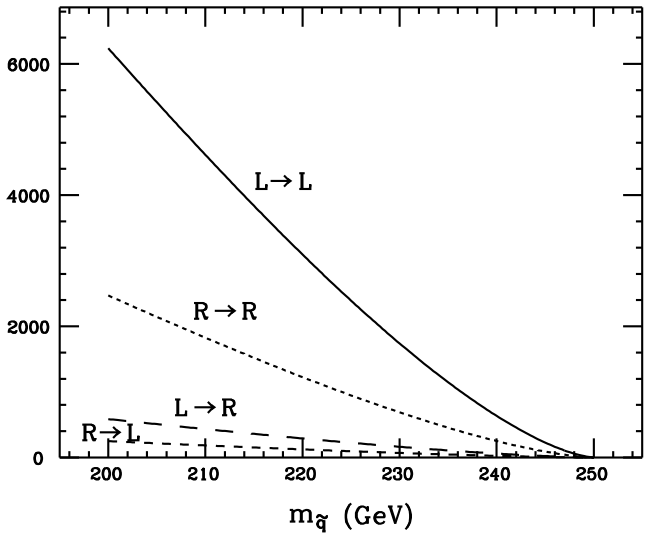

Fig. 4. The number of squark pairs of the first two generations produced at a 500 GeV e^+e^- collider with polarized e^- beams, unpolarized e^+ beams, and an integrated luminosity of 20 fb^{-1} for each e^- beam polarization. The four helicity combinations plotted are $e^-_{L,R}\,e^+ \to \widetilde{q}_{L,R}\,\overline{\widetilde{q}}$. Taken from Ref. [77].

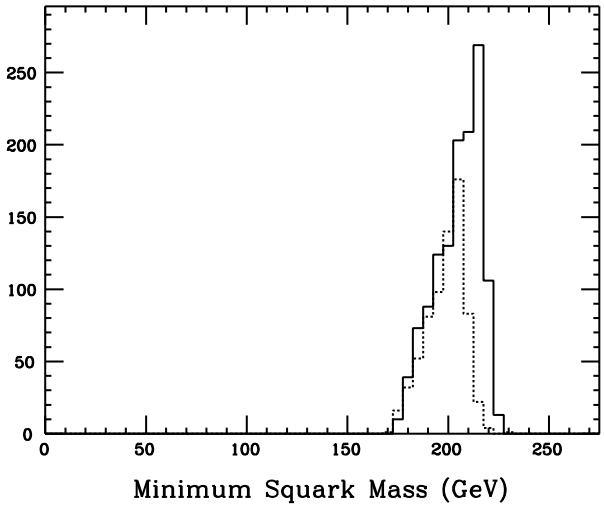

Fig. 5. The distribution of $m^{\rm min}_{\tilde{q}}$, the minimum allowed squark mass for a given event, in region 1 at the point $(\mu, M_2) = (-500\,{\rm GeV}, 300\,{\rm GeV})$. The distribution for e^-_L (e^-_R) polarized beams is given by the solid (dashed) histogram and is sharply peaked at the actual $\widetilde{q}_L$ ($\widetilde{q}_R$) mass of 220 (210) GeV. The integrated luminosity assumed is 10 fb^{-1} per polarization, and the bin size is 5 GeV. Taken from Ref. [77]

LECTURE 3:
Applications to Higgs and New Gauge Boson Searches

In this lecture, I will discuss a few more examples of utilizing polarization and spin analysis in new physics searches at future colliders. This lecture is not meant to be comprehensive. Instead, I have selected just a few examples from the search for Higgs bosons at a future e^+e^- linear collider (ILC) and new gauge bosons beyond the $W^\pm$ and Z at a future hadron supercollider (such as the LHC). Some other areas of investigation will be mentioned briefly at the end of these lectures.

3.1 Higgs bosons beyond the minimal Standard Model

In the Standard Model, the electroweak gauge symmetry is broken when the neutral component of a complex Higgs doublet (with hypercharge $Y = 1$) acquires a vacuum expectation value. The scalar spectrum of the theory then contains one neutral CP-even Higgs field; the other scalar degrees of freedom are Goldstone bosons which are absorbed by the $W^\pm$ and Z (thereby generating the gauge boson masses). In this Lecture, the Standard Model Higgs boson will be denoted by ϕ^0 in order to distinguish it from other CP-even neutral Higgs scalars that may appear in non-minimal extensions of the Standard Model. Although the Standard Model is very well tested at LEP, there is no direct experimental information on the underlying dynamics that is responsible for electroweak symmetry breaking. As remarked in the introduction to these lectures, the study of electroweak symmetry breaking is the main goal of the next generation of colliders.

If new physics exists beyond the Standard Model, then the minimal Higgs structure described above will almost certainly be supplanted by a more complicated electroweak symmetry breaking sector. What new features is this sector likely to possess? If Higgs bosons are elementary scalars (on the scale of TeV physics), then one should consider the possibility of an extended Higgs sector. Here, I shall consider the simplest of the extended Higgs sectors—the two-Higgs doublet model [78].

Consider a model with two complex Higgs doublets with hypercharges $Y = -1$ and $Y = +1$, respectively. For simplicity, I shall assume that the Higgs sector conserves CP. Moreover, I will arrange the Higgs-fermion couplings such that the Higgs doublet with $Y = -1$ [$Y = +1$] couples exclusively to down-type [up-type] fermions. (This insures that there are no Higgs-mediated tree-level flavor changing neutral currents.) Of the eight scalar degrees of freedom, three Goldstone bosons are absorbed by the gauge bosons, leaving five physical Higgs states: two CP-even neutral states h^0 and H^0, a CP-odd neutral state A^0, and a charged Higgs pair $H^\pm$. In addition, the model has two additional parameters: the ratio of Higgs

vacuum expectation values $\tan\beta = v_2/v_1$ and the CP-even Higgs mixing angle α (the latter arises after diagonalizing the CP-even neutral Higgs mass matrix in the basis of $Y = \pm 1$ states). The reader has surely noticed that this is precisely the Higgs spectrum of the MSSM. However, the MSSM is a highly constrained two-Higgs doublet model. Whereas the non-supersymmetric two-Higgs doublet model described above depends on six parameters (α, $\tan\beta$, and four Higgs masses), the Higgs sector of the MSSM (at tree-level) is fixed by two parameters (usually taken to be $\tan\beta$ and m_{A^0}). Both versions of the two-Higgs doublet model have been studied extensively in the literature [78].

In discussing the prospects for Higgs discovery at future colliders, one must consider two separate aspects: (i) the discovery of a light CP-even scalar (h^0) and (ii) the discovery of evidence for a non-minimal Higgs sector. It may appear that the discovery of h^0 would immediately address point (ii) as well, since if h^0 derives from a non-minimal Higgs sector, then it seems reasonable to assume that its properties will differ from ϕ^0 of the Standard Model. However, under a few very mild assumptions, one can show that in a two-Higgs doublet model where m_{h^0}, $m_Z \ll m_{A^0}$, m_{H^0}, $m_{H^\pm}$, the properties of h^0 approach those of the Standard Model* [79]. Thus, the discovery of h^0 is likely to shed no light on the possible existence of a non-minimal Higgs sector.

Present LEP bounds based on the search for the lightest CP-even Higgs boson imply that $m_{h^0} \geq 60$ GeV (assuming $h^0 = \phi^0$). At LEP-II with $\sqrt{s} \simeq 190$ GeV running at design luminosity, it should be possible to discover the h^0 or set a bound of $m_{h^0} \gtrsim m_Z$ [3]. As remarked in Lecture 2, in the MSSM the tree-level bound of $m_{h^0} \leq m_Z$ is significantly modified by radiative corrections. For $m_t = 180$ GeV, the bound reads $m_{h^0} \lesssim 130$ GeV, which implies that if the MSSM were correct, then there is a significant possibility that LEP will not discover the Higgs boson. In this circumstance, we will be forced to wait until the 21st century to get our first glimpse of the Higgs sector. The LHC will be able to probe a considerable Higgs mass range [80-86]. If $140 \lesssim m_{h^0} \lesssim 600$ GeV, then the LHC will discover the h^0 via the gold-plated signature:

$$gg \to h^0 \to ZZ \to \ell^+\ell^-\ell^+\ell^- \,, \tag{3.1}$$

under the assumption that the h^0ZZ coupling is equal to that of the minimal Higgs coupling in the Standard Model. [Note that for $m_{h^0} < 2m_Z$, at least one of the Z-bosons in Eq. (3.1) is off-shell.] For Higgs mass values in the "intermediate mass regime" of $m_Z \lesssim m_{h^0} \lesssim 140$ GeV, the Higgs search at a hadron collider is much

$\star$ This limit is called the *decoupling* limit. One can show that in most cases, the heavier Higgs states are nearly degenerate, with the mass degeneracy broken by terms of $\mathcal{O}(m_Z)$.

more difficult. The dominant signal, $gg \to h^0 \to b\bar{b}$, is completely swamped by the QCD background ($q\bar{q}$, $gg \to b\bar{b}$). Other signatures have been proposed, such as

$$\begin{aligned} &gg \to h^0 \to \gamma\gamma\,, \\ &gg \to t\bar{t}h^0\,, \qquad\qquad (h^0 \to b\bar{b} \ \text{ or } \ h^0 \to \gamma\gamma)\,, \\ &q\bar{q}' \to W^* \to Wh^0\,, \qquad (h^0 \to \gamma\gamma)\,. \end{aligned} \tag{3.2}$$

LHC detectors are being designed with some of these Higgs search channels in mind [86]. One would hope to be able to detect a signal in at least two channels in order to have confidence that a Higgs signal was being observed.

What about the prospects for detection of the other states of the non-minimal Higgs sector? At LEP-II, $H^\pm$ can be detected via $e^+e^- \to H^+H^-$, and A^0 can be detected via $e^+e^- \to h^0A^0$. Of course, if A^0, $H^\pm$ and H^0 are substantially heavier than h^0 then no evidence of the extended Higgs search will emerge prior to the era of the supercolliders. Moreover, LHC will be hard-pressed to find such states. Both $H^\pm$ and A^0 do not couple to gauge boson pairs, so that the signatures of these states at a hadron supercollider are notoriously difficult to separate from Standard Model backgrounds.

We therefore turn to the prospects of Higgs detection at the ILC. An e^+e^- linear collider with $\sqrt{s} \geq 300$ GeV will be able to fully explore the intermediate mass Higgs regime. The two primary mechanisms for Higgs production at the ILC are: (i) $e^+e^- \to Zh^0$ via s-channel Z-exchange (the same mechanism responsible for Higgs production at LEP-II energies); and (ii) $e^+e^- \to \nu\bar{\nu}h^0$ via W^+W^- fusion (this latter mechanism becomes increasingly important as $\sqrt{s}$ becomes larger). An ILC with CM-energy $300 \lesssim \sqrt{s} \lesssim 500$ GeV and an integrated luminosity of 10 to 20 fb^{-1} would have a discovery reach of $m_{h^0} \lesssim 0.7\sqrt{s}$, enough to cover completely the intermediate mass regime [87]. The LEP-II search for non-minimal Higgs states mentioned above also applies at higher energies. The various signatures appear to be detectable at the ILC if the processes are kinematically allowed (and not too close to threshold) [88–90].

3.2 Higgs boson production at a $\gamma\gamma$ collider

All e^+e^- colliders are also $\gamma\gamma$ colliders. However, the $\gamma\gamma$ luminosity resulting from the Weizsäcker-Williams spectrum of photons falls rapidly as a function of the $\gamma\gamma$ invariant mass. The ILC provides a more promising alternative for directly studying $\gamma\gamma$ collisions. By Compton backscattering of laser photons off the ILC electron and positron beams, one can produce high luminosity $\gamma\gamma$ collisions with a wide spectrum of $\gamma\gamma$ CM-energy ($E_{\gamma\gamma}$) [91–94]. In comparison with the Weizsäcker-Williams spectrum and luminosity, the $\gamma\gamma$ collider mode produces a

significantly harder $\gamma\gamma$ spectrum with a substantially higher luminosity at large $E_{\gamma\gamma}$. In addition, a high degree of circular polarization for each of the colliding photons can be achieved by polarizing the incoming electron and positron beams and the laser beams [92]. Both the $\gamma\gamma$ luminosity spectrum and subprocess cross sections are strongly influenced by the polarizations of the colliding photons.

Higgs bosons can be produced in $\gamma\gamma$ collisions via a one-loop diagram, in which all charged particles of the theory whose masses derive from the Higgs mechanism can appear inside the loop [95]. (The relevant formulae are conveniently summarized in section 2.1 of Ref. [32].) Thus, the detection of Higgs bosons in the $\gamma\gamma$ collider mode at the ILC can provide fundamental information about the particle spectrum and mass generation mechanism of the theory.

To illustrate the sensitivity of the $\gamma\gamma$-Higgs coupling to new particles that can appear in the loop, Gunion and I computed $\Gamma(\text{Higgs} \to \gamma\gamma)$ in a variety of model scenarios [96]. Our results are shown in Fig. 6. First, we compared the Standard Model to a model with one extra heavy generation of quarks and leptons. In Fig. 6, the results are exhibited in the case of a mass-degenerate heavy fourth generation quark doublet of mass 500 GeV and a heavy charged lepton of mass 300 GeV. These mass values were chosen so that none of the fourth generation fermions could be pair produced at an e^+e^- linear collider with $\sqrt{s} = 500$ GeV (ILC-500). Note that even a crude measurement of the $\gamma\gamma$-Higgs coupling would be sufficient to distinguish between the three and four generation Standard Model (except in a small Higgs mass region where the ratio of $\gamma\gamma$ couplings is accidentally near 1).

Next, consider the case of the MSSM. Suppose the lightest CP-even Higgs boson has been discovered, but no experimental evidence for either the heavier Higgs bosons or any supersymmetric particles has been found at the ILC. Could a measurement of the $h^0\gamma\gamma$ coupling provide indirect evidence for physics beyond the Standard Model? Unfortunately, the answer is no. If the MSSM parameters are chosen such that all new particles beyond the Standard Model are too heavy to be produced at the ILC-500, then the deviation of $\Gamma(h^0 \to \gamma\gamma)$ from the corresponding Standard Model value is less than 15%. Because of decoupling, as the supersymmetry breaking scale and the scale of the heavier Higgs bosons become large, all couplings of the h^0 approach their Standard Model values. This is illustrated in Fig. 6 where we plot the ratio $\Gamma(h^0 \to \gamma\gamma)/\Gamma(\phi^0 \to \gamma\gamma)$, as a function of the Higgs mass, for chargino mass parameters $M_2 = -\mu = 300$ GeV and a common soft-supersymmetry-breaking diagonal mass of 300 GeV for all squarks and sleptons, with all off-diagonal squark and slepton masses set to zero. Even with the MSSM parameters chosen such that the supersymmetric partners lie just beyond the reach of ILC-500, the ratio of $\gamma\gamma$ decay widths is still close to 1 (in Fig. 6, the plotted ratio lies between 0.89 and 0.94).

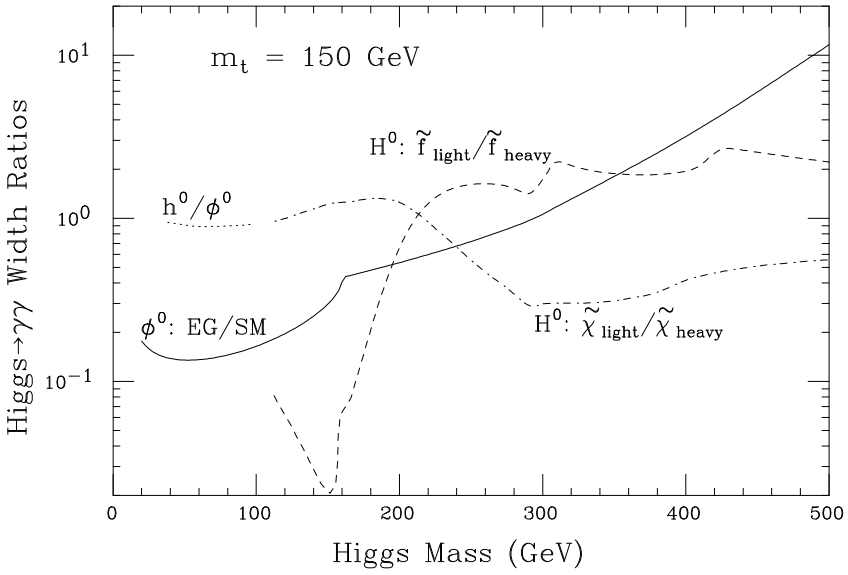

Fig. 6 The ratio of $\Gamma(\text{Higgs} \to \gamma\gamma)$ computed in two different models, for a number of model choices. For the Standard Model (SM) ϕ^0: the ratio of $\Gamma(\phi^0 \to \gamma\gamma)$ as computed in the 4-generation *vs.* the 3-generation SM, as a function of m_{ϕ^0} (solid curve). The extra generation (EG) of fermions includes a 300 GeV charged lepton and a mass-degenerate 500 GeV quark doublet. For the MSSM h^0: the ratio $\Gamma(h^0 \to \gamma\gamma)/\Gamma(\phi^0 \to \gamma\gamma)$ as a function of $m_{h^0} = m_{\phi^0}$ (dotted curve), with $m_{A^0} = 400$ GeV. Squarks and charginos have been taken to be as light as possible without being observable at ILC-500 (see text). For the MSSM H^0, two curves are shown. The dot-dashed curve is $\Gamma(H^0 \to \gamma\gamma)$ in a model with light charginos ($M_2 = -\mu = 150$ GeV) divided by the corresponding width with heavy charginos ($M_2 = -\mu = 1$ TeV), keeping the squarks and sleptons heavy (with masses of order 1 TeV); the dashed curve is $\Gamma(H^0 \to \gamma\gamma)$ in a model with light squarks and sleptons (see text) divided by the corresponding width computed with heavy squarks and sleptons, keeping the charginos heavy as before. For the latter two curves, the ratio of widths is plotted as a function of m_{H^0}, for $\tan\beta = 2$. Taken from Ref. [96].

On the other hand, suppose that some of the other Higgs bosons of the MSSM ($H^\pm$, H^0 and/or A^0) are light enough to be produced and studied at the ILC. In this case, a measurement of the $\gamma\gamma$ couplings of H^0 and A^0 can provide useful information on the spectrum of charged supersymmetric particles (even if the latter are too heavy to be directly produced at the ILC).* Figure 6 provides two examples of the sensitivity of the $H^0\gamma\gamma$ couplings to supersymmetric particle masses. Suppose that the masses of all supersymmetric particles appearing in the loop (charginos, squarks, and sleptons) are 1 TeV in mass. Consider then two different scenarios: (i) light charginos and heavy squarks and sleptons (with chargino parameters

$\star$ The widths of H^0 and A^0 into $\gamma\gamma$ will almost always differ from the width of the Standard Model Higgs boson and vary as a function of the MSSM parameters.

$M_2 = -\mu = 150$ GeV), and (ii) light squarks and sleptons and heavy charginos (with a common soft-supersymmetry breaking diagonal mass of 150 GeV for all squarks and sleptons, and with all off-diagonal squark and slepton masses set to zero).† The ratio of $H^0 \to \gamma\gamma$ widths (relative to the case of 1 TeV supersymmetric particle masses) in these two scenarios is depicted in Fig. 6 and demonstrates the sensitivity of the $H^0\gamma\gamma$ coupling to the details of the supersymmetric spectrum.

The connection between the $H\gamma\gamma$ coupling and the Higgs production rate in $\gamma\gamma$ collisions is most conveniently expressed in terms of the $H \to \gamma\gamma$ decay width.⋆ For a given value of the $\gamma\gamma$ CM-energy $E_{\gamma\gamma}$ we have:

$$\sigma(\gamma\gamma \to H \to X) = \frac{8\pi\Gamma(H \to \gamma\gamma)\Gamma(H \to X)}{(E^2_{\gamma\gamma} - m^2_H)^2 + \Gamma^2_H m^2_H}(1 + \lambda\lambda')\,, \tag{3.3}$$

where $\Gamma_H \equiv \Gamma(H \to \text{all})$ is the total decay width of H, and λ and λ' $(= \pm 1)$ are the helicities of the two colliding photons.

The final states X of greatest interest are W^+W^-, ZZ and $Q\overline{Q}$ (with $Q = b$ or t). In this section, I shall focus on $X = Q\overline{Q}$; see Refs. [94] and [96] for the analysis of other possible final state signals (and their corresponding backgrounds). In order to compute the expected number of Higgs bosons, Eq. (3.3) must be folded together with the appropriate $\gamma\gamma$ luminosity. The number of Higgs bosons produced and detected is given by:

$$N(\gamma\gamma \to H \to Q\overline{Q}) = \int_{y_-}^{y_+} dy\, \frac{d\mathcal{L}_{\gamma\gamma}}{dy}\sigma_{\gamma\gamma\to H\to Q\overline{Q}}(E_{\gamma\gamma} = yE_{e^+e^-})\,, \tag{3.4}$$

where $d\mathcal{L}_{\gamma\gamma}/dy$ is the differential $\gamma\gamma$ luminosity as a function of $y \equiv E_{\gamma\gamma}/E_{e^+e^-}$ and $y_\pm = (m_H \pm \Gamma_{\rm res}/2)/E_{e^+e^-}$. Here, $\Gamma_{\rm res}$ is a resolution factor which is chosen to maximize the significance of the $\gamma\gamma \to H \to Q\overline{Q}$ signal over the $\gamma\gamma \to Q\overline{Q}$ continuum background. In Ref. [96], Gunion and I adopted a strategy of integrating over a region of $E_{\gamma\gamma}$ of size $\Gamma_{\rm res} \equiv \max\{\Gamma_{\rm exp}, \Gamma_H\}$, where $\Gamma_{\rm exp}$ is the experimental

† In the light squark and slepton scenario (with $\tan\beta = 2$), all sleptons and squarks, with the exception of the top-squark are roughly degenerate in mass, ranging between 141 and 157 GeV, while the two top-squark masses are 208 and 210 GeV, respectively. Thus, there are two distinct thresholds for squark (and slepton) pair production, which account for the two dips on the corresponding curve in Fig. 6.

⋆ Henceforth, the symbol H will be used to denote any neutral CP-even or CP-odd Higgs boson.

$Q\overline{Q}$ mass resolution and Γ_H is the total Higgs width. If one defines

$$\frac{d\mathcal{L}_{\gamma\gamma}}{dy} \equiv F(y)\mathcal{L}_{e^+e^-} , \tag{3.5}$$

then $F(y)$ and the average value of $\lambda\lambda'$ at y [denoted by $\langle\lambda\lambda'\rangle_y$] are obtained after convoluting over the possible energies and polarizations of the colliding photons that yield a fixed value of y. Both quantities will depend upon the experimental arrangement for creating the back-scattered laser beams, the polarization of the incoming electron and positron, and the polarizations of the two initial laser beams [91–94]. In the present discussion, it is a good approximation to assume that both $F(y)$ and $\langle\lambda\lambda'\rangle_y$ are constant over the region of integration in Eq. (3.4) where the Higgs cross section is dominant.

It is a simple exercise to compute the number of detected Higgs events directly from Eq. (3.4). If $F(y)$ and $\langle\lambda\lambda'\rangle_y$ are slowly varying,

$$\begin{aligned} N(\gamma\gamma \to H \to Q\overline{Q}) =& \frac{8\pi BR(H\to X)}{E_{e^+e^-}m_H^2} \tan^{-1}\left(\frac{\Gamma_{\rm res}}{\Gamma_H}\right)\Gamma(H\to\gamma\gamma) \\ & \times F(y_H)(1+\langle\lambda\lambda'\rangle_{y_H})\mathcal{L}_{e^+e^-} , \end{aligned} \tag{3.6}$$

where $y_H \equiv m_H/E_{e^+e^-}$. Note that in the limit where $\Gamma_{\rm exp} \gg \Gamma_H$ the inverse tangent approaches $\pi/2$, and N is independent of $\Gamma_{\rm res}$.

As already noted, $F(y)$ and $\langle\lambda\lambda'\rangle_y$ can be adjusted by appropriately choosing the experimental arrangement and polarizations of the electron, positron and two initial laser beams. The basic formalism for computing these quantities appears in Ref. [92] and a large number of specific cases were examined in Ref. [94]. For the reader's convenience, the most important points are reviewed here. Define λ_e (λ_e') and P_c (P_c') to be the helicity and circular polarization of the electron and corresponding laser beam responsible for producing photon 1 (photon 2). It is useful to consider the extreme cases of $2\lambda_e P_c = \pm 1$, *i.e.*, maximal helicity for the incoming electron and full circular polarization for the initial laser photon. For $2\lambda_e P_c = -1$ the energy spectrum of photon 1 is peaked just below the highest allowed photon energy, whereas for $2\lambda_e P_c = +1$ one finds a rather flat spectrum over a broad range of photon energy falling sharply to zero as one approaches the maximum possible energy. Meanwhile, the helicity of the back-scattered photon, λ, approaches $+P_c, -P_c$ for photon energy equal to zero or the maximum allowed, respectively. In the case of $2\lambda_e P_c = 1$, $\lambda = +P_c$ over almost the entire photon energy range; only very near to the maximum allowed energy does λ change sign and approach $-P_c$. In contrast, in the case of $2\lambda_e P_c = -1$, associated with a

peaked energy spectrum, λ slowly switches sign in the middle of the allowed energy range. Note that it is unlikely that the (*a priori* unknown) Higgs boson mass will be approximately equal to the full e^+e^-energy. Thus, the flat energy spectrum obtained for $2\lambda_e P_c = +1$ will generally be preferred for Higgs boson searches. In addition, one sees that this choice will imply a relatively constant (and large) value for $|\lambda|$ over most of the energy range of interest.

The functions $F(y)$ and $\langle\lambda\lambda'\rangle_y$ are obtained by convoluting together the spectra and polarizations for the individual photons 1 and 2. In order to maximize the Higgs cross section, one sees from Eq. (3.6) that it is desirable to have as large a value for $F(y_H)$ as possible *and* to have $\langle\lambda\lambda'\rangle_{y_H} \sim +1$. Moreover, we shall see below that $Q\overline{Q}$ backgrounds are proportional to $1 - \langle\lambda\lambda'\rangle_{y_H}$ for $m_H \gg 2m_Q$, and will be suppressed if $\langle\lambda\lambda'\rangle_{y_H} \sim +1$. Typical behaviors for $F(y)$ and $\langle\lambda\lambda'\rangle_y$ are illustrated in Ref. [94] and can be summarized as follows. First, at e^+e^- energies of the order of 500 GeV, the kinematic limit for $E_{\gamma\gamma}$ is roughly $0.8E_{e^+e^-}$; *i.e.*, $y^{\rm max} \sim 0.8$ for the typical machine design. Second, one finds that large $F(y)$ and $\langle\lambda\lambda'\rangle_y \sim +1$ can be *simultaneously* achieved for all y between ~ 0.1 and $y^{\rm max}$. For Higgs searches below about $0.7E_{e^+e^-}$, it is most useful to employ the broad spectrum for $F(y)$ that results from choosing $2\lambda_e P_c$ and $2\lambda'_e P'_c$ both as close to $+1$ as possible. For these choices and typical machine design parameters at $E_{e^+e^-} = 500$ GeV, $F(y) \gtrsim 1$ for 50 GeV $\lesssim E_{\gamma\gamma} \lesssim$ 350 GeV, *i.e.*, for y values between 0.1 and 0.7. If, in addition to choosing $2\lambda_e P_c = +1$, $2\lambda'_e P'_c = +1$, we also have $P_c P'_c \sim +1$ then $\langle\lambda\lambda'\rangle_y$ is near $+1$ for this entire range, $y \lesssim 0.7$. For Higgs searches between $y \sim 0.7$ and $y \sim y^{\rm max}$, $F(y) \gtrsim 1$ and $\langle\lambda\lambda'\rangle_y \sim +1$ can again be simultaneously achieved by the alternative choices of $2\lambda_e P_c = 2\lambda'_e P'_c = -1$, $P_c P'_c = +1$. Thus, there is a fortunate conspiracy in which polarization choices can be made that yield large $\gamma\gamma$ luminosity (for $0.1 \lesssim y \lesssim y^{\rm max}$) and also maximize the Higgs cross section while tending to suppress backgrounds.

In order to establish the significance of the Higgs signal, one must consider the background from $\gamma\gamma \to Q\overline{Q}$ [94,96,97]. The differential cross section for $\gamma(\lambda) + \gamma(\lambda') \to Q\overline{Q}$ is

$$\frac{d\sigma}{dz} = \frac{4\pi\alpha^2 e_Q^4 N_c \beta \left[1 - \beta^4 + \frac{1}{2}(\lambda\lambda' - 1)(1 + \beta^2 z^2)(1 - 2\beta^2 + \beta^2 z^2)\right]}{s(1 - \beta^2 z^2)^2}\,, \qquad (3.7)$$

where $z \equiv \cos\theta$ is the cosine of the angle of the outgoing heavy quark, Q, relative to the beam direction in the $\gamma\gamma$ CM-frame, e_Q is the quark charge (in units of e), m_Q is the quark mass, $\beta \equiv (1 - 4m_Q^2/s)^{1/2}$, and $s \equiv E_{\gamma\gamma}^2$. For $m_Q = 0$, one can easily check that Eq. (3.7) reproduces the results of my Lecture 1 computation [see Eq. (1.91)]. If $E_{\gamma\gamma} \gg 2m_Q$ (*i.e.*, $\beta \to 1$) then the cross section for this

background subprocess is strongly suppressed for $\lambda\lambda' = +1$, the choice which maximizes the Higgs boson cross section as discussed above. Furthermore, for $\beta \to 1$, the cross section is strongly forward-backward peaked as a function of z, whereas the $H \to Q\overline{Q}$ decay is isotropic. Thus, to maximize the significance of the Higgs boson signal in the $b\overline{b}$ channel it is desirable to arrange for a value of $\langle\lambda\lambda'\rangle_{y_H}$ as near to $+1$ as possible, and to integrate signal and background over a region $|z| < z_0$ away from $|z| = 1$. Even in the $t\overline{t}$ channel this same procedure provides some improvement in the statistical significance of the Higgs signal, despite the fact that $2m_t$ is only somewhat smaller than m_H.

Integrating Eq. (3.7) over the region $|z| \leq z_0 < 1$ yields

$$\sigma_{Q\overline{Q}}(s,z_0) = \frac{4\pi\alpha^2 e_Q^4 N_c}{s}\Bigg\{ -\beta z_0\left[1+\frac{(1-\beta^2)^2}{(1-\beta^2 z_0^2)}\right] + \tfrac{1}{2}\left[3-\beta^4\right]\log\frac{1+\beta z_0}{1-\beta z_0} + \lambda\lambda'\beta z_0\left[1+\frac{2(1-\beta^2)}{1-\beta^2 z_0^2} - \frac{1}{\beta z_0}\log\frac{1+\beta z_0}{1-\beta z_0}\right]\Bigg\}. \tag{3.8}$$

The effectiveness of using polarization and angular cuts in reducing the $\gamma\gamma \to Q\overline{Q}$ background is clear. For example, if both β and $\lambda\lambda'$ are near 1, then Eq. (3.8) yields

$$\sigma_{Q\overline{Q}}(s,z_0) \simeq \frac{4\pi\alpha^2 e_Q^4 N_c}{s}\Bigg\{(1-\beta^2)\left[\frac{2z_0}{1-z_0^2} + \ln\left(\frac{1+z_0}{1-z_0}\right)\right] + (\lambda\lambda'-1)\left[z_0 - \ln\left(\frac{1+z_0}{1-z_0}\right)\right]\Bigg\}. \tag{3.9}$$

That is, for $\lambda\lambda' = 1$, the cross-section is suppressed by a factor of $1-\beta^2$, as expected from our previous analysis. The effectiveness of the cut on the decay angle in reducing the $Q\overline{Q}$ background can be seen in the following example. For $Q = b$ and $\sqrt{s} = E_{\gamma\gamma} = 300$ GeV, choosing $z_0 = 0.5$ reduces the $Q\overline{Q}$ cross section by a factor of 14, while retaining 50% of the Higgs events. This yields a net gain by a factor of 7 in Higgs signal over background. We can compute the net number of background events by multiplying the cross section of Eq. (3.8) by the integral of $d\mathcal{L}_{\gamma\gamma}/dy$ [Eq. (3.5)] over the interval $\Delta y = \Gamma_{\rm res}/E_{e^+e^-}$, with $\Gamma_{\rm res}$ defined below Eq. (3.4)

$$N(\gamma\gamma \to Q\overline{Q}) = \frac{\Gamma_{\rm res}}{E_{e^+e^-}} F(y_H)\mathcal{L}_{e^+e^-}\sigma_{Q\overline{Q}}(m_H^2, z_0)\,. \tag{3.10}$$

For numerical estimates, Gunion and I took $F(y_H)\mathcal{L}_{e^+e^-} = 2\times10^{33}$ cm^{-2} sec^{-1} *i.e.*, an integrated luminosity of 20 fb^{-1} for a standard collider year, and we chose

$\langle\lambda\lambda'\rangle_{y_H} = 0.8$. As discussed previously, these choices for $F(y_H)$ and $\langle\lambda\lambda'\rangle_{y_H}$ are both well within the range of possibility for $y_H \lesssim 0.8$ (*e.g.*, $E_{\gamma\gamma} \lesssim 400$ GeV at $E_{e^+e^-} = 500$ GeV). Detector resolution was assumed to be such that $\Gamma_{\rm exp} = 5$ GeV is possible for the observation of $H \to Q\overline{Q}$. When considering $Q\overline{Q}$ final states, we employed the background cross section given in Eq. (3.8). Since the Higgs decays to $Q\overline{Q}$ are uniform in $z = \cos\theta$, the effect of the angular cut on the number of Higgs events in a $Q\overline{Q}$ final state is simply to multiply the total event rate by a factor of z_0. In our numerical work, we found that the value $z_0 = 0.85$ was the most effective in reducing the $Q\overline{Q}$ background.

In Fig. 7 we present results for the Standard Model Higgs boson, ϕ^0. Results for two choices of top quark mass: $m_t = 150$ GeV and $m_t = 200$ GeV are shown. It is apparent that where $\phi^0 \to b\bar{b}$ decays are dominant, ϕ^0 masses down to roughly 40 GeV can be probed. In contrast, the $t\bar{t}$ mode never has a sufficiently large branching ratio (due to the dominance of the vector boson pair decay modes of the ϕ^0 above the W^+W^- threshold) to be useful, given the large size of the $\gamma\gamma \to t\bar{t}$ background. The importance of polarization for enhancing the statistical significance of the Higgs signal in the $b\overline{b}$ channel is illustrated in Fig. 8, which depicts the maximum and minimum masses for which the number of Higgs signal events (S) and background events (B) are such that $S > 10$ and the number of standard deviations [$N_{SD} \equiv S/\sqrt{B}$] is greater than 5. From Fig. 8, it is clear that being able to achieve large $\langle\lambda\lambda'\rangle$ greatly expands the mass range over which the ϕ^0 can be detected in the $b\overline{b}$ channel. Unfortunately, detection of the ϕ^0 in the $t\overline{t}$ channel is not possible even with perfect polarization.

In the case of the Higgs bosons of the MSSM, results will be presented for one moderate value of $\tan\beta = 2$ and one large value of $\tan\beta = 20$, and two choices of top quark mass as in the previous analysis. The masses of all the supersymmetric partners, in particular, the charginos, neutralinos, squarks, and sleptons are assumed to be large. This means not only that they will not enter into the Higgs decay modes, but also, in the case of the charged supersymmetric particles, their contributions to the $\gamma\gamma$ couplings at one-loop will be small. Results for the heavier CP-even state H^0 and for the CP-odd A^0 are given in Figs. 9 and 10, respectively. Sensitivity of the $m_t = 150$ GeV, $\tan\beta = 2$ results for the H^0, A^0 and h^0 to the degree of polarization that can be achieved is illustrated in Figs. 8 and 11, for the $b\overline{b}$ and $t\overline{t}$ channels, respectively. Figure 8 shows the minimal and maximal observable masses, $m_{H^0}^{\rm max,min}$, $m_{A^0}^{\rm min}$, and $m_{h^0}^{\rm min}$, as defined using the criteria stated earlier for ϕ^0. Not explicitly plotted are: $m_{A^0}^{\rm max}$, which is always very close to $2m_t = 300$ GeV; and $m_{h^0}^{\rm max}$ which is equal to the theoretical upper limit for m_{h^0} within the MSSM [see Eq. (2.3)]. That is, the $h^0 \to b\overline{b}$ channel satisfies the criteria for observability for all m_{h^0} masses above $m_{h^0}^{\rm min}$. Note how close $m_{h^0}^{\rm min}$

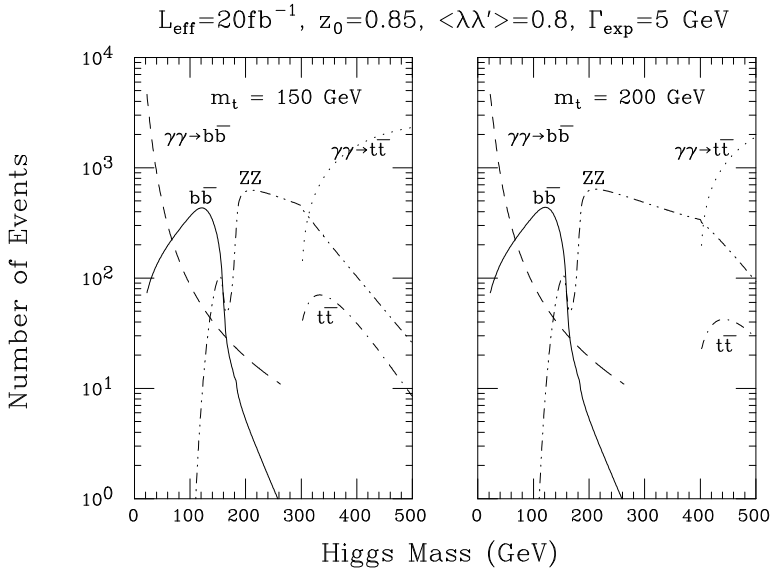

Fig. 7. Number of events per year for the Standard Model Higgs boson ($\phi^0 \to b\bar{b}$, $\phi^0 \to t\bar{t}$, $\phi^0 \to ZZ$) and for the $Q\overline{Q}$ backgrounds ($\gamma\gamma \to b\bar{b}$ and $\gamma\gamma \to t\bar{t}$). In computing event rates for the $Q\overline{Q}$ ($Q = b, t$) final states, an angular cut of $|\cos\theta| \leq z_0 = 0.85$ is imposed and a $Q\overline{Q}$ mass resolution of 5 GeV has been assumed. Taken from Ref. [96].

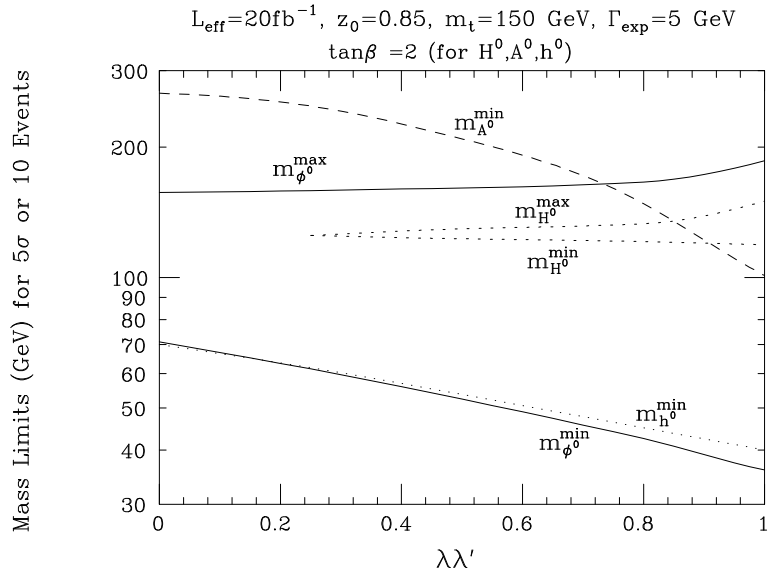

Fig. 8. Minimum and maximum Higgs masses for which the number of standard deviations of the Higgs signal in the $b\bar{b}$ channel $N_{SD} \geq 5$ and the number of signal Higgs events $S \geq 10$, as a function of $\langle\lambda\lambda'\rangle$. Both Standard Model and MSSM Higgs boson signals are exhibited, with $m_t = 150$ GeV and $\tan\beta = 2$. Not shown explicitly is $m^{\max}_{A^0}$ which is always very close to $2m_t = 300$ GeV. The $h^0 \to b\bar{b}$ signal is statistically significant for all m_{h^0} masses from $m^{\min}_{h^0}$ up to its theoretical limit. Taken from Ref. [96].

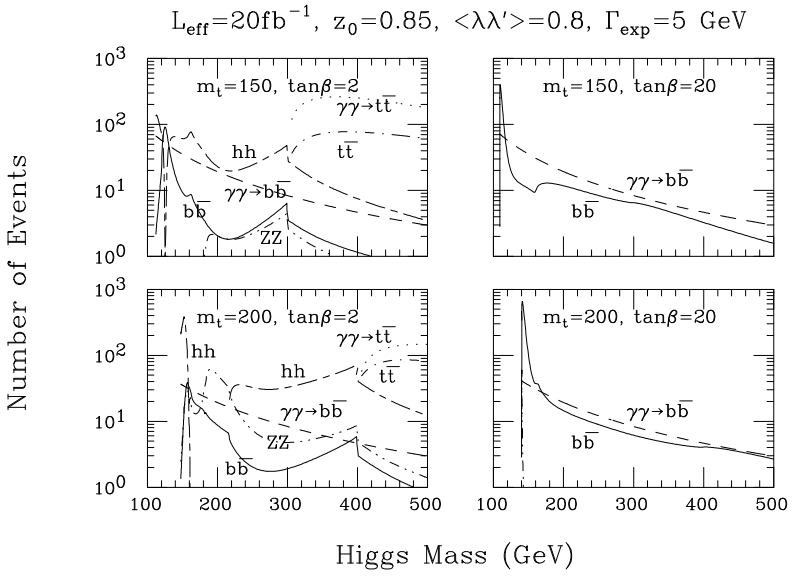

Fig. 9. As in Fig. 7, but for the heavy CP-even Higgs boson of the MSSM, H^0. The exotic $H^0 \to h^0 h^0$ decay mode event rate is also shown. (It should be noted that in the region $165 \lesssim m_{H^0} \lesssim 220$ GeV, the decay $H^0 \to h^0 h^0$ is kinematically forbidden for the MSSM parameters chosen.) Supersymmetric partners are assumed to be sufficiently heavy that they do not influence the $H^0\gamma\gamma$ coupling or H^0 decays. Radiative corrections to the MSSM Higgs sector are incorporated with $M_{\rm SUSY} = 1$ TeV and squark mixing neglected. Results for $m_t = 150$ GeV and $m_t = 200$ GeV are displayed for both $\tan\beta = 2$ and $\tan\beta = 20$.

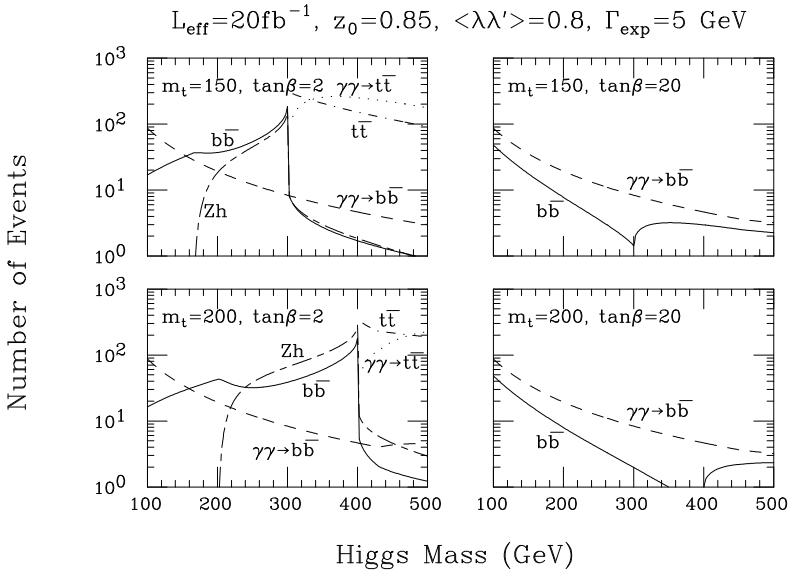

Fig. 10. As in Fig. 9, but for the CP-odd Higgs boson of the MSSM, A^0. The exotic $A^0 \to Zh^0$ decay mode event rate is shown. The A^0 has no tree-level couplings to vector boson pairs, so that the ZZ final state is not present.

is to the corresponding Standard Model Higgs result [see Fig. 7]; this is simply a reflection of how similar the h^0 is to the ϕ^0 of the same mass once m_{A^0} is large enough. Clearly, the range of masses for which the A^0 and h^0 are detectable is greatly diminished if a high degree of polarization cannot be achieved. For the $t\bar{t}$ channel, detection of the H^0 and A^0 for Higgs masses above $2m_t$ should generally be possible for $\langle\lambda\lambda'\rangle = 0.8$. Figure 11 shows the value of N_{SD} achieved in the $t\bar{t}$ channel at $m_{A^0}, m_{H^0} = 500$ GeV as a function of $\langle\lambda\lambda'\rangle$. These results clearly indicate that in spite of the large t-quark mass, polarization can still play a critical role in the observability of the A^0 and H^0 in the $t\bar{t}$ channel.

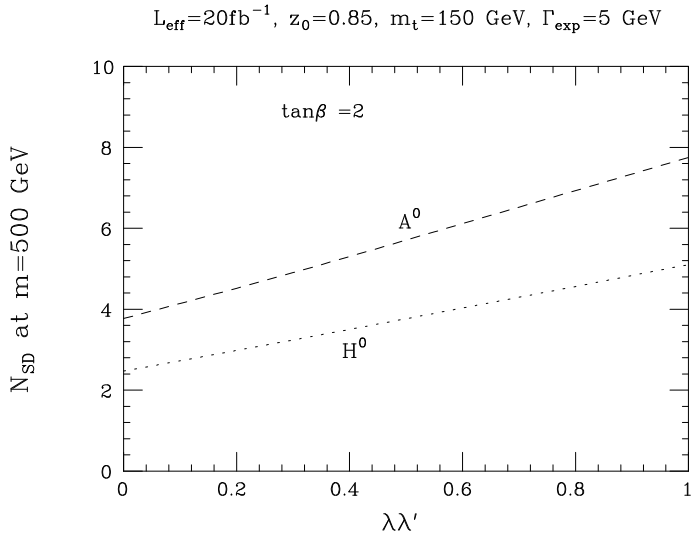

Fig. 11. Statistical significance (*i.e.*, number of standard deviations N_{SD}) of the $A^0 \to t\bar{t}$ and $H^0 \to t\bar{t}$ Higgs signals at $m_{A^0}, m_{H^0} = 500$ GeV as a function of $\langle\lambda\lambda'\rangle$, for $m_t = 150$ GeV and $\tan\beta = 2$. $\Gamma_{\rm res}$ and z_0 are chosen as in Fig. 7.

In summary, detection of the Standard Model ϕ^0 should be possible for all Higgs masses between the present day LEP lower limit up to the $\gamma\gamma$ collider kinematic limit (roughly $E_{\gamma\gamma}^{\rm max} \simeq 0.8E_{e^+e^-}$). That is, the kinematic reach of the ILC for ϕ^0 detection is somewhat increased (relative to the limit of $m_{\phi^0} \lesssim 0.7E_{e^+e^-}$ achievable in conventional e^+e^- collisions) using the $\gamma\gamma$ collider mode option, while at the same time the $\gamma\gamma$ coupling of the ϕ^0 is determined. In the case of the MSSM Higgs bosons, the $\gamma\gamma$ collider mode at the ILC proves to be an enormously powerful tool. For moderate $\tan\beta$, detection of the H^0 and A^0 will be possible for all masses up to roughly the $\gamma\gamma$ collider kinematical limit, often in more than one final state decay mode. This represents a significant increase in Higgs mass reach as compared to a Higgs mass limit of roughly $0.4E_{e^+e^-}$ obtained by using the ILC in its search for $e^+e^- \to h^0A^0, H^0A^0$. For large $\tan\beta$, a four-fold increase in $\gamma\gamma$ luminosity

beyond that assumed in this section would allow H^0 detection for all masses up to the $E_{\gamma\gamma}$ kinematic limit. In reaching these optimistic conclusions, the ability to achieve substantial polarization for the colliding photon beams has been assumed. We have illustrated the fact that the mass ranges for which the Standard Model and MSSM Higgs bosons can be detected deteriorate significantly as the degree of polarization decreases, especially in the $b\overline{b}$ and $t\overline{t}$ channels. Every effort should be made to achieve the highest possible polarization for the colliding photons.

3.3 Search for CP-violating effects in the Higgs sector

In the Standard Model with one Higgs weak doublet, the physical Higgs boson is a CP-even scalar with CP-conserving tree-level interactions. In the MSSM, the Higgs sector consists of two scalar weak doublets. But, due to the supersymmetric constraints which restrict the form of the scalar potential, the physical scalar mass eigenstates are states of definite CP, with tree-level CP-conserving interactions.[⋆] However, in non-supersymmetric models with a non-minimal Higgs sector, and in non-minimal supersymmetric models, the scalar sector typically contains sources of CP-violation. It is possible that Higgs-sector CP-violation effects could be detected in low-energy processes (such as in the interactions of K and B-mesons, or the neutron electric dipole moment). However, the absence of such low-energy effects does not necessarily imply that CP-violating Higgs effects must be absent. It could turn out that Higgs induced CP-violating effects can only be seen directly in high-energy processes in which the Higgs bosons are produced. One consequence of CP-violation in the Higgs self-interactions is that the neutral scalar Higgs mass eigenstates are no longer eigenstates of CP. In other words, the neutral Higgs mass eigenstates are mixtures of CP$= \pm 1$ scalar states.

In this section, I shall discuss a technique suggested by Gunion and collaborators [98,99] for detecting the existence of CP-violating Higgs interactions by searching for scalar states with mixed CP quantum numbers. One might think that if the Higgs boson were discovered, its CP-quantum numbers could be determined from its production characteristics and/or the energy and angular distribution of its decay products. Such methods will fail if the Higgs boson is detected through its interactions with massive gauge bosons. For example, at e^+e^- colliders, the Higgs boson is typically produced either by bremsstrahlung off the Z-boson or via W^+W^- fusion. In addition, in many cases, W^+W^- and Z^0Z^0 are the dominant decay modes of the heavy Higgs boson. However, at tree-level, the ZZ or W^+W^- couples only to the CP-even part of a CP-mixed scalar state.[†]

⋆ Soft-supersymmetry breaking terms do not affect this conclusion [see Eq. (2.1)].

† The coupling of a CP-odd scalar to two gauge bosons takes the form $\epsilon^{\mu\nu\alpha\beta}F^a_{\mu\nu}F^a_{\alpha\beta}$ which can only arise in one-loop (or higher-loop) radiative corrections.

The $\gamma\gamma$ collider provides an efficient environment for the detection of mixed CP properties (if present) of the neutral Higgs bosons since $\gamma\gamma$ does not possess tree-level couplings to the neutral Higgs states. At one-loop, $\gamma\gamma$ couples to both the CP= ± 1 pieces of the scalar state. The corresponding matrix elements are proportional to

$$\begin{aligned} \mathcal{M}(\gamma\gamma h^0) &\sim \hat{\boldsymbol{\epsilon}} \cdot \hat{\boldsymbol{\epsilon}}' \,, \\ \mathcal{M}(\gamma\gamma A^0) &\sim \hat{\boldsymbol{\epsilon}} \times \hat{\boldsymbol{\epsilon}}' \,. \end{aligned} \tag{3.11}$$

where $\hat{\boldsymbol{\epsilon}}$ is the space components of the spin-1 polarization vector [Eq. (1.54)]. The availability of polarized bosons is particularly useful, and provides a number of CP-violating asymmetries:

$$\begin{aligned} \mathcal{A}_1 &\equiv \frac{|\mathcal{M}_{++}|^2 - |\mathcal{M}_{--}|^2}{|\mathcal{M}_{++}|^2 + |\mathcal{M}_{--}|^2} \,, \\ \mathcal{A}_2 &\equiv \frac{2\,\mathrm{Im}\,(\mathcal{M}_{++}\mathcal{M}_{--}^*)}{|\mathcal{M}_{++}|^2 + |\mathcal{M}_{--}|^2} \,, \\ \mathcal{A}_3 &\equiv \frac{2\,\mathrm{Re}\,(\mathcal{M}_{++}\mathcal{M}_{--}^*)}{|\mathcal{M}_{++}|^2 + |\mathcal{M}_{--}|^2} \,, \end{aligned} \tag{3.12}$$

where $\mathcal{M}_{\lambda\lambda'}$ is the amplitude for $\gamma(\lambda) + \gamma(\lambda') \to H$. Each asymmetry can lie between -1 and 1. $\mathcal{A}_1 \neq 0$, $\mathcal{A}_2 \neq 0$, and/or $|\mathcal{A}_3| < 1$ would all constitute signals of CP-violation.

Grzadkowski and Gunion [98] have computed the three asymmetries above for a scalar Higgs field arising from the most general CP-nonconserving two-Higgs doublet model. They repeat the asymmetry calculation many times, searching over the model parameter space for the maximum CP-violating signal. This is accomplished by choosing a particular value of m_t, $\tan\beta$ and Higgs mass, and varying at random the Higgs mixing angles, *i.e.*, the parameters that specify the Higgs mass eigenstates (relative to the interaction eigenstate basis). In Fig. 12, the asymmetries defined in Eq. (3.12) are plotted as a function of the Higgs mass for $m_t = 150$ GeV and $\tan\beta = 2$. Each asymmetry plotted is the maximum asymmetry achievable as the Higgs mixing angles are varied, for the specified Higgs mass. The maximal CP-violating asymmetries can be large, and the statistical significance of the signal scales with the square root of the number of events. Under plausible operating conditions for a $\gamma\gamma$ collider operating at a CM energy of 500 GeV, with an integrated luminosity of 20 fb^{-1}, the authors of Ref. [98] show that the asymmetry $\mathcal{A}_1$ is the most promising for the detection of a CP-violating signal.

At hadron supercolliders, the dominant mechanism for Higgs production is gluon-gluon fusion to the Higgs boson through a heavy quark loop. Since the same

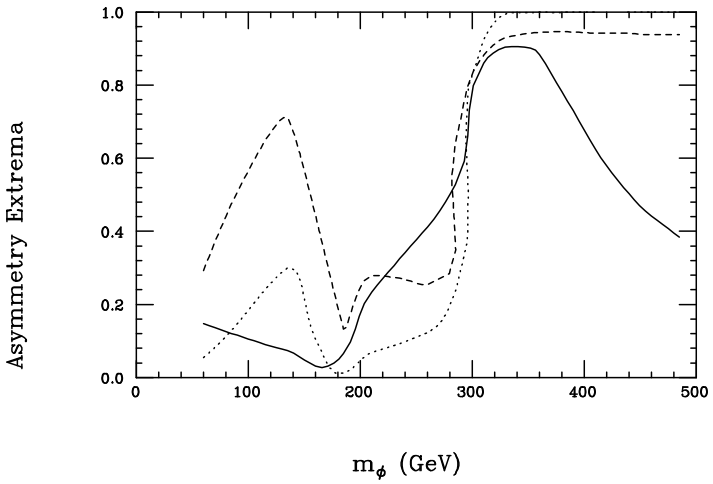

Fig. 12. The values for $|\mathcal{A}_1|$ (———) and $|\mathcal{A}_2|$ ($-\ -\ -\ -$) and $(1-|\mathcal{A}_3|)$ ($\cdot\ \cdot\ \cdot\ \cdot\ \cdot\ \cdot$) which yield the largest standard scenario statistical significances, as a function of m_{ϕ^0}, for $\tan\beta = 2$ and $m_t = 150$ GeV. Extrema are obtained for 150,000 random choices of Higgs mixing angles subject to the requirement that there be at least 80 events in the $b\overline{b}$ decay channel of the ϕ^0, or 20 events in the ZZ (one $Z \to \ell^+\ell^-$) channel, or 80 events in the $t\overline{t}$ channel when the colliding photon polarizations are averaged over. Taken from Ref. [98].

diagram gives rise to the Higgs coupling to $\gamma\gamma$ (where the gluons are replaced by photons), one can also search for a CP-violating asymmetry at hadron supercolliders with polarized beams. Of course, in this case, the theoretical prediction for the asymmetry and its experimental detection are not as clean (compared to the case of the $\gamma\gamma$ collider discussed above). For example, one does not polarize the gluons directly; rather one must polarize the initial proton beams, and attempt to determine the resulting gluon polarization, based on a model (making the best possible use of polarized deep inelastic scattering data to determine the polarized gluon distribution function). In order to detect a CP-violating signal, it is sufficient to polarize one of the proton beams. The CP-violating asymmetry of interest is

$$\mathcal{A} \equiv \frac{\sigma_+ - \sigma_-}{\sigma_+ + \sigma_-}\,, \tag{3.13}$$

where σ_λ is the Higgs production cross-section for the case of one proton beam with helicity λ. To evaluate $\mathcal{A}$, one must compute the asymmetry at the partonic level, and then fold in the helicity-dependent gluon distribution function. Let $\Delta g(x) \equiv g_+(x) - g_-(x)$, where $g_+(x)$ $[g_-(x)]$ is the probability of finding a gluon

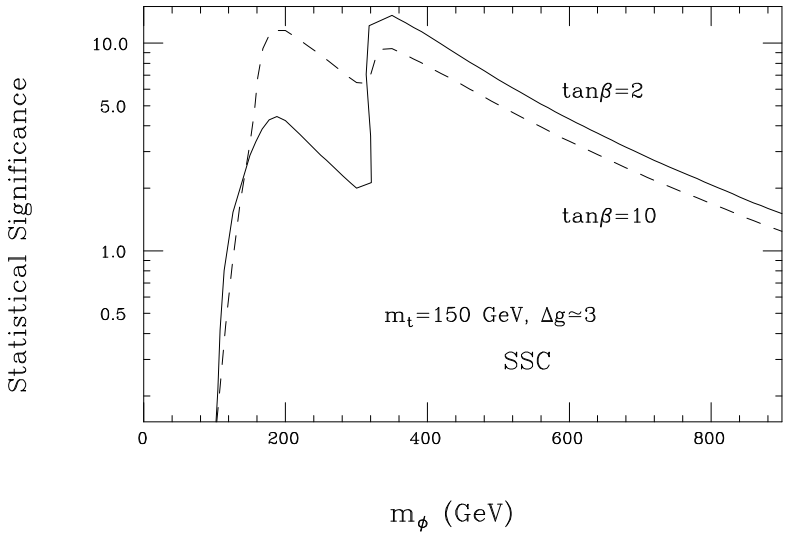

Fig. 13. Maximal statistical significance achieved for an asymmetry signal as a function of m_{ϕ^0} at the SSC with $L = 10$ fb^{-1}. The branching ratio for $\phi^0 \to ZZ \to \ell^+\ell^- X$ is included. A model for the polarized gluon distribution function is used where $\Delta g(x) = g(x)$ for $x > 0.2$ and $\Delta g(x) = 5xg(x)$ for $x < 0.2$ [100]. This yields $\Delta g \equiv \int g(x)dx \simeq 3$ over the Higgs mass range depicted above (where $g(x) \equiv g(x,Q)$ is evaluated at $Q = m_{\phi^0}$). Taken from Ref. [99].

with positive [negative] helicity inside a proton of *positive* helicity.* The unpolarized gluon distribution is given by $g(x) \equiv g_+(x) + g_-(x)$. If $\mathcal{M}_{\lambda\lambda'}$ denotes the amplitude for $g(\lambda) + g(\lambda') \to H$, then†

$$\mathcal{A} = \frac{\int_{m_H^2/s}^1 dx\, g\left(m_H^2/sx\right) \Delta g(x) \left[|\mathcal{M}_{++}|^2 - |\mathcal{M}_{--}|^2\right]}{\int_{m_H^2/s}^1 dx\, g\left(m_H^2/sx\right) g(x) \left[|\mathcal{M}_{++}|^2 + |\mathcal{M}_{--}|^2\right]}\,. \tag{3.14}$$

Note that $\mathcal{A}$ vanishes if H is an eigenstate of CP. This can be understood from Eq. (1.29) which implies that $|\mathcal{M}_{++}| = |\mathcal{M}_{--}|$ if P is conserved. However, for neutral scalars, eigenstates of P are necessarily eigenstates of CP, since there are no scalar interactions with fermion pairs or vector boson pairs that conserve P without conserving CP. Thus, the detection of a nonzero value for $\mathcal{A}$ would be an indication of CP-violation. The distribution function difference $\Delta g(x)$ is not very well constrained by data, and thus introduces model dependence into the calculation. As a result, the evaluation of the statistical significance of the signal is more uncertain than in the previous case of $\gamma\gamma \to H$. Figure 13, taken from Ref. [99],

$\star$ Note that $g_+(x)$ [$g_-(x)$] is also the probability of finding a gluon with negative [positive] helicity inside a proton of *negative* helicity.

$\dagger$ Recall that for $\gamma\gamma \to H$ (and $gg \to H$), $\mathcal{M}_{\lambda\lambda'}$ vanishes unless $\lambda = \lambda'$ [see Eq. (3.3)].

depicts a typical result. Although the detection of a CP-violating signal of this kind presents a real challenge for experimentalists working at a hadron supercollider, Fig. 13 does suggest that a polarized proton beam at hadron supercolliders can play a useful role in probing the details of new physics.

3.4 New gauge bosons beyond the $W^\pm$ and Z

In this section, I present the final example of these lectures. One of the key questions that one hopes to answer with the next generation of supercolliders is: what is the correct electroweak gauge group of the low-energy effective TeV-scale theory? Is it $\mathrm{SU}(2)_L\times\mathrm{U}(1)$ or is the gauge group larger, implying the existence of new gauge bosons beyond the $W^\pm$ and Z whose masses are of $\mathcal{O}$ (1 TeV). To answer this question with full confidence requires a collider that can probe deep into the TeV energy region. Clearly (unless we are very lucky), the ILC will not be sufficient for this task. If new W' and/or Z' gauge bosons are discovered, it will be essential to measure their couplings to fermions. At a hadron supercollider, there are a variety of techniques that can be employed for this purpose [101]. Here, I shall briefly mention two techniques.

If one of the proton beams is polarized, then one can consider the single helicity asymmetry

$$A_L = \frac{d\sigma_- - d\sigma_+}{d\sigma_- + d\sigma_+}\,, \tag{3.15}$$

where $d\sigma_\lambda$ is the differential cross-section (integrated either partially or completely over the available phase space) for $p(\lambda) + p \to$ heavy gauge boson. This is a similar asymmetry to the one defined in the previous section in the case of Higgs production. However, in this case, $A_L \neq 0$ implies only parity nonconservation, since vector boson interactions can violate P without violating CP. The production mechanism for new gauge bosons at a hadron collider is $q\bar{q}$ fusion. For very heavy gauge bosons, the momentum fractions of the initial partons are not particularly small.* Hence, one would expect that the polarization of a valence parton would reflect the polarization of the corresponding proton. Thus, it seems plausible that in new gauge boson production, large single helicity asymmetries should be observed. This is illustrated by a calculation of Ref. [73], which demonstrates that values for A_L as large as 25% are possible in the production of a neutral heavy gauge boson of a few TeV in mass. Moreover, the obtained value of A_L is a sensitive function of the vector boson mass and its quantum numbers. By changing the assumptions of the

$\star$ Recall that in the parton model computation, $x_1x_2s = m_V^2$, where s is the CM energy squared of the supercollider and x_1 and x_2 are the momentum fractions of the quark and antiquark, respectively [102].

Z' quantum numbers, one can find dramatic shifts in A_L by an order of magnitude. Finally, if both proton beams are polarized, then additional observables can be used to probe the new gauge boson couplings to fermion pairs. For example, Ref. [73] shows that in the production of left-handed and/or right-handed charged gauge bosons, σ_{--}/σ_{++} may deviate substantially from 1.

If no polarized beams are available, there are other tools for determining the nature of the new gauge boson interactions. I will conclude these lectures by discussing one powerful technique, in which one studies the decay of the heavy gauge boson to τN (where N is a neutral heavy lepton which may or may not be the ν_τ). This is a particularly useful decay mode, because the τ-lepton decays are self-analyzing. By studying the energy distribution of the τ decay products, one deduces information about the τ polarization, and hence learns about the coupling of the gauge boson to τN [103,104].

To illustrate the method, consider the decay of a new charged gauge boson, W'_L, where the subscript L indicates that W'_L has the same couplings to fermions as the $W^\pm$ of electroweak interactions. The following decay chain is assumed.

$$\begin{array}{l} W'_L \to \tau N \\ \qquad \Big\lfloor\!\!\longrightarrow \begin{cases} \mu\nu\bar{\nu} \qquad [\text{or } e\nu\bar{\nu}] \\ \pi\nu \\ \rho\nu \end{cases} \end{array} \tag{3.16}$$

In what follows, I shall provide details of the computation of the differential cross-section for W'_L production followed by the decay chain

$$W'_L \to \tau N \to e\nu\bar{\nu}N\,, \tag{3.17}$$

and quote the results for the other two decay chains shown above. In this calculation, I will make the (very good) approximation that all final state masses are negligible compared to W'_L.

The basic formula for the cross-section for the scattering process $a+b\to c+d$ followed by the decay $d\to 1+2+\ldots+n$ was described in section 1.7 as a trace over the product of the production and decay density matrix elements [see Eq. (1.107)]. Here, I shall write out the relevant formula in complete detail [10]

$$\begin{aligned} \sigma = {} & \frac{1}{4p_{\rm CM}\sqrt{s}}\sum_{\lambda\lambda'}\int \mathcal{M}(ab\to cd_\lambda)\mathcal{M}^*(ab\to cd_{\lambda'})\,\frac{ds_d}{2\pi}\,d\text{Lips}(s;p_c,p_d) \\ & \times\frac{\mathcal{M}(d_\lambda\to 1+2+\ldots+n)\mathcal{M}^*(d_{\lambda'}\to 1+2+\ldots+n)}{(m^2-s_d)^2+m^2\Gamma^2}\,d\text{Lips}(s_d\,;\,p_1,\ldots,p_n)\,, \end{aligned} \tag{3.18}$$

where $s=(p_a+p_b)^2$ is the CM energy squared for the process, m and Γ are the

mass and width of particle d, $p_{\rm CM}$ is the CM-momentum of particle a (or b) [if initial state masses are neglected, $p_{\rm CM} = \sqrt{s}/2$], $s_d = p_d^2$ is the invariant mass squared of the decaying particle d, and

$$d\mathrm{Lips}(s\,;\,p_1,\ldots,p_n) = (2\pi)^{4-3n}\prod_{i=1}^{n}\frac{d^3p_i}{2E_i}\,\delta^4(p_a+p_b-\sum_i p_i) \tag{3.19}$$

is Lorentz invariant phase space for an n-body final state with total CM-energy squared equal to s. Using the above formula, the computation proceeds in the seven steps sketched out below [105].

Step 1: Since $m_\tau \ll m_{W_L'}$, the emitted τ's are completely left-handed. Thus, only the $\lambda = \lambda' = -1$ term in the sum over λ, λ' in Eq. (3.18) survives. This observation simplifies this calculation immensely, and is special to this particular problem.

Step 2: Use the narrow width approximation

$$\frac{1}{(m^2-s_d)^2+m^2\Gamma^2} \longrightarrow \frac{\pi}{m\Gamma}\delta(m^2-s_d) \tag{3.20}$$

to integrate over s_d in Eq. (3.18). In this calculation,

$$B_e\Gamma = \frac{G_F^2 m_\tau^5}{192\pi^3}\,, \tag{3.21}$$

where $B_e \equiv \Gamma(\tau\to e\nu\bar\nu)/\Gamma$ is the tau-lepton branching ratio into electrons.

Step 3: The squared matrix elements for $a+b\to c+d$ and $d\to 1+2+3$ are well-known and are given below.

(i) $\bar u d \to W_L'^- \to \tau^- N$

The squared amplitude for this process, averaged over initial and summed over final spins and colors, is easily computed. The result is

$$|\mathcal{M}(\bar u d\to W_L'^-\to\tau^- N)|^2 = \left(\frac{1}{12}\right)\frac{4g^4 p_d\cdot p_\nu\, p_{\bar u}\cdot p_\tau}{(m_W^2-s)^2+\Gamma_W^2 m_W^2}\,, \tag{3.22}$$

where p_i is the four-momentum of particle i, and the $1/12$ inside the parentheses consists of a factor of $1/4$ for the spin-average and a color factor of $1/3$. As remarked above, the produced τ^- is purely left-handed (to a very good approximation), since $m_\tau \ll m_{W'}$.

(ii) $\tau^- \to e^-\nu\bar{\nu}$

In order to apply Eq. (3.18), we need the squared matrix element for the decay of a left-handed τ^-. This computation is most easily done using the spin projection operator method described in section 1.4. We introduce the spin four-vector [Eq. (1.48)] for a negative helicity τ^- of four-momentum $p_\tau = (E_\tau, \vec{\boldsymbol{p}}_{\boldsymbol{\tau}})^\star$

$$S = -\left(\frac{|\vec{\boldsymbol{p}}_{\boldsymbol{\tau}}|}{m_\tau}\,;\,\frac{E_\tau \hat{\boldsymbol{p}}_{\boldsymbol{\tau}}}{m_\tau}\right) . \tag{3.23}$$

The calculation of the squared decay amplitude is straightforward. Here, I simply quote the well known formula for the decay rate of a polarized muon found in Ref. [21], which can also be used here

$$E_\tau E_e \frac{d\Gamma}{d^3p_e} = \frac{G_F^2}{3(2\pi)^4}\left[\, q^2 p_e\cdot(p_\tau - m_\tau S) + 2q\cdot(p_\tau - m_\tau S) q\cdot p_e \,\right] ,$$

where $p_e = (E_e; \vec{\boldsymbol{p}}_{\boldsymbol{e}})$ is the electron four-momentum, $q \equiv p_\tau - p_e$ and S is the spin four-vector of the negative-helicity τ^-.

Step 4: Using Eq. (3.18) and the results given above, we integrate over s_d and obtain

$$\sigma = \frac{B_e g^4}{192\pi^3 m_\tau^6\, s\,[(m_W^2 - s)^2 + \Gamma_W^2 m_W^2]} \int d\Omega_\tau \frac{d^3p_e}{E_e}\, 4p_d\cdot p_\nu\, p_{\bar{u}}\cdot p_\tau \\ \times\left[q^2 p_e\cdot(p_\tau - m_\tau S) + 2q\cdot(p_\tau - m_\tau S)\, q\cdot p_e\right] , \tag{3.24}$$

where $d\Omega_\tau$ is the differential solid angle of the τ^-.

Step 5: It is convenient to choose the rest frame of the $W_L^{\prime -}$ to evaluate the integral above. Explicitly,

$$q^2 p_e\cdot(p_\tau - m_\tau S) + 2q\cdot(p_\tau - m_\tau S)\, q\cdot p_e = E_e\left[m_\tau^2 z + \sqrt{s}(m_\tau^2 - 2E_e z)(1 - \hat{\boldsymbol{p}}_{\boldsymbol{\tau}}\cdot\hat{\boldsymbol{p}}_{\boldsymbol{e}})\right] , \tag{3.25}$$

where

$$z \equiv \frac{s + m_\tau^2 - (s - m_\tau^2)\hat{\boldsymbol{p}}_{\boldsymbol{\tau}}\cdot\hat{\boldsymbol{p}}_{\boldsymbol{e}}}{\sqrt{s}} , \tag{3.26}$$

and

$$4p_d\cdot p_\nu\, p_{\bar{u}}\cdot p_\tau = \tfrac{1}{4}s^2(1 + \hat{\boldsymbol{p}}_{\boldsymbol{d}}\cdot\hat{\boldsymbol{p}}_{\boldsymbol{\tau}})^2 + \mathcal{O}(m_\tau^2) . \tag{3.27}$$

Since $m_\tau \ll m_{W'}$, we can drop the $\mathcal{O}(m_\tau^2)$ term in Eq. (3.27).

$\star$ A capital S is used here since s is already being used for the CM-energy squared.

Step 6: Insert the above expressions into the integral [Eq. (3.24)]. Choosing the direction of the d-quark to lie along the z-axis, and the direction of the electron to lie in the x–z plane, we write $\hat{\boldsymbol{p}}_{\boldsymbol{d}} = \hat{\boldsymbol{z}}$ and $\hat{\boldsymbol{p}}_{\boldsymbol{e}} = (\sin\theta_e, 0, \cos\theta_e)$. Our plan is to integrate over all possible τ directions, $\hat{\boldsymbol{p}}_{\boldsymbol{\tau}}$, holding the electron direction fixed. For this purpose, it is somewhat easier to rotate the z-axis to lie along the electron direction. That is, we take $\hat{\boldsymbol{p}}_{\boldsymbol{e}} = (0,0,1)$ and $\hat{\boldsymbol{p}}_{\boldsymbol{d}} = (-\sin\theta_e, 0, \cos\theta_e)$. Relative to this choice, we integrate over $\hat{\boldsymbol{p}}_{\boldsymbol{\tau}} = (\sin\theta\cos\phi, \sin\theta\sin\phi, \cos\theta)$. Then,

$$\begin{aligned} \hat{\boldsymbol{p}}_{\boldsymbol{\tau}} \cdot \hat{\boldsymbol{p}}_{\boldsymbol{e}} &= \cos\theta\,, \\ \hat{\boldsymbol{p}}_{\boldsymbol{d}} \cdot \hat{\boldsymbol{p}}_{\boldsymbol{\tau}} &= \cos\theta\cos\theta_e - \sin\theta\sin\theta_e\cos\phi\,. \end{aligned} \tag{3.28}$$

In the integration over $\hat{\boldsymbol{p}}_{\boldsymbol{\tau}}$ at fixed electron energy, the limits of integration depend on E_e. This is most easily obtained by noting that $(p_\tau - p_e)^2 \geq 0$ implies that $z \leq m_\tau^2/E_e$. From the definitions of z [Eq. (3.26)] and $\cos\theta$ [Eq. (3.28)], one sees that $y \leq \cos\theta \leq 1$, where

$$y \equiv \frac{E_e(s+m_\tau^2) - m_\tau^2\sqrt{s}}{E_e(s-m_\tau^2)}\,. \tag{3.29}$$

It follows that

$$\begin{aligned} \frac{d\sigma}{d\Omega_e dE_e} = {} & \frac{g^4 s E_e^2 B_e}{768\pi^3 m_\tau^6[(m_W^2-s)^2 + m_W^2\Gamma_W^2]} \\ & \times \int_0^{2\pi} d\phi \int_y^1 d\cos\theta\,(1+\cos\theta\cos\theta_e - \sin\theta\sin\theta_e\cos\phi)^2 \\ & \times \left[m_\tau^2 z + \sqrt{s}\,(1-\cos\theta)(m_\tau^2 - 2E_e z)\right]\,. \end{aligned} \tag{3.30}$$

Step 7: The above integration can be performed analytically. Recall that we are working in the limit of small m_τ. Although the factor of m_τ^6 in the denominator of Eq. (3.30) may be a cause for concern, it is easy to see that the leading m_τ behavior of the integral is $\mathcal{O}(m_\tau^6)$. Since $y \to 1$ as $m_\tau \to 0$, one can expand the integrand in Eq. (3.30) around $\cos\theta = 1$. Furthermore, for $\cos\theta \simeq 1$, one sees from Eq. (3.26) that $z = \mathcal{O}(m_\tau^2)$. Thus, it is sufficient to keep terms in Eq. (3.30) up to $(1-\cos\theta)^2$ and drop all higher terms. One therefore ends up with a finite value for the differential cross-section in the limit of $m_\tau \to 0$:

$$\frac{d\sigma}{dE_e\,d\cos\theta_e} = \frac{\pi\alpha^2\sqrt{s}\,(1+\cos\theta_e)^2 B_e}{36\sin^4\theta_W[(m_W^2-s)^2 + \Gamma_W^2 m_W^2]}\left[1 - \left(\frac{2E_e}{\sqrt{s}}\right)^3\right]\,, \tag{3.31}$$

where $\alpha \equiv g^2/4\pi\sin^2\theta_W$. Note that the allowed range of electron energies is $0 \leq E_e \leq \frac{1}{2}\sqrt{s}$.

Two features of this result are immediately apparent. First, the $(1+\cos\theta_e)^2$ angular distribution matches precisely the $(1+\cos\theta)^2$ angular distribution of the τ^- obtained in Eq. (3.22), in the $m_\tau = 0$ limit [see Eq. (3.27)]. This angular distribution can be understood using simple helicity arguments as shown in the figure below.

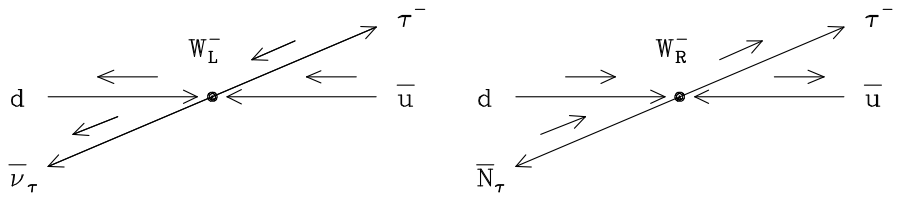

The arrows above the fermion lines denote helicity. The $W_L'^-$ couples to a left-handed d-quark and τ^-, and a right-handed u-quark and anti-neutrino. Angular momentum conservation favors θ near 0° and disfavors θ near 180°. It is interesting to note that precisely the same angular factor would arise in $W_R'^-$ production, assuming that the $W_R'^-$ couples to right-handed fermions and left-handed anti-fermions. In the figure above, the configurations shown are both favored by angular momentum conservation, and one concludes that the electron angular distribution will be the same for both W_L' and W_R' production!

Second, let us define $x \equiv 2E_e/\sqrt{s}$. From Eq. (3.31), one sees that the polarization of the τ^- is reflected in the $1-x^3$ energy distribution of the electron. Furthermore, by repeating the above calculation for $W_R'^-$ production, one finds that although the final state electron angular distribution is the same, the electron energy distribution is proportional to $(1+2x)(1-x)^2$. Thus, the electron energy distribution is *softer* for W_R' production as compared with W_L' production. Thus, by measuring the energy distribution of the observed electron, one gains information about the τ polarization and thereby obtains a probe of the W' coupling to τN.

Other τ decay modes can be used in a similar fashion. The relevant calculations are similar to the one presented above, so I shall simply summarize the results below [103].

(i) $\bar{u}d \to W_{L,R}'^- \to \tau^- N$, $\tau^- \to e^-\nu\bar{\nu}$

$$\frac{d\sigma}{dE_e\, d\cos\theta_e} = B_e C(\theta_e) \times \begin{cases} \frac{2}{3}(1-x^3) & , W_L' \\ (1+2x)(1-x)^2 & , W_R' \end{cases} \tag{3.32}$$

(ii) $\bar{u}d \to W'^{-}_{L,R} \to \tau^- N,\ \tau^- \to \rho^- \nu$

$$\frac{d\sigma}{dE_\rho\, d\cos\theta_\rho} = \frac{B_\rho m_\tau^2 C(\theta_\rho)}{(m_\tau^2 - m_\rho^2)^2(m_\tau^2 + 2m_\rho^2)} \times \begin{cases} 2m_\rho^2(m_\tau^2 - m_\rho^2) + m_\tau^2(m_\tau^2 - 2m_\rho^2)(1-x) & , W'_L \\ m_\tau^2\left[m_\rho^2 + (m_\tau^2 - 2m_\rho^2)x\right] & , W'_R \end{cases} \tag{3.33}$$

(iii) $\bar{u}d \to W^-_{L,R} \to \tau^- N,\ \tau^- \to \pi^- \nu$

$$\frac{d\sigma}{dE_\pi\, d\cos\theta_\pi} = B_\pi C(\theta_\pi) \times \begin{cases} 1-x & , W'_L \\ x & , W'_R \end{cases} \tag{3.34}$$

where m_π has been set to zero in the last computation. In all the above expressions, B is the relevant τ branching ratio,

$$C(\theta) \equiv \frac{\pi\alpha^2\sqrt{s}\,(1+\cos\theta)^2}{24\sin^4\theta_W[(m_W^2 - s)^2 + \Gamma_W^2 m_W^2]}\,, \tag{3.35}$$

and $x \equiv 2E/\sqrt{s}$, where E is the energy of the final state negatively charged particle.

There is a simple way to rederive the form of Eq. (3.34) for $\bar{u}d \to W'^{-}_{L,R} \to \tau^- N$, $\tau^- \to \pi^- \nu$. Choose the quantization axis of the τ-spin to lie along the z-axis. Let k be the four-momentum of the π in the rest frame of the τ. Then, setting $m_\pi = 0$, $k = \frac{1}{2}m_\tau\,(1;\,\sin\theta, 0, \cos\theta)$. Now, boost to a frame where the τ is moving along $\hat{z}$ with velocity v. In this frame,

$$\begin{aligned} E_\pi &= \tfrac{1}{2}\gamma m_\tau(1 + v\cos\theta)\,, \\ E_\tau &= \gamma m_\tau\,, \end{aligned} \tag{3.36}$$

where $\gamma \equiv (1-v^2)^{1/2}$ and

$$x \equiv \frac{E_\pi}{E_\tau} = \tfrac{1}{2}(1 + v\cos\theta) \longrightarrow \cos^2\tfrac{1}{2}\theta \tag{3.37}$$

as $v \to 1$. But, using Eq. (1.25), we know that the decay rate for $\tau^-(\lambda) \to \pi^-\nu$ is

$$\Gamma(\tau^-(\lambda) \to \pi\nu) \propto |d^{1/2}_{\lambda,1/2}(\theta)|^2 = \begin{cases} \cos^2\frac{\theta}{2}, & \lambda = +\frac{1}{2} \\ \sin^2\frac{\theta}{2}, & \lambda = -\frac{1}{2} \end{cases} \tag{3.38}$$

which corresponds to pion energy distributions of x and $1-x$, respectively, in agreement with the previously quoted result.

This result also has a simple physical interpretation. The τ^- is either left or right-handed depending on whether it came from W_L' or W_R'. But the neutrino emitted in τ^- decay is always left-handed. Thus, because the π is spinless, conservation of angular momentum implies that the π is emitted preferentially forward in the case of W_R' decay and backward in the case of W_L' decay. This is illustrated in the figure below.

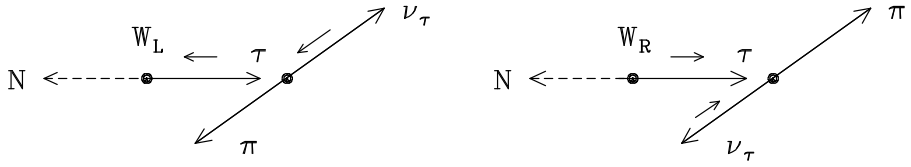

The arrows above the τ and ν denote helicity. Angular momentum conservation implies that the configurations shown above are the ones favored. Therefore, in the $\bar{u}d$ CM-frame, the energy spectrum of the π is harder in W_R decay and softer in W_L decay.

Finally, one must convolute the partonic cross-sections given above with parton distribution functions to obtain predictions for the energy distributions of τ-lepton decay products in the laboratory frame. The computations of Ref. [106] show that it may be possible to distinguish between W_L' and W_R' on the basis of their τ-decay spectra.

CODA

In these lectures, I presented an introduction to spin formalism and illustrated its use in a number of examples of searches for new physics beyond the Standard Model at future colliders. I have only touched the surface; many important topics have been omitted. Some of the important applications not included in these lectures involve the search for evidence of physics beyond the Standard Model in precision measurements of top-quarks and gauge bosons. For example, a crucial test of the Standard Model consists of checking the details of the W^+W^-Z and $W^+W^-\gamma$ vertices [107]. Similarly, it may be possible to see hints of non-Standard Model effects in $t\bar{t}$ couplings to γ and/or Z [108]. In both cases, one can search for anomalous moments, CP-violating form-factors, evidence for form-factors, *etc.* Using spin information to separate out definite helicity final states could enhance a particular signal as well as help control backgrounds.

There are many other precision tests of electroweak theory and QCD which become available with polarized beams and/or spin analysis of final state particles. Some of these have been addressed in other lectures presented at this summer school. Another method for searching for evidence of new physics is to detect the presence of four-fermion operators, which would be remnants of new physics

at a higher energy scale [109]. There are many such operators possible. These could be detected at a future hadron supercollider if deviations are seen from Standard Model predictions in two-jet and/or Drell-Yan cross-sections (to give just two examples). The ability to separate out the definite helicity properties of such operators (if they exist) would play a crucial role in trying to interpret their origin.

The discovery of new physics beyond the Standard Model hopefully lies ahead in the not too distant future. In the first decade of the third millennium, powerful supercolliders will be ready to fully explore the TeV-energy scale and reveal its secrets. Once deviations from the Standard Model are found, the challenge to theorists and experimentalists will be to interpret the results and build a new Standard Model of particle physics. Spin techniques will surely play an important role in unraveling the true nature of TeV-scale physics. We have only just begun to explore its power.

ACKNOWLEDGMENTS

I would like to thank Roberto Vega for fruitful discussions pertaining to Lecture 1, Hitoshi Murayama and Jonathan Feng for their help in presenting some of the material of Lecture 2, and Jack Gunion for his assistance and collaboration in various aspects of Lecture 3. I am also very grateful to Mayling and Lance Dixon and to Valerie and Michael Peskin for their gracious hospitality during my stay at the SLAC Summer School. I am pleased to acknowledge the Institute for Theoretical Physics in Santa Barbara for their support during the preparation of the written version of these lectures. Finally, I wish to extend my special thanks and appreciation to Nora Rogers at SCIPP and Darla Sharp at the ITP for their assistance in the TEX input and processing.

REFERENCES

[1] See *e.g.*, D. Schaile, CERN-PPE/93-213 (1993).

[2] F. Abe *et al.* [CDF Collaboration] FERMILAB-PUB-94/097-E (1994).

[3] E. Gross and P. Yepes, *Int. J. Mod. Phys.* **A8** (1993) 407.

[4] S. Weinberg, *Phys. Rev.* **D13** (1976) 974; **D19** (1979) 1277; L. Susskind, *Phys. Rev.* **D20** (1979) 2619; G. 't Hooft, in *Recent Developments in Gauge Theories,* Proceedings of the NATO Advanced Summer Institute, Cargese, 1979, edited by G. 't Hooft *et al.* (Plenum, New York, 1980) p. 135.

[5] H.E. Haber, in *Testing the Standard Model*, Proceedings of the 1990 Theoretical Advanced Study Institute in Elementary Particle Physics, edited by M. Cvetič and Paul Langacker (World Scientific, Singapore, 1991) pp. 340–475.

[6] M. Jacob and G.C. Wick, Ann. Phys. (NY) **7** (1959) 404.

[7] See *e.g.*, K. Gottfried, *Quantum Mechanics* (W.A. Benjamin, Inc., New York, 1966), §35.3; A. Galindo and P. Pascual, *Quantum Mechanics I* (Springer-Verlag, Berlin, 1990), §5.10.

[8] For a comprehensive treatment of angular momentum theory in quantum mechanics and a guide to the literature, see D.A. Varshalovich, A.N. Moskalev and V.K. Khersonskii, *Quantum Theory of Angular Momentum* (World Scientific, Singapore, 1988).

[9] J. Werle, *Relativistic Theory of Reactions* (North-Holland, Amsterdam, 1966); A.D. Martin and T.D. Spearman, *Elementary Particle Physics* (North-Holland, Amsterdam, 1970); S.U. Chung, *Spin Formalisms*, CERN Yellow Report 71-8 (1971); Martin L. Perl, *High Energy Hadron Physics* (John Wiley & Sons, New York, 1974).

[10] H. Pilkuhn, *The Interactions of Hadrons* (North-Holland, Amsterdam, 1967).

[11] Peter A. Carruthers, *Spin and Isospin in Particle Physics* (Gordon and Breach, New York, 1971); M.D. Scadron, *Advanced Quantum Theory* (Springer-Verlag, Berlin, 1991).

[12] J.D. Bjorken and S.D. Drell, *Relativistic Quantum Mechanics* (McGraw Hill, New York, 1964).

[13] M.E. Peskin and D.V. Schroeder, *An Introduction to Quantum Field Theory* (Addison-Wesley, Reading, MA), to be published.

[14] F.M. Renard, *Basics of Electron Positron Collisions* (Editions Frontières, Gif sur Yvette, France, 1981).

[15] R. Gastmans and T.T. Wu, *The Ubiquitous Photon: Helicity Method for QED and QCD* (Oxford University Press, Oxford, England, 1990).

[16] F.A. Berends, P.H. Daverveldt and R. Kleiss, *Nucl. Phys.* **B253** (1985) 441; R. Kleiss and W.J. Stirling, *Nucl. Phys.* **B262** (1985) 235; C. Mana and M. Martinez, *Nucl. Phys.* **B287** (1987) 601.

[17] Z. Xu, D.-H. Zhang and L. Chang, Tsinghua University preprints TUTP-84/3 (1984), TUTP-84/4 (1985); TUTP-84/5a (1985); *Nucl. Phys.* **B291** (1987) 392.

[18] P. de Causmaecker, R. Gastmans, W. Troost, and T.T. Wu, *Phys. Lett.* **105B** (1981) 215; *Nucl. Phys.* **B206** (1982) 53; F.A. Berends, P. de Causmaecker, R. Gastmans, R. Kleiss, W. Troost, and T.T. Wu, *Nucl. Phys.* **B206** (1982) 61; **B239** (1984) 382; **B239** (1984) 395; **B264** (1986) 243; 265.

[19] M.L. Mangano and S.J. Parke, *Phys. Rep.* **200** (1991) 301.

[20] See *e.g.*, Z. Bern, in *Recent Directions in Particle Theory*, Proceedings of the 1992 Theoretical Advanced Study Institute in Elementary Particle Physics, Boulder, CO, 1–26 June, 1992, edited by J. Harvey and J. Polchinski (World Scientific, Singapore, 1993) pp. 471–535; C.S. Lam, McGill preprint 93-20 (1993).

[21] D. Bailin, *Weak Interactions* (Adam Hilger, Bristol, England, 1982).

[22] C. Bouchiat and L. Michel, *Nucl. Phys.* **5** (1958) 416; L. Michel, *Suppl. Nuovo Cim.* **14** (1959) 95.

[23] H.W. Fearing and R.R. Silbar, *Phys. Rev.* **D6** (1972) 471; M. Caffo and E. Remiddi, *Helv. Phys. Acta* **55** (1982) 339; G. Passarino, *Phys. Rev.* **D28** (1983) 2867; *Nucl. Phys.* **B237** (1984) 249; K. Hagiwara and D. Zeppenfeld, *Nucl. Phys.* **B274** (1986) 1; E. Yehudai, FERMILAB-PUB-92/256-T (1992); A. Ballestrero and E. Maina, Turin Univ. preprint DFTT-76/93 (1994); D.A. Dicus and R. Vega, unpublished.

[24] C. Bourrely, E. Leader and J. Soffer, *Phys. Rep.* **59** (1980) 95; T.B. Anders, A.O. Barut, and W. Jachmann, *Int. J. Mod. Phys.* **A6** (1991) 4223; **A8** (1993) 5383.

[25] F. Bletzacker and H.T. Nieh, *Phys. Rev.* **D14** (1976) 1251.

[26] B.R. Martin, E. de Rafael and J. Smith, *Phys. Rev.* **D2** (1970) 179.

[27] Y.-S. Tsai, *Phys. Rev.* **D4** (1971) 2821).

[28] S. Kawasaki, T. Shirafuji and S.Y. Tsai, *Prog. Theor. Phys.* **49** (1973) 1656.

[29] J.-L. Cortes, M. Gourdin and X.Y. Pham, PAR-LPTHE 79/22 (1979); M. Gourdin and X.Y. Pham, *Nucl. Phys.* **B164** (1980) 399.

[30] G. Jarlskorg and D. Rein, editors, *Proceedings of the ECFA Large Hadron Collider Workshop*, Vols I–III, Aachen, Germany, 4–9 October 1990, CERN Report 90-10 (1990).

[31] R. Orava, P. Eerola and M. Nordberg (editors), *Physics and Experiments with Linear Collers*, Workshop Proceedings, Saariselkä, Finland, 9–14 September, 1991 (World Scientific, Singapore, 1992); F.A. Harris, S.L. Olsen, S. Pakvasa and X. Tata (editors), *Physics and Experiments with Linear e^+e^- Colliders*, Workshop Proceedings, Waikoloa, Hawaii, 26–30 April, 1993 (World Scientific, Singapore, 1993).

[32] J.F. Gunion, H.E. Haber, G. Kane, and S. Dawson, *The Higgs Hunter's Guide* (Addison-Wesley Publishing Company, Redwood City, CA, 1990).

[33] E. Farhi and L. Susskind, *Phys. Rep.* **74** (1981) 277; R.K. Kaul, *Rev. Mod. Phys.* **55** (1983) 449.

[34] J. Maalampi and M. Roos, *Phys. Rep.* **186** (1990) 53.

[35] J.L. Hewett and T.G. Rizzo, *Phys. Rep.* **183** (1989) 193.

[36] P. Langacker, *Phys. Rep.* **72** (1981) 185; G.G. Ross, *Grand Unified Theories* (Addison-Wesley Publishing Company, Reading, MA, 1984).

[37] E. Gildener, *Phys. Rev.* **B14** (1976) 1667; S. Weinberg, *Phys. Lett.* **82B** (1979) 387.

[38] L. Susskind, *Phys. Rep.* **104** (1984) 181.

[39] I.A. D'Souza and C.S. Kalman, *Preons* (World Scientific, Singapore, 1992).

[40] M. Veltman, *Acta Phys. Pol.* **B12** (1981) 437; R.K. Kaul and P. Majumdar, *Nucl. Phys.* **B199** (1982) 36; T. Inami, H. Nishino and S. Watamura, *Phys. Lett.* **117B** (1982) 197; N.G. Deshpande, R.J. Johnson and E. Ma, *Phys. Lett.* **130B** (1983) 61; *Phys. Rev.* **D29** (1984) 2851.

[41] H.E. Haber, *The Supersymmetric Top-Ten Lists*, SCIPP-93/22 (1993), to appear in the Proceedings of the Workshop on Recent Advances in the Superworld, Houston Advanced Research Center, April 14–16, 1993.

[42] H.P. Nilles, *Phys. Rep.* **110** (1984) 1; A.B. Lahanas and D.V. Nanopoulos, *Phys. Rep.* **145** (1987) 1.

[43] P. Nath, R. Arnowitt, and A. H. Chamseddine, *Applied $N = 1$ Supergravity* (World Scientific, Singapore, 1984).

[44] M.B. Green, J.S. Schwarz, and E. Witten, *Superstring Theory* (Cambridge University Press, Cambridge, 1987).

[45] E. Witten, *Nucl. Phys.* **B188** (1981) 513; S. Dimopoulos and H. Georgi, *Nucl. Phys.* **B193** (1981) 150; N. Sakai, *Z. Phys.* **C11** (1981) 153; R.K. Kaul, *Phys. Lett.* **109B** (1982) 19.

[46] H.E. Haber and G.L. Kane, *Phys. Rep.* **117** (1985) 75.

[47] K. Inoue, A. Kakuto, H. Komatsu, and S. Takeshita, *Prog. Theor. Phys.* **68**, (1982) 927; [E: **70** (1983) 330]; **71** (1984) 413; R. Flores and M. Sher, *Ann. Phys. (NY)* **148** (1983) 95.

[48] J.F. Gunion and H.E. Haber, *Nucl. Phys.* **B272** (1986) 1 [E: **B402** (1993) 567].

[49] L. Girardello and M. Grisaru, *Nucl. Phys.* **B194** (1982) 65.

[50] For a recent discussion, see B. de Carlos and J.A. Casas, *Phys. Lett.* **B309** (1993) 320.

[51] S. Bertolini, F. Borzumati, A. Masiero, and G. Ridolfi, *Nucl. Phys.* **B353** (1991) 591.

[52] P. Fayet, *Phys. Lett.* **69B** (1977) 489; G. Farrar and P. Fayet, *Phys. Lett.* **76B** (1978) 575.

[53] J. Ellis, J.S. Hagelin, D.V. Nanopoulos, K. Olive, and M. Srednicki, *Nucl. Phys.* **B238** (1984) 453.

[54] See *e.g.*, S. Dimopoulos, R. Esmailzadeh, L.J. Hall, and G.D. Starkman, *Phys. Rev.* **D41** (1990) 2099; H. Dreiner and G.G. Ross, *Nucl. Phys.* **B365** (1991) 597.

[55] H.E. Haber, in *Recent Directions in Particle Theory*, Proceedings of the 1992 Theoretical Advanced Study Institute in Particle Physics, edited by J. Harvey and J. Polchinski (World Scientific, Singapore, 1993) pp. 589–686.

[56] W. Fischler, S. Paban, and S. Thomas, *Phys. Lett.* **B289** (1992) 373; S.M. Barr, *Int. J. Mod. Phys.* **A8** (1993) 209.

[57] H.E. Haber and R. Hempfling, *Phys. Rev. Lett.* **66** (1991) 1815.

[58] Y. Okada, M. Yamaguchi, and T. Yanagida, *Prog. Theor.* **85** (1991) 1; J. Ellis, G. Ridolfi, and F. Zwirner, *Phys. Lett.* **B257** (1991) 83.

[59] See *e.g.*, Appendix A of Ref. [48].

[60] See *e.g.*, D. Decamp *et al.* [ALEPH Collaboration], *Phys. Rep.* **216** (1992) 253.

[61] J. Ellis and S. Rudaz, *Phys. Lett.* **128B** (1983) 248.

[62] F. Gabbiani and A. Masiero, *Nucl. Phys.* **B322** (1989) 235.

[63] For a recent discussion, see M. Dine, R. Leigh, and A. Kagan, *Phys. Rev.* **D48** (1993) 4269. For an alternate approach, see Y. Nir and N. Seiberg, *Phys. Lett.* **B309** (1993) 337.

[64] Recent works include: G.G. Ross and R.G. Roberts, *Nucl. Phys.* **B377** (1992) 571; S. Kelley, J.L. Lopez, D.V. Nanopoulos, H. Pois, and K. Yuan, *Nucl. Phys.* **B398** (1993) 3; M. Olechowski and S. Pokorski, *Nucl. Phys.* **B404** (1993) 590; D.J. Castaño, E.J. Piard, and P. Ramond, UFIFT-HEP-93-18 (1993); V. Barger, M.S. Berger, and P. Ohmann, MAD/PH/801 (1993); G.L. Kane, C. Kolda, L. Roszkowski, and J.D. Wells, UM-TH-93-24 (1993).

[65] For recent reviews, see R. Arnowitt and P. Nath, CTP-TAMU-52/93 (1993); W. de Boer, IEKP-KA/94-01 (1994).

[66] U. Amaldi, W. de Boer, and H. Furstenau, *Phys. Lett.* **B260** (1991) 447; U. Amaldi *et al.*, *Phys. Lett.* **B281** (1992) 374.

[67] H. Arason *et al.*, *Phys. Rev.* **D46** (1992) 3945.

[68] J. Ellis, S. Kelly, and D.V. Nanopoulos, *Nucl. Phys.* **B373** (1992) 55; F. Anselmo, L. Cifarelli, A. Peterman, and A. Zichichi, *Nuovo Cim.* **105A** (1992) 1817; **105A** (1992) 581; **105A** (1992) 1201; P. Langacker and N. Polonsky, *Phys. Rev.* **D47** (1993) 4028; M. Carena, S. Pokorski, and C.E.M. Wagner, *Nucl. Phys.* **B406** (1993) 59; V. Barger, M.S. Berger, and P. Ohmann, *Phys. Rev.* **D47** (1993) 1093.

[69] See *e.g.*, B. Anantharayan, G. Lazarides, and Q. Shafi, *Phys. Rev.* **D44** (1991) 1613; S. Dimopoulos, L.J. Hall, and S. Raby, *Phys. Rev.* **D45** (1992) 4192; L.J. Hall, R. Rattazzi, and U. Sarid, LBL-33997 (1993).

[70] P.R. Harrison and C.H. Llewellyn Smith, *Nucl. Phys.* **B213** (1983) 223 [E: **B223** (1983 542]; S. Dawson, E. Eichten and C. Quigg, *Phys. Rev.* **D31** (11985) 1581.

[71] X. Tata, in *The Standard Model and Beyond*, Proceedings of the 9th Symposium in Theoretical Physics, Mt. Sorak, Korea, 20–25 August 1990, edited by J.E. Kim (World Scientific, Singapore, 1991) pp. 304–378.

[72] N.S. Craigie, K. Hidaka, M. Jacob and F.M. Renard, *Phys. Rep.* **99** (1983) 69.

[73] C. Bourrely, J. Soffer, R.M. Renard and P. Taxil, *Phys. Rep.* **177** (1989) 319.

[74] N.S. Craigie, K. Hidaka and P. Ratcliffe, *Phys. Lett.* **129B** (1983) 310.

[75] T. Tsukamoto, K. Fujii, H. Murayama, M. Yamaguchi, and Y. Okada, KEK Preprint 93-146 (1993).

[76] R.M. Barnett, H.E. Haber, and K.S. Lackner, *Phys. Rev. Lett.* **51** (1983) 176; *Phys. Rev.* **D29** (1984) 1381.

[77] J.L. Feng and D.E. Finnell, *Phys. Rev.* **D49** (1994) 2369.

[78] For an extensive review and guide to the literature, see chapter 4 of Ref. [32].

[79] H.E. Haber and Y. Nir, *Nucl. Phys.* **B335** (1990) 363; H.E. Haber and S. Thomas, SCIPP-94/08 (1994).

[80] V. Barger, M.S. Berger and A.L. Stange, *Phys. Rev.* **D45** (1992) 4128; V. Barger, K. Cheung, R.J.N. Phillips and A.L. Stange, *Phys. Rev.* **D46** (1992) 4914.

[81] R. Bork, J.F. Gunion, H.E. Haber and A. Seiden, *Phys. Rev.* **D46** (1992) 2040.

[82] J.F. Gunion, H.E. Haber, and C. Kao, *Phys. Rev.* **D46** (1992) 2907.

[83] J.F. Gunion and L.H. Orr, *Phys. Rev.* **D46** (1992) 2052.

[84] Z. Kunszt and F. Zwirner, *Nucl. Phys.* **B385** (1992) 3.

[85] H. Baer, C. Kao, M. Bisset, X. Tata and D. Dicus, *Phys. Rev.* **D46** (1992) 1067; **D47** (1993) 1062.

[86] A. Rubbia, in *Proceedings of the 1992 Workshop on High Energy Physics with Colliding Beams*, Volume 3, "Electroweak Symmetry Breaking at Colliding Beam Facilities," December 11-12, 1992, Santa Cruz, CA, edited by J. Rogers, SLAC-Report-428 (1993) p. 800–836.

[87] V. Barger, K. Cheung, B.A. Kniehl, and R.J.N. Phillips, *Phys. Rev.* **D46** (1992) 3725.

[88] P. Janot, in *Physics and Experiments with Linear e^+e^- Colliders*, Workshop Proceedings, Waikoloa, Hawaii, 26–30 April, 1993, edited by F.A. Harris, S.L. Olsen, S. Pakvasa and X. Tata, (World Scientific, Singapore, 1993) pp. 192–217.

[89] H.E. Haber, in *Physics and Experiments with Linear Colliders*, Proceedings of the Linear Collider Workshop, Saariselkä, Finland, 9–14 September, 1991, edited by R. Orava, P. Eerola and M. Nordberg (World Scientific, Singapore, 1992) pp. 235–275; J.F. Gunion, in *Physics and Experiments with Linear e^+e^- Colliders*, Workshop Proceedings, Waikoloa, Hawaii, 26–30 April, 1993, edited by F.A. Harris, S.L. Olsen, S. Pakvasa and X. Tata, (World Scientific, Singapore, 1993) pp. 166–191.

[90] A. Yamada, *Mod. Phys. Lett.* **A7** (1992) 2789.

[91] H.F. Ginzburg, G.L. Kotkin, V.G. Serbo and V.I. Telnov, *Nucl. Inst. and Methods* **205** (1983) 47.

[92] H.F. Ginzburg, G.L. Kotkin, S.L. Panfil, V.G. Serbo and V.I. Telnov, *Nucl. Inst. and Methods* **219** (1984) 5.

[93] T.L. Barklow, in *Research Directions for the Decade*, Proceedings of the 1990 Summer Study on High Energy Physics, Snowmass, CO, June 25–July 13, 1990, edited by E.L. Berger (World Scientific, Singapore, 1992), pp. 440–450.

[94] D.L. Borden, D.A. Bauer and D.O. Caldwell, *Phys. Rev.* **D48** (1993) 4018.

[95] A.I. Vainshtein, M.B. Voloshin, V.I. Zakharov and M. Shifman, *Yad. Fiz.*, **30** (1979) 1368 [*Sov. J. Nucl. Phys.* **30** (1979) 711].

[96] J.F. Gunion and H.E. Haber, *Phys. Rev.* **D48** (1993) 5109.

[97] O.J.P. Eboli, M.C. Gonzalez-Garcia, F. Halzen and D. Zeppenfeld, *Phys. Rev.* **D48** (1993) 1430.

[98] B. Grzadkowski and J.F. Gunion, *Phys. Lett.* **B294** (1992) 361.

[99] J.F. Gunion, T.C. Yuan and B. Grzadkowski *Phys. Rev. Lett.* **71** (1993) 488 [E: **71** (1993) 2681]; J.F. Gunion, UCD-92-26 (1992).

[100] E. Berger and J. Qui, *Phys. Rev.* **D40** (1989) 778.

[101] P. Langacker, R. W. Robinett and J. L. Rosner, *Phys. Rev.* **D30** (1984) 1470; F. del Aguila, M. Cvetic and P. Langacker, *Phys. Rev.* **D48** (1993) 969; M. Cvetic, P. Langacker, and J. Liu, *Phys. Rev.* **D49** (1994) 2405.

[102] E. Eichten, I. Hinchliffe, K. Lane and C. Quigg, *Rev. Mod. Phys.* **56** (1984) 579 [E: **58** (1986) 1065].

[103] H. Haber, in *Proceedings of the 1984 Summer Study on the Design and Utilization of the Superconducting Super Collider*, Snowmass, Colorado, June 23-July 13, 1984, edited by R. Donaldson and J.G. Morfin (Fermilab, Batavia, IL, 1985) pp. 125–143; and pp. 157–159.

[104] B.K. Bullock, K. Hagiwara and A.D. Martin, *Nucl. Phys.* **B395** (1993) 499.

[105] R.M. Barnett, H.E. Haber and K.S. Lackner, *Phys. Rev.* **D29** (1984) 1381.

[106] J.F. Gunion and H.E. Haber, in *Proceedings of the 1984 Summer Study on the Design and Utilization of the Superconducting Super Collider*, Snowmass, Colorado, June 23-July 13, 1984, edited by R. Donaldson and J.G. Morfin (Fermilab, Batavia, IL, 1985) pp. 150–152.

[107] See *e.g.*, K. Hagiwara, R.D. Peccei, D. Zeppenfeld and K. Hikasa, *Nucl. Phys.* **B282** (1987) 253; E. Yehudai, *Phys. Rev.* **D41** (1990) 33; **D44** (1991) 3434; SLAC-383 (1991); G.J. Gounaris, J. Layssac, G. Moultaka and F. Renard, *Int. J. Mod. Phys.* **A8** (1993) 3285; G.J. Gounaris, J. Layssac and F. Renard, Montpelier preprint PM-93-26 (1993).

[108] G.L. Kane, G.A. Ladinsky and C.P. Yuan, *Phys. Rev.* **D45** (1992) 124; C.P. Yuan, *Phys. Rev.* **D45** (1992) 782; G.A. Ladinsky, *Phys. Rev.* **D46** (1992) 3789 [E: **D47** (1993) 3086]; C.R. Schmidt and M.E. Peskin, *Phys. Rev. Lett.* **69** (1992) 410; C.R. Schmidt, *Phys. Lett.* **B293** (1992) 111; W. Bernreuther, J.P. Ma, and T. Schroder, *Phys. Lett.* **B297** (1992) 318.

[109] E. Eichten, K. Lane and M.E. Peskin, *Phys. Rev. Lett.* **50** (1983) 811.